(12) INTERNATIONAL APPLICATION PUBLISHED UNDER THE PATENT COOPERATION TREATY (PCT)

(19) World Intellectual Property Organization
International Bureau

(43) International Publication Date
20 December 2012 (20.12.2012)

WIPO | PCT

(10) International Publication Number
WO 2012/174344 A2

(51) International Patent Classification:
B01J 31/12 (2006.01) *H01M 4/90* (2006.01)
B01J 38/02 (2006.01)

(21) International Application Number:
PCT/US2012/042609

(22) International Filing Date:
15 June 2012 (15.06.2012)

(25) Filing Language: English

(26) Publication Language: English

(30) Priority Data:

61/497,444	15 June 2011 (15.06.2011)	US
61/606,109	2 March 2012 (02.03.2012)	US
61/621,084	6 April 2012 (06.04.2012)	US
61/621,095	6 April 2012 (06.04.2012)	US

(71) Applicant *(for all designated States except US)*: **STC.UNM** [US/US]; MSC 04 2750, 801 University Blvd. SE, Suite 101, Albuquerque, NM 87106 (US).

(72) Inventors; and
(75) Inventors/Applicants *(for US only)*: **SEROV, Alexey** [RU/US]; 5300 Eubank Blvd Apt 9J, Albuquerque, NM 87111 (US). **HALEVI, Barr** [US/US]; 1510 Gold Ave SE Apt C, Albuquerque, NM 87102 (US). **ARTYUSHKOVA, Kateryna** [US/US]; 412 Mankin St. NE, Albuquerque, NM 87123 (US). **ATANASSOV, Plamen, B.** [US/US]; 1642 Villa Strada, Santa Fe, NM 87506 (US).

(74) Agent: **GONZALES, Ellen**; Gonzales Patent Services, 4605 Congress Ave NW, Albuquerque, NM 87114 (US).

(81) Designated States *(unless otherwise indicated, for every kind of national protection available)*: AE, AG, AL, AM, AO, AT, AU, AZ, BA, BB, BG, BH, BR, BW, BY, BZ, CA, CH, CL, CN, CO, CR, CU, CZ, DE, DK, DM, DO, DZ, EC, EE, EG, ES, FI, GB, GD, GE, GH, GM, GT, HN, HR, HU, ID, IL, IN, IS, JP, KE, KG, KM, KN, KP, KR, KZ, LA, LC, LK, LR, LS, LT, LU, LY, MA, MD, ME, MG, MK, MN, MW, MX, MY, MZ, NA, NG, NI, NO, NZ, OM, PE, PG, PH, PL, PT, QA, RO, RS, RU, RW, SC, SD, SE, SG, SK, SL, SM, ST, SV, SY, TH, TJ, TM, TN, TR, TT, TZ, UA, UG, US, UZ, VC, VN, ZA, ZM, ZW.

(84) Designated States *(unless otherwise indicated, for every kind of regional protection available)*: ARIPO (BW, GH, GM, KE, LR, LS, MW, MZ, NA, RW, SD, SL, SZ, TZ, UG, ZM, ZW), Eurasian (AM, AZ, BY, KG, KZ, RU, TJ, TM), European (AL, AT, BE, BG, CH, CY, CZ, DE, DK, EE, ES, FI, FR, GB, GR, HR, HU, IE, IS, IT, LT, LU, LV, MC, MK, MT, NL, NO, PL, PT, RO, RS, SE, SI, SK, SM, TR), OAPI (BF, BJ, CF, CG, CI, CM, GA, GN, GQ, GW, ML, MR, NE, SN, TD, TG).

Published:

— *without international search report and to be republished upon receipt of that report (Rule 48.2(g))*

WO 2012/174344 A2

(54) Title: NON-PGM CATHODE CATALYSTS FOR FUEL CELL APPLICATION DERIVED FROM HEAT TREATED HETEROATOMIC AMINES PRECURSORS

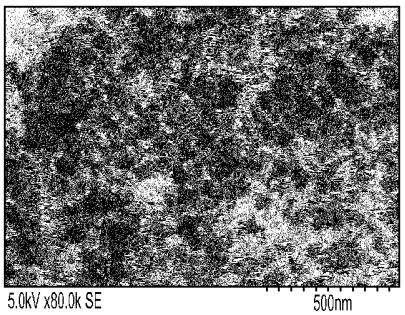

FIG. 2

(57) Abstract: A method of preparing M-N-C catalysts utilizing a sacrificial support approach and inexpensive and readily available polymer precursors as the source of nitrogen and carbon is disclosed. Exemplary polymer precursors include non-porphyrin precursors with no initial catalytic activity. Examples of suitable non-catalytic non-porphyrin precursors include, but are not necessarily limited to low molecular weight precursors that form complexes with iron such as 4-aminoantipirine, phenylenediamine, hydroxysuccinimide, ethanolamine, and the like.

NON-PGM CATHODE CATALYSTS FOR FUEL CELL APPLICATION DERIVED FROM HEAT TREATED HETEROATOMIC AMINES PRECURSORS

Cross-reference to Related Applications

[001] The following application claims benefit of U.S. Provisional Application Nos. 61/497,444, filed June 15, 2011, 61/606,109, filed March 2, 2012, 61/621084, filed April 6, 2012 and 61/621,095, filed April 6, 2012, each of which is hereby incorporated by reference in its entirety.

Background

[002] Fuel cells are receiving increasing attention as a viable energy-alternative. In general, fuel cells convert electrochemical energy into electrical energy in an environmentally clean and efficient manner. Fuel cells are contemplated as potential energy sources for everything from small electronics to cars and homes. In order to meet different energy requirements, there are a number of different types of fuel cells in existence today, each with varying chemistries, requirements, and uses.

[003] As one example, Direct Methanol Fuel Cells (DMFCs) rely upon the oxidation of methanol on an electrocatalyst layer to form carbon dioxide. Water is consumed at the anode and produced at the cathode. Positive ions (H+) are transported across a proton exchange membrane to the cathode where they react with oxygen to produce water. Electrons can then be transported via an external circuit from anode to cathode providing power to external sources.

[004] As another example, polymer electrolyte membrane (PEM) fuel cells (also called proton exchange membrane fuel cells) use pure hydrogen (typically supplied by a hydrogen tank) as a fuel. A stream of hydrogen is delivered to the anode side of a membrane-electrode assembly (MEA), where it is catalytically split into protons and electrons. As with the DMFC, the positive ions are transported across a proton exchange membrane to the cathode where they react with oxygen to produce water.

[005] Currently, one of the limiting factors in the wide scale commercialization of PEM and DMFC fuel cells is the cost associated with precious metals. Both DMFC and PEM fuel cells commonly use platinum as an electrocatalyst. Nobel metals such as platinum are needed to catalyze the sluggish oxygen reduction reaction (ORR) at the cathode. One of the major routes to overcome this limitation is to increase the platinum utilization in noble-metal based electrocatalysts. Another viable route is to use a less expensive, yet still sufficiently active catalyst in larger quantities. Several classes of non-platinum electrocatalysts have been

identified as having adequate oxygen reduction activity to be considered as potential electrocatalysts in commercial fuel cell applications.

[006] Generally, known non-platinum electrocatalysts are supported on high surface area carbon blacks. This is done to increase dispersion, active surface area, and conductivity of the catalytic layer. The synthesis procedure usually includes precipitation of the precursor molecules onto the supporting substrate and pyrolyzation of the supported precursor.

[007] M-N-C catalysts have been found to be very promising for electrochemical oxygen reduction applications in fuel cell membrane electrode assemblies (MEAs), stacks and fuel cell systems. Critical aspects of the materials include the presence of metallic particles, conjugated carbon-nitrogen-oxide-metallic networks, and nitrogen-bonded carbon. The metallic phase includes metallic, oxide, carbide, nitride, and mixtures of these states. The chemical states and bonding of the N/C/M networks and N/C networks influences performance, for example, increased overall nitrogen content improves ORR performance. However, these systems still suffer from several significant drawbacks including: low stability in acidic environments, low durability in acid and alkaline environments, high costs of nitrogen precursors and low activity in ORR compared with platinum. The problem of low stability in acid is connected to leaching of metal from carbon-nitrogen network. Low durability in acid and alkaline solutions is explained by the evolution of significant amount of H_2O_2 in these environments which is corrosive for both metal and carbon-nitrogen networks. The low activity is possibly due to the low metal loading, and as a result in low concentration of active sites in such catalysts due to using external carbon source (high surface carbons like Vulcan, KetjenBlack etc).

[008] A previously described pyrolysis-based methods for synthesizing unsupported M-N-C catalysts that overcame a number of the problems identified above involved templating a nitrogen and carbon containing porphyrins that are known to have some initial catalytic activity on a sacrificial support such as silica, pyrolyzing the templated support, and then removing the support, for example via etching. See e.g., U.S. Patent No. 7,678,728 issued March 15, 2010, which is hereby incorporated by reference.

Summary

[009] The M-N-C systems are known catalysts for oxygen reduction reaction (ORR). However, they possess a number of significant disadvantages including: low stability in acid media, low activity compared to conventional ORR catalyst (platinum), and high cost of precursors. In the present disclosure a method of preparation of M-N-C catalysts utilizing a sacrificial support approach and using inexpensive and readily available polymer precursors

is described. The synthesized catalysts made using this approach perform well in both alkaline and acid media are highly durable, and inexpensive to manufacture.

Brief Description of the Drawings

[010] Fig. 1 is an X-ray diffractogram of an Fe-M-C catalyst prepared as described herein.

[011] Fig. 2 is an SEM image of Fe-AApyr catalysts prepared using the methods described herein.

[012] Fig. 3 is a Rotating Disc Electrode electro-voltamogram illustrating oxygen reduction for Fe-AApyr catalysts prepared using the methods described herein.

[013] Fig. 4 is a Rotating Disc Electrode electro-voltamogram illustrating oxygen reduction for Fe-AAPyr prepared with a variety of heat treatment temperatures.

[014] Fig. 5 is a graph of the number of electrons participating in ORR for a variety Fe-AAPyr catalysts prepared as described herein.

[015] Fig. 6 is a graph of hydrogen peroxide yield for a variety of Fe-AAPyr catalysts prepared as described herein.

[016] Fig. 7 is a graph of the number of electrons participating in ORR for Fe-AAPyr catalysts prepared as described herein.

[017] Fig. 8 is a graph of hydrogen peroxide yield for a variety of Fe-AAPyr catalysts prepared as described herein.

[018] Fig. 9 is a schematic illustration of a method for producing catalysts having a multimodal pore size distribution, as described herein.

[019] Fig. 10A is an SEM image of a mono-modal catalyst derived from Fe-AAPyr and HS5 silica with a scale bar at 500nm.

[020] Fig. 10B is an SEM image of a mono-modal catalyst derived from Fe-AAPyr and HS5 silica with a scale bar at 300nm.

[021] Fig. 11A is an SEM image of a bi-modal catalyst derived from Fe-AAPyr and M5 silica with a scale bar at 500nm.

[022] Fig. 11B is an SEM image of a bi-modal catalyst derived from Fe-AAPyr and M5 silica with a scale bar at 300nm.

[023] Fig. 12A is an SEM image of a bi-modal catalyst derived from Fe-AAPyr and LM130 silica with a scale bar at 500nm.

[024] Fig. 12B is an SEM image of a bi-modal catalyst derived from Fe-AAPyr and LM130 silica with a scale bar at 300nm.

[025] Fig. 13A is an SEM image of a catalyst derived from Fe-AAPyr and A90 silica with a scale bar at 500nm.

[026] Fig. 13B is an SEM image of a catalyst derived from Fe-AAPyr and A90 silica with a scale bar at 300nm.

[027] Fig. 14 is an SEM image of a bi-modal catalyst derived from Fe-AAPyr and mixture of L90 and A90 silicas.

[028] Fig. 15A is an SEM image of a tri-modal catalyst derived from Fe-AAPyr and mixture of L90 and EH5 silicas with a scale bar at 500nm.

[029] Fig. 15B is an SEM image of a tri-modal catalyst derived from Fe-AAPyr and mixture of L90 and EH5 silicas with a scale bar at 400nm.

[030] Fig. 15C is an SEM image of a tri-modal catalyst derived from Fe-AAPyr and mixture of L90 and EH5 silicas with a scale bar at 300nm.

[031] Fig. 16 is an SEM image of a bi-modal catalyst derived from Fe-AAPyr and mixture of L90 and M5 silicas with a scale bar at 500nm.

[032] Fig. 17 is an SEM image of a bi-modal catalyst derived from Fe-AAPyr and mixture of L90 and LM130 silicas with a scale bar at 500nm.

[033] Fig. 18 is an SEM image of a bi-modal catalyst derived from Fe-AAPyr and mixture of L90 and A200 silicas.

[034] Fig. 19 is an SEM image of a bi-modal catalyst derived from Fe-AAPy and mixture of L90 and A380 silicas.

[035] Fig. 20A is an SEM image of a spherical catalyst derived from Fe-AAPyr and M5 silica.

[036] Fig. 20B is another SEM image of a spherical catalyst derived from Fe-AAPyr and M5 silica.

[037] Fig. 20C is another SEM image of a spherical catalyst derived from Fe-AAPyr and M5 silica.

[038] Fig. 20E is another SEM image of a spherical catalyst derived from Fe-AAPyr and M5 silica.

[039] Fig. 21 is a Rotating Disc Electrode electro-voltamogram illustrating oxygen reduction for RDE data for catalysts prepared from Fe-AAPyr and HS5, L90 and L90 + EH5 silicas.

[040] Fig 22 is a Rotating Disc Electrode electro-voltamogram illustrating oxygen reduction for RDE data for catalysts prepared from Fe-AAPyr and L90, LM130, and L90 + LM130 silicas.

[041] Fig. 23 is a Rotating Disc Electrode electro-voltamogram illustrating oxygen reduction for RDE data for catalysts prepared from Fe-AAPyr and L90, L90 + A90, and A90 silicas.

[042] Fig. 24 is a Rotating Disc Electrode electro-voltamogram illustrating oxygen reduction for RDE data for catalysts prepared from Fe-AAPyr and L90 and L90 + EH5 silicas.

[043] Fig. 25 is a Rotating Disc Electrode electro-voltamogram illustrating oxygen reduction for RDE data for catalysts prepared from Fe-AAPyr and L90, M5 and L90 + M5 silicas.

[044] Fig. 26 is an SEM image of Fe_3Co-AAPyr catalyst prepared using the methods described herein.

[045] Fig 27 is an SEM image of FeCo-AAPyr catalyst prepared using the methods described herein.

[046] Fig. 28 is an SEM image of $FeCo_3$-AAPyr catalyst prepared using the methods described herein.

[047] Fig. 29A is an SEM image of $FeCu_3$-AAPyr bi-metallic catalyst prepared using the methods described herein.

[048] Fig. 29B is another SEM image of $FeCu_3$-AAPyr bi-metallic catalyst prepared using the methods described herein.

[049] Fig. 30A is an SEM image of $FeMn_3$-AAPyr bi-metallic catalyst prepared using the methods described herein.

[050] Fig. 30B is another SEM image of $FeMn_3$-AAPyr bi-metallic catalyst prepared using the methods described herein.

[051] Fig. 31A is an SEM image of $FeNi_3$-AAPyr bi-metallic catalyst prepared using the methods described herein.

[052] Fig. 31B is another SEM image of $FeNi_3$-AAPyr bi-metallic catalyst prepared using the methods described herein.

[053] Fig. 32A is an SEM image of FeCoCu-AAPyr tri-metallic catalyst prepared using the methods described herein.

[054] Fig. 32B is another SEM image of FeCoCu-AAPyr tri-metallic catalyst prepared using the methods described herein.

[055] Fig. 33A is an SEM image of FeCoMn-AAPyr tri-metallic catalyst prepared using the methods described herein.

[056] Fig. 33B is another SEM image of FeCoMn-AAPyr tri-metallic catalyst prepared using the methods described herein.

[057] Fig. 34A is an SEM image of FeCuMn-AAPyr tri-metallic catalyst prepared using the methods described herein.

[058] Fig. 34B is another SEM image of FeCuMn-AAPyr tri-metallic catalyst prepared using the methods described herein.

[059] Fig. 35 is a Rotating Disc Electrode electro-voltamogram illustrating oxygen reduction for Fe_xCo_y-AAPyr bi-metallic catalysts compared to Co-AAPyr.

[060] Fig. 36 is a Rotating Disc Electrode electro-voltamogram illustrating oxygen reduction for Fe_xNi_y-AAPyr bi-metallic catalysts compared to Ni-AAPyr.

[061] Fig. 37 is a Rotating Disc Electrode electro-voltamogram illustrating oxygen reduction for Fe_xCu_y-AAPyr bi-metallic catalysts compared to Cu-AAPyr.

[062] Fig. 38 is a Rotating Disc Electrode electro-voltamogram illustrating oxygen reduction for Fe_xCr_y-AAPyr bi-metallic catalysts compared to Cr-AAPyr.

[063] Fig. 39 is a Rotating Disc Electrode electro-voltamogram illustrating oxygen reduction for Fe_xMn_y-AAPyr bi-metallic catalysts compared to Mn-AAPyr.

[064] Fig 40 is a Rotating Disc Electrode electro-voltamogram illustrating oxygen reduction for FeM^IM^{II}-AAPyr tri-metallic catalysts.

[065] Fig. 41 is a schematic illustration of a batch-wise process for producing M-N-C catalysts according to the present disclosure.

[066] Fig. 42A is an SEM image of spherical, highly porous Fe-N-C catalysts prepared on low surface area silica with a scale bar at 10μm.

[067] Fig. 42B is an SEM image of spherical, highly porous Fe-N-C catalysts prepared on low surface area silica with a scale bar at 2μm.

[068] Fig. 42C is an SEM image of spherical, highly porous Fe-N-C catalysts prepared on low surface area silica with a scale bar at 1μm.

[069] Fig. 42D is an SEM image of spherical, highly porous Fe-N-C catalysts prepared on low surface area silica with a scale bar at 500nm.

[070] Fig. 43A is an SEM image of a first batch of spherical, highly porous Fe-N-C catalysts prepared on high surface area silica with a scale bar of 5μm.

[071] Fig. 43B is an SEM image of the first batch of spherical, highly porous Fe-N-C catalysts prepared on high surface area silica with a scale bar of 2μm.

[072] Fig. 43C is an SEM image of the first batch of spherical, highly porous Fe-N-C catalysts prepared on high surface area silica with a scale bar of 500nm.

[073] Fig. 44A is an SEM image of a second batch of spherical, highly porous Fe-N-C catalysts prepared on high surface area silica with a scale bar of 3μm.

[074] Fig. 44B is an SEM image of a second batch of spherical, highly porous Fe-N-C catalysts prepared on high surface area silica with a scale bar of 2μm.

[075] Fig. 45 is a Rotating Disc Electrode electro-voltamogram illustrating oxygen reduction for RDE data for spherical F-N-C catalysts prepared by the presently described method in 0.5M H_2SO_4 saturated with O_2 (catalysts loading: 600 μg cm^{-2}, 1200RPM, 5mV s^{-1}).

Detailed Description

[076] According to an embodiment the present disclosure provides novel catalysts and methods for making the same. In previously described methods for forming M-N-C catalysts, the source of nitrogen and carbon is typically a porphyrin precursor having an initial catalytic activity. This initial catalytic activity is them improved upon by complexing with metallic particles. The present disclosure relies on the surprising and unexpected discovery that M-N-C catalysts can be synthesized by using non-porphyrin precursors with no initial catalytic activity, as the source of nitrogen and carbon. Examples of suitable non-catalytic non-porphyrin precursors include, but are not necessarily limited to low molecular weight precursors that form complexes with iron such as 4-aminoantipirine, phenylenediamine, hydroxysuccinimide, ethanolamine, and the like. According to some embodiments, the non-catalytic precursors may be selected due to their ability to complex with iron. According to yet other embodiments, the non-catalytic precursors may be selected because they contain moieties that are the same or similar to the active sites in precursors that have initial catalytic activity, the crystal structure of which is then stabilized by means of high temperature heat treatment.

[077] According to an embodiment, an M-N-C catalyst according to the present disclosure may be prepared via wet impregnation of iron precursors in the form of iron nitrate and C-N precursors in the form of 4-aminoantipirine (AAPyr) onto the surface of a sacrificial support of fumed silica. Other suitable iron precursors include, but are not limited to iron sulfate, iron acetate, iron chloride etc.

[078] It will be appreciated that other transition metals such as Ce, Cr, Cu Mo, Ni, Ru, Ta, Ti, V, W, and Zr can be substituted in place of iron, by simply using precursors of those metals instead. Examplary transition metal precursors include, but are not limited to cerium nitrate, chromium nitrate, copper nitrate, ammonium molybdate, nickel nitrate, ruthenium chloride, tantalum isopropoxide, titanium ethoxide, vanadium sulfate, ammonium tunstanate and zirconium nitrate. Furthermore, according to some embodiments and as described in greater detail below, the presently described methodologies may utilize precursors of two or more metals to produce multi-metallic catalysts.

[079] Suitable sacrificial supports include, but are not limited to silicas, zeolites, aluminas, and the like. The support may take the form of spheres, particles, or other two or three dimensional regular, irregular, or amorphous shapes. The spheres, particles, or other shapes may be monodisperse, or irregularly sized. The spheres, particles, or other shapes may or may not have pores and such pores may be of the same or different sizes and shapes.

[080] It should be appreciated, and as described in greater detail below, the size and shape of the silica particles may be selected according to the desired shape(s) and size(s) of the voids within the electrocatalyst material. Accordingly, by selecting the particular size and shape of silica particles, one can produce a electrocatalyst having voids of a predictable size and shape. For example, if the silica particles are spheres, the electrocatalyst will contain a plurality of spherical voids. Those of skill in the art will be familiar with the electrocatalyst Pt-Ru black, which consists of a plurality of platinum-ruthenium alloy spheres. An electrocatalyst formed from using silica spheres with the above-described method looks like a negative image of the Pt-Ru black; the space that existed as a void in the Pt-Ru black is filled with metal electrocatalyst, and the space that existed as metal electrocatalyst in the Pt-Ru black is void.

[081] As stated above, according to some embodiments, silica spheres of any diameter may be used. In some preferred embodiments, silica particles having an characteristic lengths of between 1 nm and 100 nm, in more preferred embodiments, silica particles having an characteristic lengths of between 100 nm and 1000 nm may be used and in other preferred embodiments, silica particles having an characteristic lengths of between 1 mm and 10 mm may be used. Further mesoporous silica can also be used in the templating synthesis approach. In this case the templating involves intercalating the mesopores of the material and results in a self-supported electrocatalysts with porosity in the 2-20 nm range. In one particular embodiment, the silica template is Cabosil amorphous fumed silica (325 m^2/g). As stated above, because the spheres serve as the template for the formation of the electrocatalyst, in an embodiment where silica particles having an average diameter of 20 nm is used, the spherical voids in the electrocatalyst will typically have a diameter of approximately 20 nm. Those of skill in the art will be familiar with a variety of silica particles that are commercially available, and such particles may be used. Alternatively, known methods of forming silica particles may be employed in order to obtain particles of the desired shape and/or size.

[082] After deposition and/or impregnation of the C-N and metal precursors on the sacrificial support, the catalysts is heat treated either in an inert atmosphere such as N_2, Ar, or He, or in a reactive atmosphere such as NH_3 or acetonitrile. Inert atmospheres are typically

used when the C-N precursor is nitrogen rich, as the inert atmosphere enables the production of a high number of active sites with Fe (or other metal) N4 centers. However, it may be desired to use a nitrogen rich atmosphere if the C-N precursor is rich in carbon and depleted in nitrogen, as the nitrogen rich atmosphere will enable production of the Fe (or other metal) N4 centers.

[083] According to an embodiment, optimal temperatures for heat treatment are between 500 and 1100°C. According to some embodiments, heat treatment between 800 and 900 °C is preferred, as this temperature is high enough to pyrolize the material, but is typically not high enough to destroy the active sites.

[084] After heat treatment, the sacrificial support is removed using suitable means. For example, the sacrificial support may be removed via chemical etching. Examples of suitable etchants include NaOH, KOH, and HF. According to some embodiments, it may be preferable to use KOH, as it preserves all metal and metal oxide in the catalyst and, if the species are catalytically active, use of KOH may, in fact, increase catalytic activity. Alternatively, in some embodiments, HF may be preferred as it is very aggressive and can be used to remove some poisonous species from the surface of the catalyst. Accordingly, those of skill in the art will be able to select the desired etchants based on the particular requirements of the specific catalytic material being formed.

[085] According to a specific exemplary embodiment, Fe-AAPyr catalysts were prepared via wet impregnation of iron and aminoantipyrine precursors onto the surface of fumed silica (Cab-O-Sil™ EH-5, surface area: ~400 m^2 g^{-1}). First, 1g of silica was dispersed in water using the sonobath. Then, a solution of 1g of AAPyr in water was added to the silica, and sonicated for 20 minutes. Then, an aqueous solution of 1g iron nitrate ($Fe(NO_3)_3 \bullet 9H_2O$, Sigma-Aldrich) was added to the SiO_2-AAPyr solution and then sonicated for 8 hours in the sonobath. After sonication, a viscous solution of silica and Fe-AApyr was dried overnight at T=85 °C. The solid was ground to a fine powder in an agate mortar, and then subjected to the heat treatment (HT). The conditions of HT were: UHP N_2 atmosphere flowing at a rate of 100 cc min^{-1}, HT temperatures of 800°C, HT temperature ramp rates of 10°C min^{-1}, and HT durations of 1 hour.

[086] Figs. 1-2 illustrate structural and morphological data for selected M-N-C catalysts prepared using the methods described herein.

[087] Fig. 1 is an X-ray diffractogram illustrating that the Fe-M-C catalyst prepared from iron nitrate as a metal source and AAPyr as a source of nitrogen and carbon mainly consists of nanoparticles (less than 2nm) of iron imbedded into a carbon matrix.

[088] Fig. 2 is an SEM image of Fe-AApyr catalysts prepared using the methods described herein illustrating that this material possesses a highly developed porous structure with pore size of about 50-70nm. The porosity is thought to improve catalytic properties towards oxygen reduction.

[089] Figs. 3 and 4 show the results of oxygen reduction tests and thus demonstrate the utility of the materials described herein.

[090] Fig. 3 is a Rotating Disc Electrode electro-voltamogram illustrating oxygen reduction for Fe-AApyr catalysts prepared with different amounts of aminoantipiryne precursor in 0.5M H_2SO_4 saturated with O_2 (catalyst loading 160 mg cm^{-2}, 1600 RPM, scan rate 20mV s^{-1}).

[091] Fig. 4 is a Rotating Disc Electrode electro-voltamogram illustrating oxygen reduction for Fe-AAPyr prepared with a variety of heat treatment temperatures in 0.5M H_2SO_4 saturated with O_2 (catalyst loading: 160 mg cm^{-2}, 1600 RPM, scan rate 20mV s^{-1})

[092] The reaction tests demonstrate that M-N-C catalysts prepared using inexpensive heteroatomic amines precursors and the methods disclosed herein, possess high activity in both alkaline and acid media, and should therefore also be active in neutral pH.

[093] Figs. 5-8 illustrate mechanistic studies of the catalysts prepared as described herein and show low H_2O_2 production yield, thus indicating a reaction pathway that proceeds via the more efficient 4 electron mechanism.

[094] Fig. 5 is a graph of the number of electrons participating in ORR for Fe-AAPyr catalysts, with variation of the amount of aminoantipiryen precursor in 0.5M H_2SO_4 saturated with O_2 (catalyst loading: 160mg cm^{-2}, 1600RPM, 20mV s^{-1})

[095] Fig. 6 is a graph of hydrogen peroxide yield for Fe-AAPyr catalysts prepared with different amounts of aminoantipiryen precursor in 0.5M H_2SO_4 saturated with O_2 (catalyst loading: 160mg cm^{-2}, 1600RPM, 20mV s^{-1}).

[096] Fig. 7 is a graph of the number of electrons participating in ORR for Fe-AAPyr catalysts prepared with variation of heat treatment temperature in 0.5M H_2SO_4 saturated with O_2 (catalyst loading: 160mg cm^{-2}, 1600RPM, 20mV s^{-1})

[097] Fig. 8 is a graph of hydrogen peroxide yield for Fe-AAPyr prepared with variation of heat treatment temperature in 0.5M H_2SO_4 saturated with O_2 (catalyst loading: 160mg cm^{-2}, 1600RPM, 20mV s^{-1}).

[098] As stated above, the mechanism of oxygen reduction shows the direct reduction of oxygen to water by the preferred 4 electron pathway, thus avoiding corrosive peroxide production and therefore improving the stability and durability of the resulting catalysts.

[099] As demonstrated in Figs. 3, 5, and 6, the properties of the resulting catalyst can be varied by selecting the amount of nitrogen-containing precursor to use in the preparation method. In general, the higher concentration of nitrogen in the catalyst, the higher the activity in ORR. Furthermore, as demonstrated in Figs. 4, 7 and 8, the properties of the catalysts can also be altered by varying the heat treatment temperature. It will be appreciated that it is desirable to optimize the heat treatment temperature for each combination of transition metals and C-N precursors, as too low a temperature will not create active sites, and too high a temperature will decompose the materials.

[0100] As mentioned above, the presently described methods can be used to produce catalysts from non-iron metals such as Co, Ni, Cu, Cr, Mn, and the like.

[0101] As a specific non-limiting example, Fe-AAPyr catalysts were prepared via wet impregnation of iron and aminoantipyrine precursors onto the surface of fumed silica (Cab-O-Sil™ EH-5, surface area: ~400 m^2 g^{-1}). First, 1g of silica was dispersed in water using the sonobath. Then, a solution of 1g of AAPyr in water was added to the silica, and sonicated for 20 minutes. Then, an aqueous solution of 1g iron nitrate ($Fe(NO_3)_3 \bullet 9H_2O$, Sigma-Aldrich) was added to the SiO_2-AAPyr solution and then sonicated for 8 hours in the sonobath. After sonication, a viscous solution of silica and Fe-AApyr was dried overnight at T=85 °C. The solid was ground to a fine powder in an agate mortar, and then subjected to the heat treatment (HT). The conditions of HT were: UHP N_2 atmosphere flowing at a rate of 100 cc min^{-1}, HT temperatures of 800°C, HT temperature ramp rates of 10°C min^{-1}, and HT durations of 1 hour.

[0102] According to yet another non-limiting example, Fe-Mn-AAPyr catalysts were prepared via wet impregnation of iron, manganese and aminoantipyrine precursors onto the surface of fumed silica (Cab-O-Sil™ EH-5, surface area: ~400 m^2 g^{-1}). First, 3g of silica was dispersed in water using the sonobath. Then, a solution of 1.98g of AAPyr in water was added to silica, and sonicated for 20 minutes. Then, an aqueous solution of 1.4g iron nitrate ($Fe(NO_3)_3 \bullet 9H_2O$, Sigma-Aldrich) and 3.2g of manganese nitrate were added to the SiO_2-AAPyr solution and then sonicated for 8 hours in the sonobath. After sonication, a viscous solution of silica and Fe-Mn-AApyr was dried overnight at T=85 °C. The solid was ground to a fine powder in an agate mortar, and then subjected to the heat treatment (HT). The conditions of HT were: UHP N_2 atmosphere flowing at a rate of 100 cc min^{-1}, HT temperatures of 800°C, HT temperature ramp rates of 10°C min^{-1}, and HT durations of 1 hour.

[0103] According to still another non-limiting embodiment, Fe-Cr-AAPyr catalysts were prepared via wet impregnation of iron and aminoantipyrine precursors onto the surface of

fumed silica (Cab-O-Sil™ EH-5, surface area: ~400 m^2 g^{-1}). First, 2g of silica was dispersed in water using the sonobath. Then, a solution of 3.5g of AAPyr in water was added to the silica, and sonicated for 20 minutes. Then, an aqueous solution of 1g iron nitrate ($Fe(NO_3)_3 \bullet 9H_2O$, Sigma-Aldrich) and 1.25g of chromium nitrate were added to the SiO_2-AAPyr solution and then sonicated for 8 hours in the sonobath. After sonication, a viscous solution of silica and Fe-AApyr was dried overnight at T=85 °C. The solid was ground to a fine powder in an agate mortar, and then subjected to the heat treatment (HT). The conditions of HT were: UHP N_2 atmosphere flowing at a rate of 100 cc min^{-1}, HT temperatures of 850°C, HT temperature ramp rates of 10°C min^{-1}, and HT durations of 4 hour.

[0104] According to embodiment, the M-N-C catalysts described herein can be deposited onto conductive dispersed supports (both carbon and non-carbon) in a fashion that facilitates the charge transfer of the heteroatom atom and the support. According to some embodiments, usage of non-carbon support, like conductive Mo or W oxides can significantly decrease hydrogen peroxide production, increase durability and stability of catalysts in acid and alkaline media.

[0105] As described above, sacrificial supports of different sizes and shapes may be used together to produce catalysts having a variety of different morphologies. For example, in some embodiments it may be desirable to produce catalysts having multi-modal porosity, that is, where the catalyst comprises two or more distinct populations of pores, wherein each population consists of pores having an average diameter that is differentiable from the other population(s). For example, a catalyst that has one population of pores with an average diameter of approximately 10nm, a second population of pores with an average diameter of approximately 50nm and a third population of pores with an average diameter of between 150-200 nm would be considered to have a multi-modal pore size distribution.

[0106] Turning to Fig. 9, according to an embodiment, such multi-modal pore size distribution could be produced by templating the above-described precursors onto sacrificial supports formed from spheres (or otherwise shaped particles) having different diameters. As shown, larger spheres 10 having a diameter d1 and smaller spheres 12 having a diameter d2 are mixed together to form a sacrificial support on which the precursor materials are deposited and pyrolized. Once the support is removed, the resulting catalytic material 16 contains differently sized pores 18, 20 corresponding to the different particle diameters.

[0107] It will be appreciated that in order to have complete control over the morphology of the resulting catalytic material, it will be desirable to template the precursors into sacrificial supports with known shapes and sizes. According to a particular embodiment where the sacrificial support is formed from silica particles, the different shapes and sizes of sacrificial

supports may be produced by using different types of silica to reliably and reproducibly produce differently sized silica particles. The resulting catalysts will then have a multi-modal pore distribution, where the specific size and shape of the pores is known.

[0108] According to a specific example, a catalyst as described herein formed on EH5 and LM130 silica was prepared via wet impregnation of iron and aminoantipyrine precursors onto the surface of different fumed silicas and their mixtures (Cab-O-Sil™ surface areas 90-400 m^2 g^{-1}). First, 1g of silica EH5 and 1g of silica LM130 were dispersed in water using the sonobath. Then, a solution of 1g of AAPyr in water was added to silica, and sonicated for 20 minutes. Then, an aqueous solution of 1g iron nitrate ($Fe(NO_3)_3 \bullet 9H_2O$, Sigma-Aldrich) was added to the SiO_2-AAPyr solution and then sonicated for 8 hours in the sonobath. After sonication, a viscous solution of silica and Fe-AApyr was dried overnight at T=85 °C. The solid was ground to a fine powder in an agate mortar, and then subjected to the heat treatment (HT). The conditions of HT were: UHP N_2 atmosphere flowing at a rate of 100 cc min^{-1}, HT temperatures of 800°C, HT temperature ramp rates of 10°C min^{-1}, and HT durations of 1 hour.

[0109] According to yet another specific example, a catalyst as described herein formed on M5D and A90 silica was prepared via wet impregnation of iron and aminoantipyrine precursors onto the surface of different fumed silicas and their mixtures (Cab-O-Sil™ surface areas 90-400 m^2 g^{-1}). First, 2g of silica M5D and 0.25g of silica A90 were dispersed in water using the sonobath. Then, a solution of 1.3g of AAPyr in water was added to silica, and sonicated for 20 minutes. Then, an aqueous solution of 4g iron nitrate ($Fe(NO_3)_3 \bullet 9H_2O$, Sigma-Aldrich) was added to the SiO_2-AAPyr solution and then sonicated for 8 hours in the sonobath. After sonication, a viscous solution of silica and Fe-AApyr was dried overnight at T=85 °C. The solid was ground to a fine powder in an agate mortar, and then subjected to the heat treatment (HT). The conditions of HT were: UHP N_2 atmosphere flowing at a rate of 100 cc min^{-1}, HT temperatures of 800°C, HT temperature ramp rates of 10°C min^{-1}, and HT durations of 1 hour.

[0110] Figs. 10-20 depict the morphological data for a various M-N-C catalysts having multi-modal porosity and prepared as described herein.

[0111] Fig. 10 is an SEM image of a mono-modal catalyst derived from Fe-AAPyr and HS5 silica. It can be seen that pore size is in the range of 40-60nm.

[0112] Fig. 11 is an SEM image of a bi-modal catalyst derived from Fe-AAPyr and M5 silica. It can be seen that first type of pores have diameter 40-60nm, while second type of pores have diameter <10nm.

[0113] Fig. 12 is an SEM image of a bi-modal catalyst derived from Fe-AAPyr and LM130 silica. It can be seen that first type of pores have diameter ~100nm, while second type of pores have diameter ~30nm.

[0114] Fig. 13 is an SEM image of a catalyst derived from Fe-AAPyr and A90 silica. It can be seen that pores have diameter ~30nm, while there is also nano-channels with diameter 40-60nm.

[0115] Fig. 14 is an SEM image of a bi-modal catalyst derived from Fe-AAPyr and mixture of L90 and A90 silicas. It can be seen that first type of pores have diameter ~150nm, while second type of pores have diameter ~20nm.

[0116] Fig. 15 is an SEM image of a tri-modal catalyst derived from Fe-AAPyr and mixture of L90 and EH5 silicas. It can be seen that first type of pores have diameter ~150-200nm, second type of pores have diameter ~40-60nm, and third is about 20nm.

[0117] Fig. 16 is an SEM image of a bi-modal catalyst derived from Fe-AAPyr and mixture of L90 and M5 silicas. It can be seen that first type of pores have diameter ~100nm, while second type of pores have diameter ~25nm.

[0118] Fig. 17 is an SEM image of a bi-modal catalyst derived from Fe-AAPyr and mixture of L90 and LM130 silicas. It can be seen that first type of pores have diameter ~150-200nm, while second type of pores have diameter ~30nm.

[0119] Fig. 18 is an SEM image of a bi-modal catalyst derived from Fe-AAPyr and mixture of L90 and A200 silicas. It can be seen that first type of pores have diameter ~100-200nm, while second type of pores have diameter ~50nm.

[0120] Fig. 19 is an SEM image of a bi-modal catalyst derived from Fe-AAPy and mixture of L90 and A380 silicas. It can be seen that first type of pores have diameter ~100nm, while second type of pores have diameter <20nm.

[0121] Fig. 20 is an SEM image of a spherical catalyst derived from Fe-AAPyr and M5 silica. It can be seen that spheres of catalyst are in the range of 1-3μm, while pores have diameter about 50-70nm.

[0122] Figs. 21-25 show the results of oxygen reduction tests on a selection of the multi-modal catalysts in Figs. 10-20 and thus demonstrate the utility of the materials described herein.

[0123] Fig. 21 is a Rotating Disc Electrode electro-voltamogram illustrating oxygen reduction for RDE data for catalysts prepared from Fe-AAPyr and HS5, L90 and L90 + EH5 silicas in 0.5M H_2SO_4 saturated with O_2 (catalysts loading: 600 mg cm^{-2}, 1200RPM, 5mV s^{-1}).

[0124] Fig 22 is a Rotating Disc Electrode electro-voltamogram illustrating oxygen reduction for RDE data for catalysts prepared from Fe-AAPyr and L90, LM130, and L90 + LM130 silicas in 0.5M H_2SO_4 saturated with O_2 (catalysts loading: 600 mg cm^{-2}, 1200RPM, 5mV s^{-1}).

[0125] Fig. 23 is a Rotating Disc Electrode electro-voltamogram illustrating oxygen reduction for RDE data for catalysts prepared from Fe-AAPyr and L90, L90 + A90, and A90 silicas in 0.5M H_2SO_4 saturated with O_2 (catalysts loading: 600 mg cm^{-2}, 1200RPM, 5mV s^{-1}).

[0126] Fig. 24 is a Rotating Disc Electrode electro-voltamogram illustrating oxygen reduction for RDE data for catalysts prepared from Fe-AAPyr and L90 and L90 + EH5 silicas in 0.5M H_2SO_4 saturated with O_2 (catalysts loading: 600 mg cm^{-2}, 1200RPM, 5mV s^{-1}).

[0127] Fig. 25 is a Rotating Disc Electrode electro-voltamogram illustrating oxygen reduction for RDE data for catalysts prepared from Fe-AAPyr and L90, M5 and L90 + M5 silicas in 0.5M H_2SO_4 saturated with O_2 (catalysts loading: 600 mg cm^{-2}, 1200RPM, 5mV s^{-1}).

[0128] It will be appreciated that some in some applications a mono-metallic catalyst may not be sufficiently stable or active to replace traditional platinum- or platinum alloy- based catalysts. Accordingly, as indicated above, according to some embodiments, the presently described method may incorporate the use of precursors of multiple metals in order to achieve a desired stability and/or activity.

[0129] According to various specific embodiments, Fe-AAPyr catalysts were prepared via wet impregnation of iron and second transition metal, or iron, second and third transition metal (transition metals=Co, Ni, Cu, Cr and Mn) and aminoantipyrine precursors onto the surface of fumed silica (Cab-O-Sil™ EH-5, surface area: ~400 m^2 g^{-1}). First, a 1g of silica was dispersed in water using the sonobath. Then, a solution of 1g of AAPyr in water was added to silica, and sonicated for 20 minutes. Then, an aqueous solution of 1g iron nitrate ($Fe(NO_3)_3 \bullet 9H_2O$, Sigma-Aldrich) and 1g of manganese nitrate was added to the SiO_2-AAPyr solution and then sonicated for 8 hours in the sonobath. After sonication, a viscous solution of silica and Fe-Mn-AApyr was dried overnight at T=85 °C. The solid was ground to a fine powder in an agate mortar, and then subjected to the heat treatment (HT). The conditions of HT were: UHP N_2 atmosphere flowing at a rate of 100 cc min^{-1}, HT temperatures of 800°C, HT temperature ramp rates of 10°C min^{-1}, and HT durations of 1 hour.

[0130] Figs. 26-34 illustrate structural and morphological data for selected multi-metallic M-N-C catalyst prepared by the above described methods.

[0131] Figs. 26-28 show three different catalysts Fe_3Co-AAPyr, FeCo-AAPyr and $FeCo_3$-AAPyr, respectively, prepared using the methods described herein. The materials possess a highly developed porous structure with a pore size of about 100nm.

[0132] Figs. 29A and B are SEM images of $FeCu_3$-AAPyr bi-metallic catalyst illustrating that this material possesses a highly developed porous structure with pore size about 70nm.

[0133] Figs. 30A and B are SEM images of $FeMn_3$-AAPyr bi-metallic catalyst illustrating that this material possesses a highly developed porous structure with pore size about 50nm.

[0134] Figs. 31A and B are SEM images of $FeNi_3$-AAPyr bi-metallic catalyst illustrating that this material possesses a highly developed porous structure with pore size about 200nm.

[0135] Figs. 32A and B are SEM images of FeCoCu-AAPyr tri-metallic catalyst illustrating that this material possesses a highly developed porous structure with pore size about 150nm.

[0136] Figs. 33A and B are SEM images of FeCoMn-AAPyr tri-metallic catalyst illustrating that this material possesses a highly developed porous structure with pore size about 100nm.

[0137] Figs. 34A and B are SEM images of FeCuMn-AAPyr tri-metallic catalyst illustrating that this material possesses a highly developed porous structure with pore size about 100nm.

[0138] The utility of the multi-metallic catalysts described herein is demonstrated by the results of oxygen reduction tests illustrated in Figs. 35-40.

[0139] Fig. 35 is a Rotating Disc Electrode electro-voltamogram illustrating oxygen reduction for Fe_xCo_y-AAPyr bi-metallic catalysts compared to Co-AAPyr in 0.5M H_2SO_4 saturated with O_2 (catalyst loading: 600 mg cm^{-2}, 1200RPM, 5mV s^{-1}).

[0140] Fig. 36 is a Rotating Disc Electrode electro-voltamogram illustrating oxygen reduction for Fe_xNi_y-AAPyr bi-metallic catalysts compared to Ni-AAPyr in 0.5M H_2SO_4 saturated with O_2 (catalyst loading: 600 mg cm^{-2}, 1200RPM, 5mV s^{-1}).

[0141] Fig. 37 is a Rotating Disc Electrode electro-voltamogram illustrating oxygen reduction for Fe_xCu_y-AAPyr bi-metallic catalysts compared to Cu-AAPyr in 0.5M H_2SO_4 saturated with O_2 (catalyst loading: 600 mg cm^{-2}, 1200RPM, 5mV s^{-1}).

[0142] Fig. 38 is a Rotating Disc Electrode electro-voltamogram illustrating oxygen reduction for Fe_xCr_y-AAPyr bi-metallic catalysts compared to Cr-AAPyr in 0.5M H_2SO_4 saturated with O_2 (catalyst loading: 600 mg cm^{-2}, 1200RPM, 5mV s^{-1}).

[0143] Fig. 39 is a Rotating Disc Electrode electro-voltamogram illustrating oxygen reduction for Fe_xMn_y-AAPyr bi-metallic catalysts compared to Mn-AAPyr in 0.5M H_2SO_4 saturated with O_2 (catalyst loading: 600 mg cm^{-2}, 1200RPM, 5mV s^{-1}).

[0144] Fig. 40 is a Rotating Disc Electrode electro-voltamogram illustrating oxygen reduction for FeM^IM^{II}-AAPyr tri-metallic catalysts in 0.5M H_2SO_4 saturated with O_2 (catalyst loading: 600 mg cm^{-2}, 1200RPM, 5mV s^{-1}).

[0145] These reaction tests demonstrate that the multi-metallic M-N-C catalysts prepared from inexpensive C-N precursors using the methods described herein possess activity significantly higher than mono-metallic catalysts. Such high activity makes these materials suitable for us in fuel cell applications as cathode catalysts as they possess high activity in ORR in alkaline, neutral, and acid environments.

[0146] According to some embodiments, it may be desirable to produce large amounts of the catalysts described herein, for example in a batch-wise process. Accordingly, the present disclosure further provides a method for large-scale preparation of the presently described catalysts. According to an embodiment, the present disclosure provides a method which combines a sacrificial support-based methodology with spray pyrolysis to produce self-supported catalysts. According to this method, the spray pyrolysis method is a continuous method while the sacrificial support-based methodology is performed batch-wise. Turning to Fig. 41, it can be seen that the precursor materials described above are mixed with a silica support, atomized, and dried in a tube furnace. The powder obtained from this procedure is then collected on a filter. The collected powder is then heat treated, as needed, depending on the desired application of the catalyst. Finally, the sacrificial support is removed, for example by leaching with HF or KOH.

[0147] It will be appreciated that the above-described large-scale production method is suitable for use for a wide variety of precursors and materials and thus not necessarily limited to the catalysts disclosed herein. Figs. 42-44 illustrate morphological data for selected self-supported metal-nitrogen-carbon (M-N-C) catalyst prepared by the above described method.

[0148] Figs. 42A-D are SEM images of spherical, highly porous Fe-N-C catalysts prepared on low surface area silica.

[0149] Figs. 43A-C are SEM images of spherical, highly porous Fe-N-C catalysts prepared on high surface area silica (Batch 1).

[0150] Fig. 44 is an SEM image of spherical, highly porous Fe-N-C catalysts prepared on high surface area silica (Batch 2).

[0151] Fig. 45 is a Rotating Disc Electrode electro-voltamogram illustrating oxygen reduction for RDE data for spherical F-N-C catalysts prepared by the presently described method in 0.5M H_2SO_4 saturated with O_2 (catalysts loading: 600 μg cm^{-2}, 1200RPM, 5mV s^{-1}).

[0152] It can clearly be seen that the morphological properties of the materials are very consistent from batch to batch. The utility of these materials is illustrated in oxygen reduction tests, an example of which is shown in Fig. 5.

[0153] The specific methods and compositions described herein are representative of preferred embodiments and are exemplary and not intended as limitations on the scope of the invention. Other objects, aspects, and embodiments will occur to those skilled in the art upon consideration of this specification, and are encompassed within the spirit of the invention as defined by the scope of the claims. It will be readily apparent to one skilled in the art that varying substitutions and modifications may be made to the invention disclosed herein without departing from the scope and spirit of the invention. The invention illustratively described herein suitably may be practiced in the absence of any element or elements, or limitation or limitations, which is not specifically disclosed herein as essential. The methods and processes illustratively described herein suitably may be practiced in differing orders of steps, and that they are not necessarily restricted to the orders of steps indicated herein or in the claims. As used herein and in the appended claims, the singular forms "a," "an," and "the" include plural reference unless the context clearly dictates otherwise. Thus, for example, a reference to "a catalyst" includes a plurality of such catalysts, and so forth.

[0154] Under no circumstances may the patent be interpreted to be limited to the specific examples or embodiments or methods specifically disclosed herein. Under no circumstances may the patent be interpreted to be limited by any statement made by any Examiner or any other official or employee of the Patent and Trademark Office unless such statement is specifically and without qualification or reservation expressly adopted in a responsive writing by Applicants.

[0155] The terms and expressions that have been employed are used as terms of description and not of limitation, and there is no intent in the use of such terms and expressions to exclude any equivalent of the features shown and described or portions thereof, but it is recognized that various modifications are possible within the scope of the invention as claimed. Thus, it will be understood that although the present invention has been specifically disclosed by preferred embodiments and optional features, modification and variation of the concepts herein disclosed may be resorted to by those skilled in the art, and that such modifications and variations are considered to be within the scope of this invention as defined by the appended claims.

[0156] All patents and publications referenced below and/or mentioned herein are indicative of the levels of skill of those skilled in the art to which the invention pertains, and each such referenced patent or publication is hereby incorporated by reference to the same extent as if it had been incorporated by reference in its entirety individually or set forth herein in its entirety. Applicants reserve the right to physically incorporate into this specification any and all materials and information from any such cited patents or publications.

What is claimed is:

1. A method for producing a Metal-Nitrogen-Carbon catalyst suitable for use in a fuel cell comprising:

providing sacrificial template particles;

precipitating one or more transition metal precursors and a non-porphyrin precursor with no initial catalytic activity onto the sacrificial template particles to produce dispersed precursors;

pyrolyzing the dispersed precursors; and

removing the sacrificial template particles to produce a highly dispersed, self-supported, high surface area electrocatalytic material.

2. The method of claim 1 wherein the non-porphyrin precursor forms a complex with iron.

3. The method of claim 1 wherein the non-porphyrin precursor is 4-aminoantipirine.

4. The method of claim 1 wherein the transition metal precursor is an iron precursor.

5. The method of claim 1 wherein the one or more transitional metal precursors is selected from the group consisting of precusors of Ce, Cr, Cu, Mo, Ni, Ru, Ta, Ti, V, W, and Zr.

6. The method of claim 1 wherein at least two different metal precursors are used resulting in a multi-metallic catalyst.

7. The method of claim 1 wherein the wherein the sacrificial template particles and non-porphyrin precursors are selected for use so as to shift the reaction mechanism of the electrocatalytic material towards the 4 e- pathway.

8. The method of claim 1 wherein the sacrificial template particles comprise at least two populations of particles wherein each population has an average particle diameter that is different from the other populations, resulting in an electrocatalytic material having a multimodal pore distribution.

9. The method of claim 8 wherein the electrocatalytic material contains a population of pores having an average diameter between 20 and 60nm and a second population of pores having an average diameter between 100 and 200nm.

10. The method of claim 9 wherein the sacrificial template particles are formed from silica.

11. The method of claim 10 wherein each population of silica particles is formed from a different type of silica.

12. The method of claim 11 wherein the silica that forms the particles in each population is selected from the group consisting of: HS5, M4, LM130, A90, L90, A200 and A380 silica.

13. The method of claim 1 further comprising

mixing the transition metal and non-porphyrin precursors with the sacrificial template particles;

atomizing the mixture to form a powder;

collecting the powder; and

heat treating the powder.

14. A highly dispersed, unsupported, catalytic material substantially consisting of nitrogen and carbon from a non-porphyrin precursor with no initial catalytic activity and at least one transition metal from pyrolyzed metal precursors manufactured using the method of claim 1.

15. A highly dispersed, unsupported, catalytic material substantially consisting of nitrogen and carbon from a non-porphyrin precursor with no initial catalytic activity and at least one transition metal from pyrolyzed metal precursors.

16. The material of claim 15 further comprising a multi-modal pore distribution.

17. The material of claim 16 wherein the material comprises a first population of pores having an average diameter between 20 and 60nm and a second population of pores having an average diameter between 100 and 200nm.

18. The material of claim 16 further comprising a tri-modal pore distribution wherein the material comprises a first population of pores having an average diameter of less than or approximately equal to 20nm, a second population of pores having an average diameter of between approximately 40 and 60nm, and a third population of pores having an average diameter between 150 and 200nm.

19. The material of claim 15 comprising multiple transition metals.

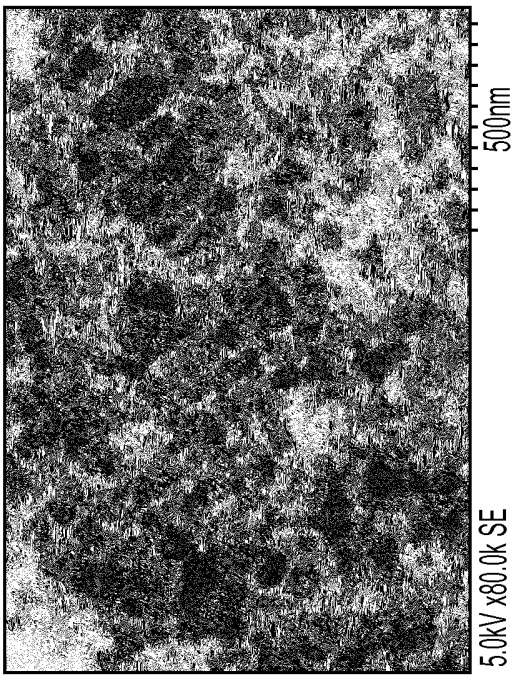

FIG. 2

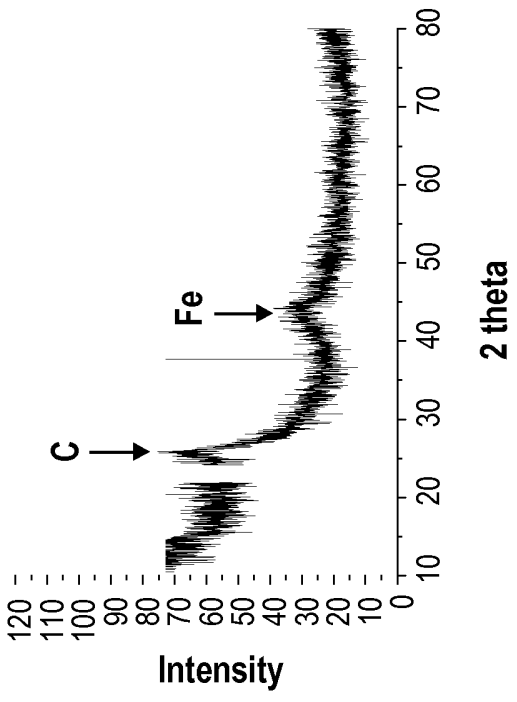

FIG. 1

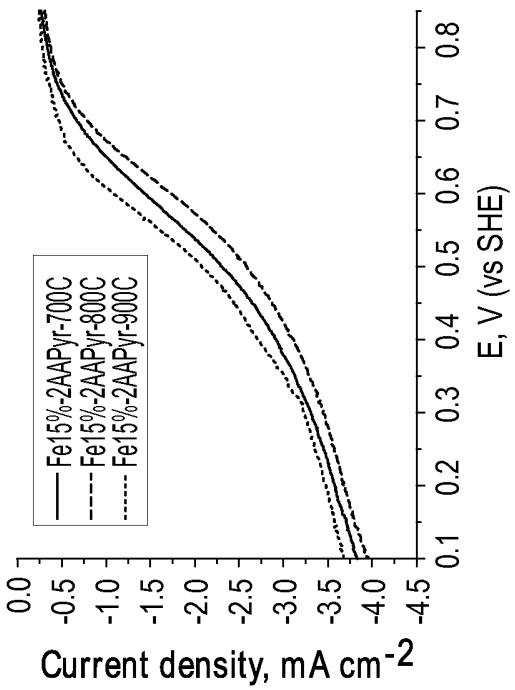

FIG. 4

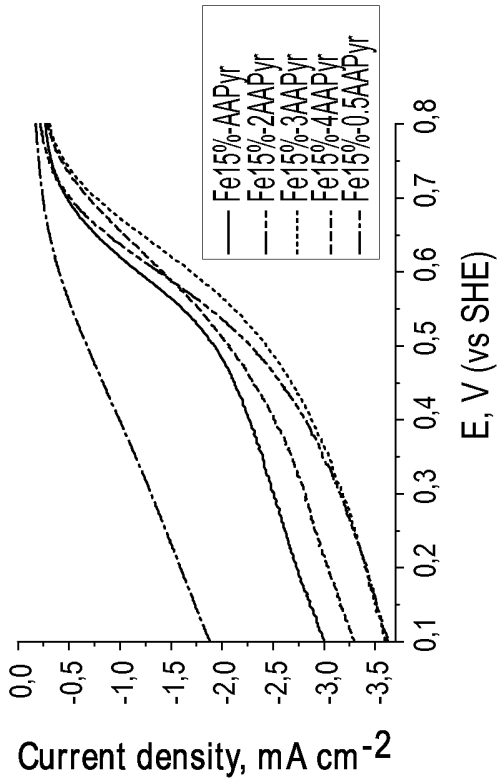

FIG. 3

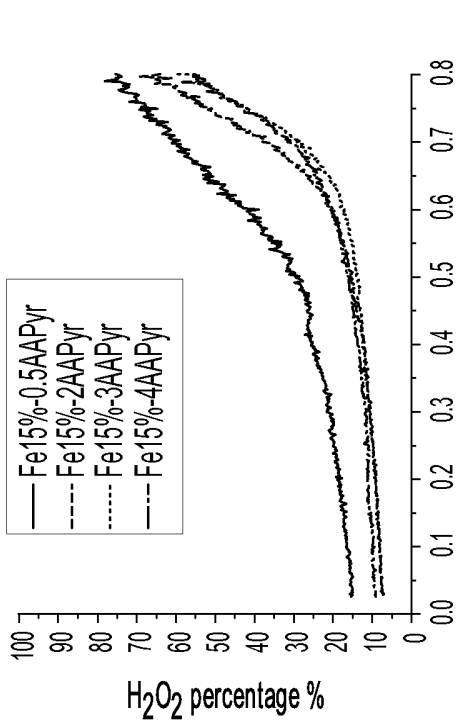

FIG. 6

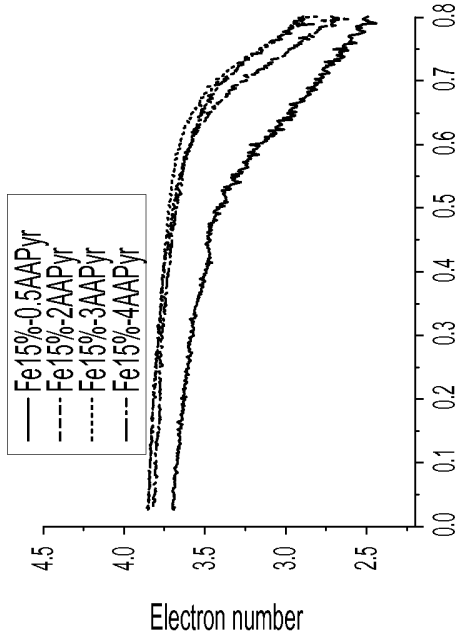

FIG. 5

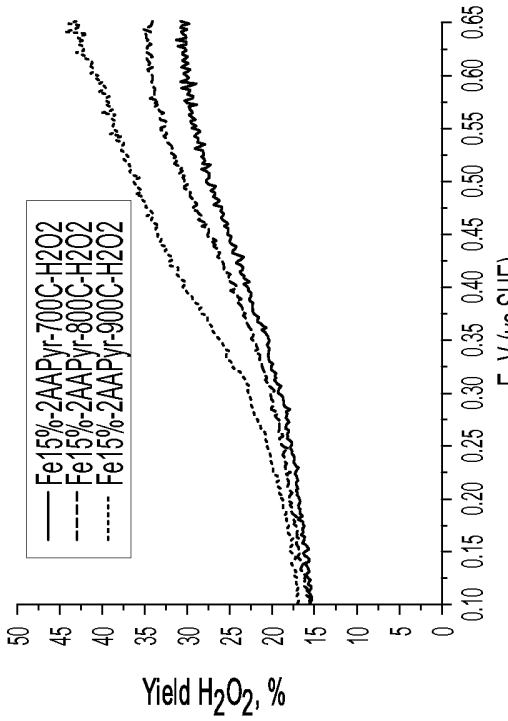

FIG. 8

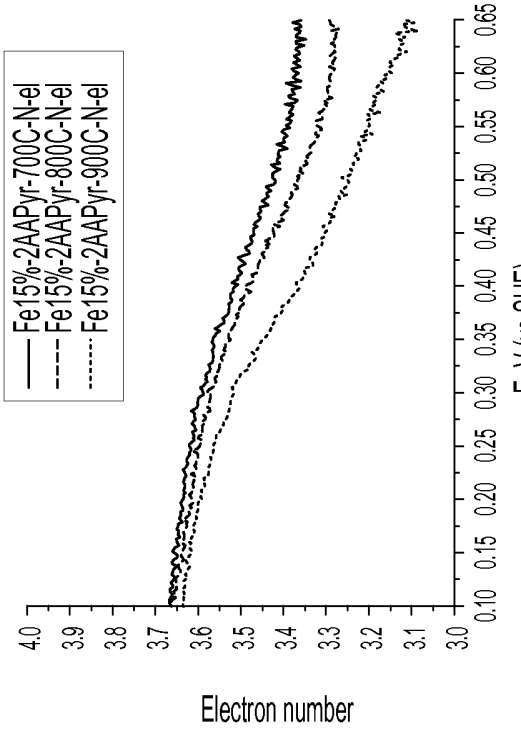

FIG. 7

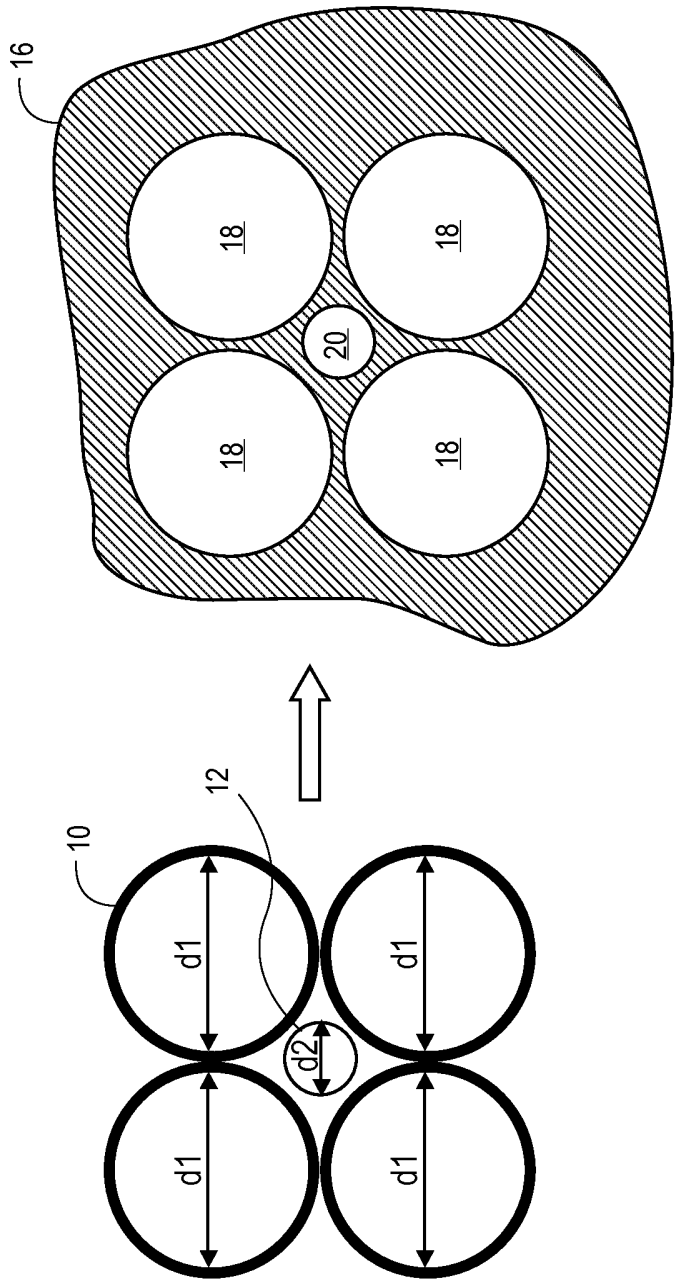

FIG. 9

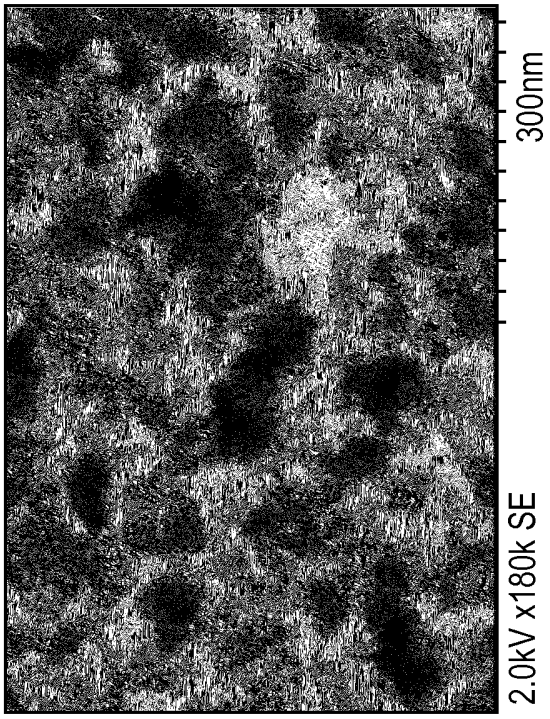

FIG. 10B

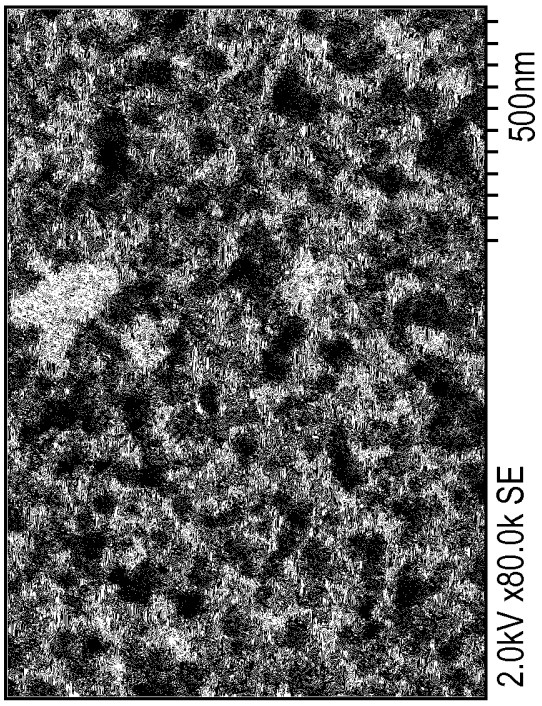

FIG. 10A

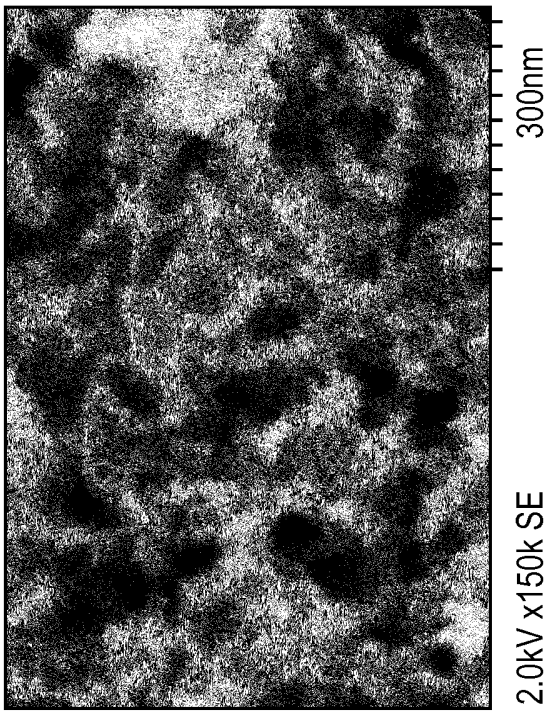

FIG. 11B

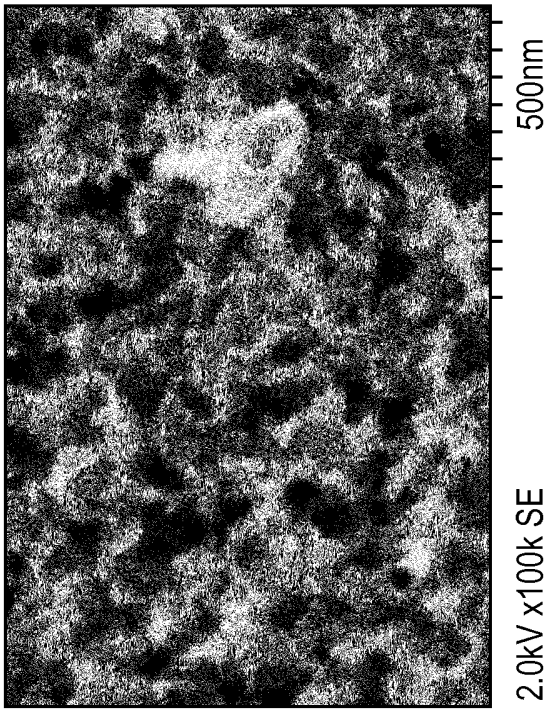

FIG. 11A

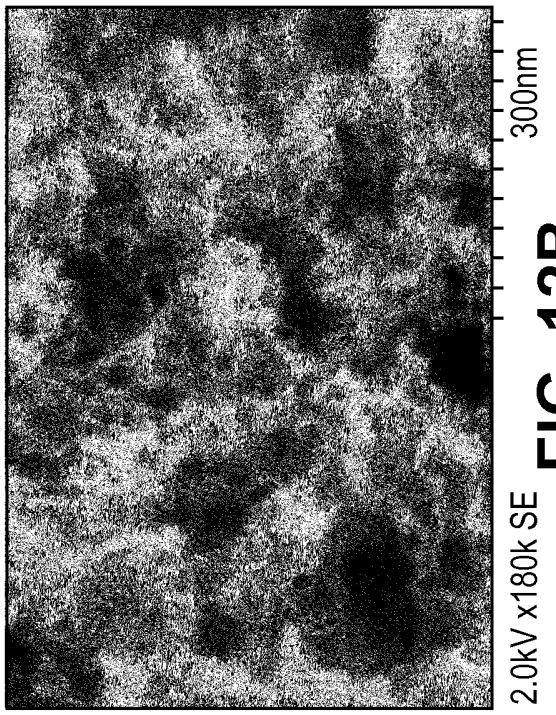

FIG. 12B

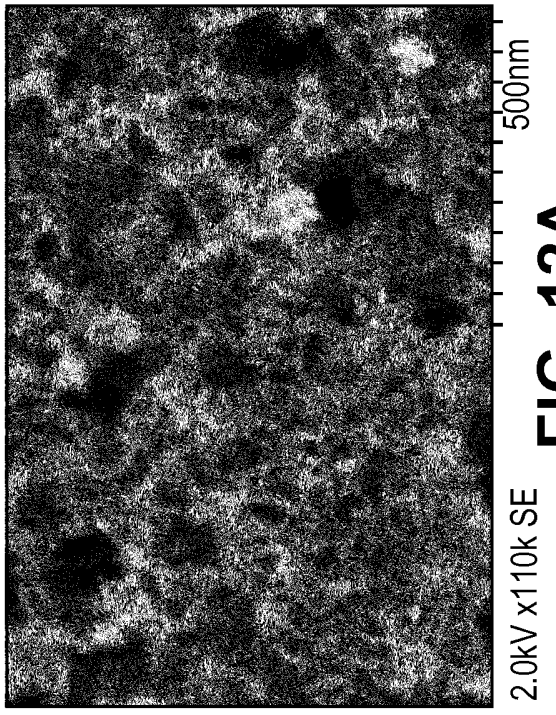

FIG. 12A

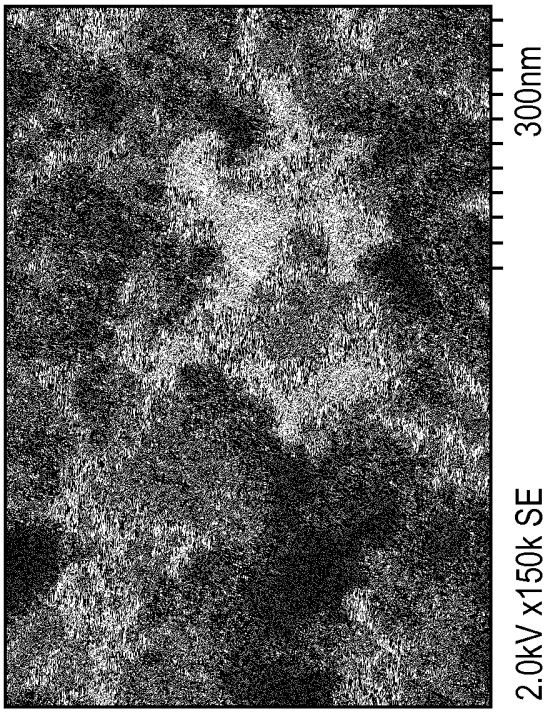

FIG. 13B

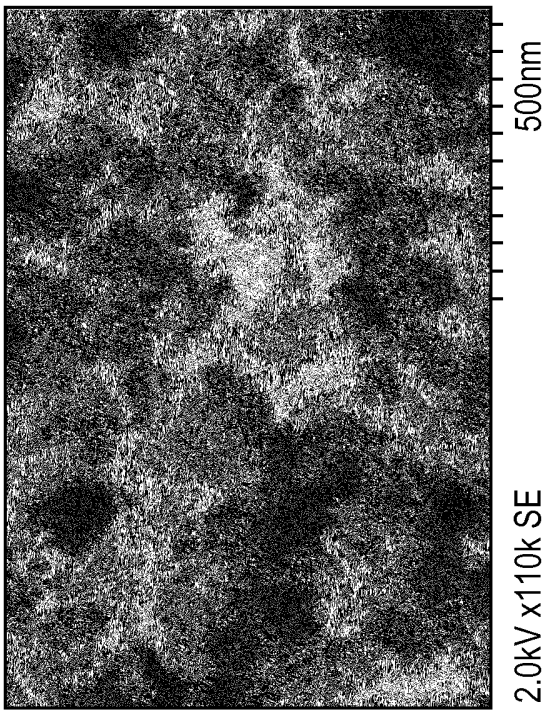

FIG. 13A

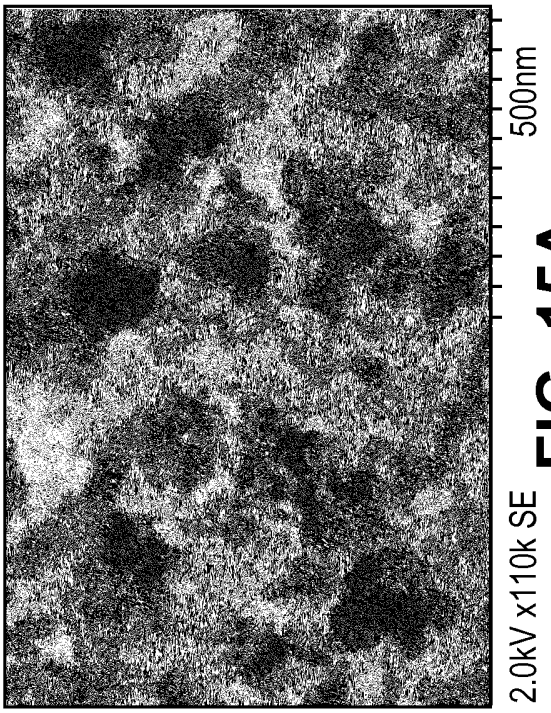

FIG. 15A

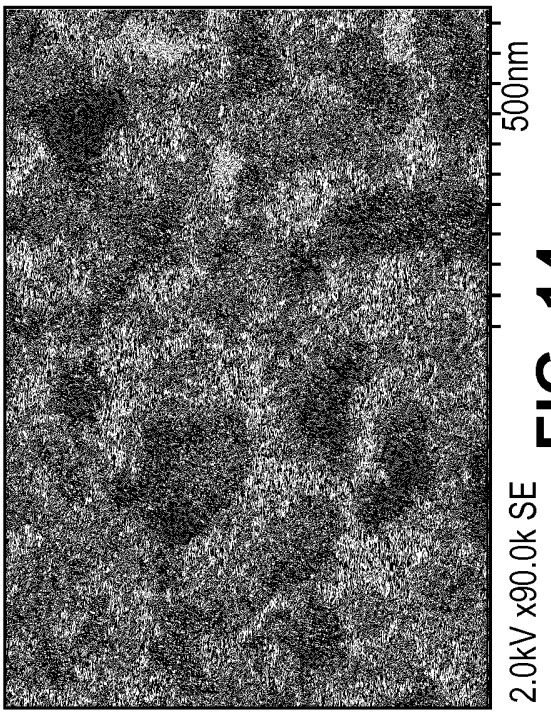

FIG. 14

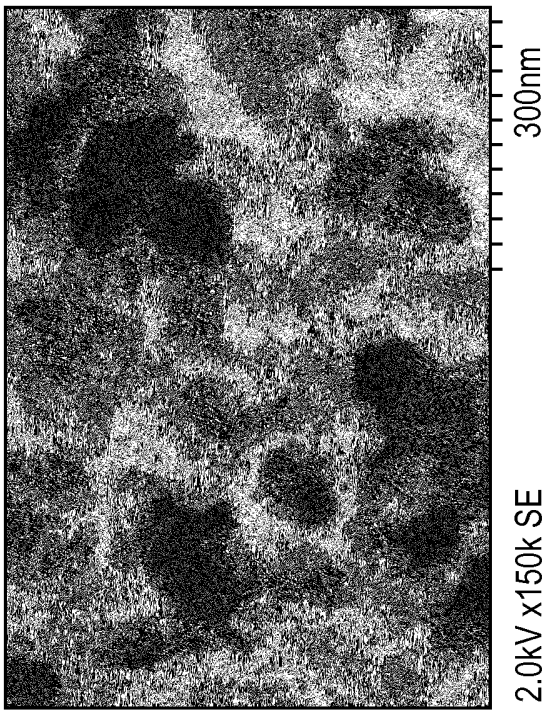

FIG. 15C

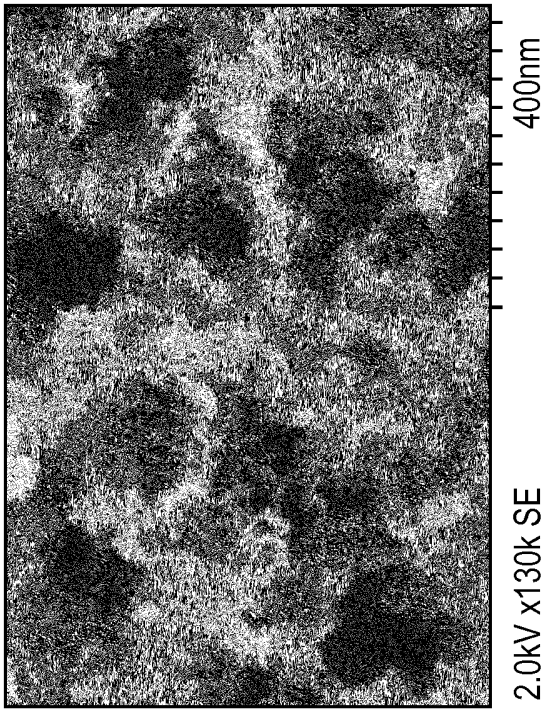

FIG. 15B

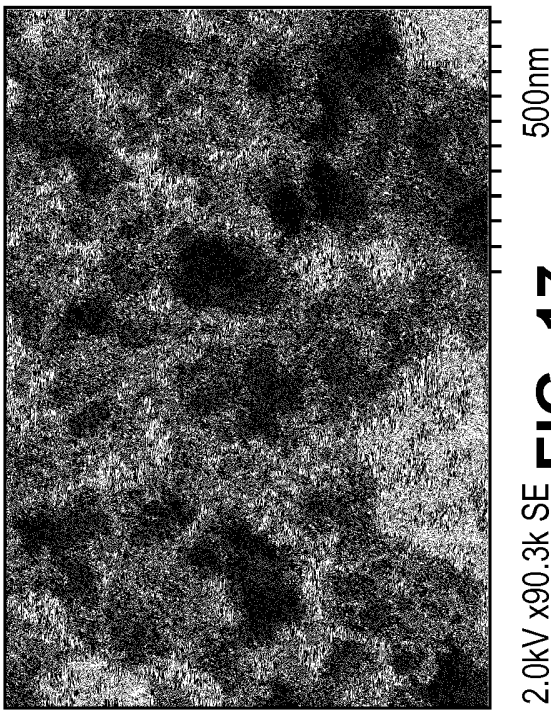

FIG. 17

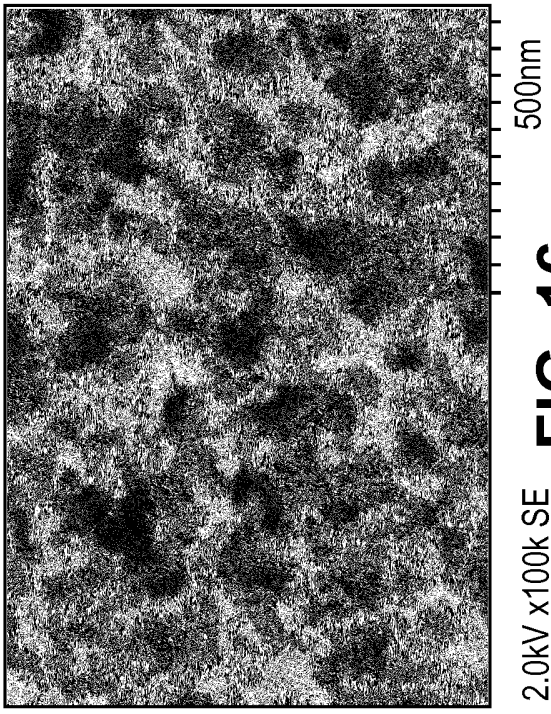

FIG. 16

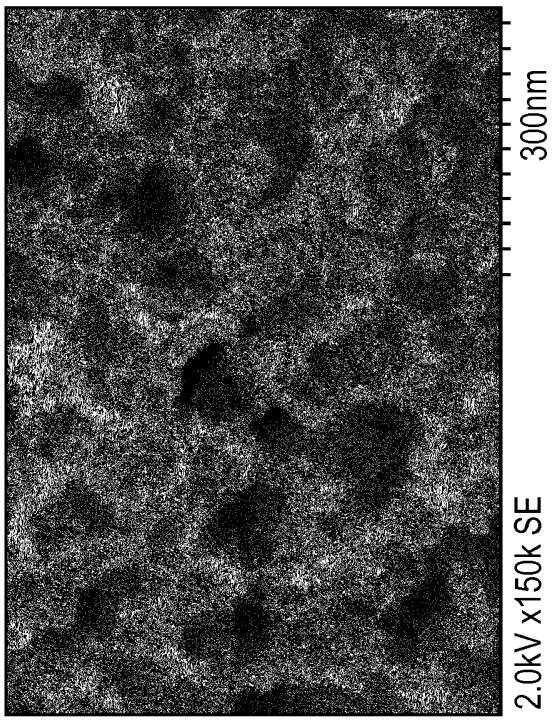

FIG. 19

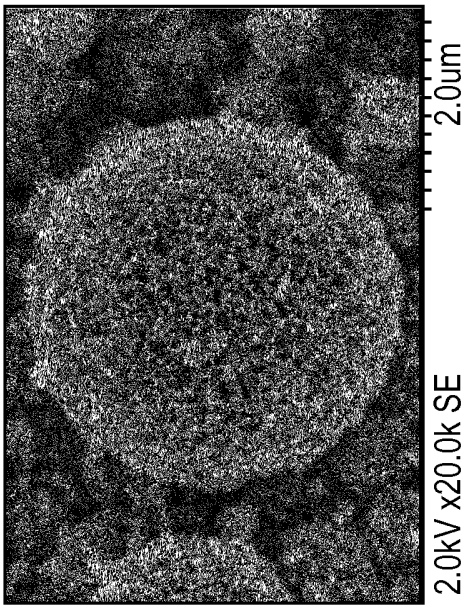

FIG. 20B

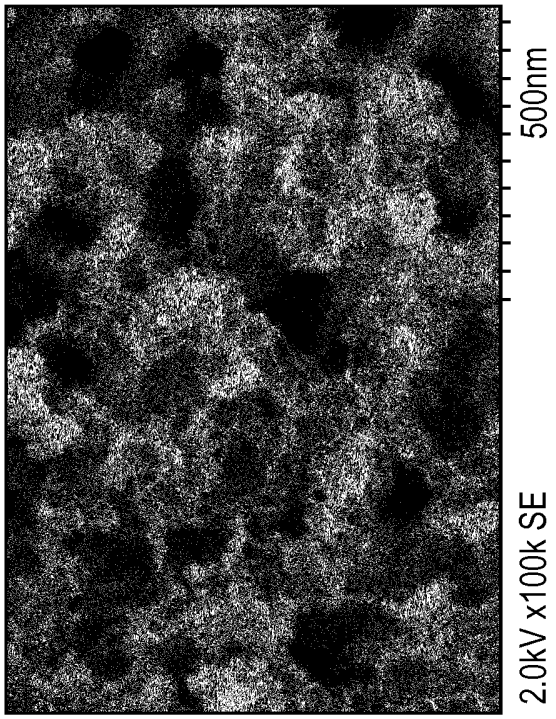

FIG. 18

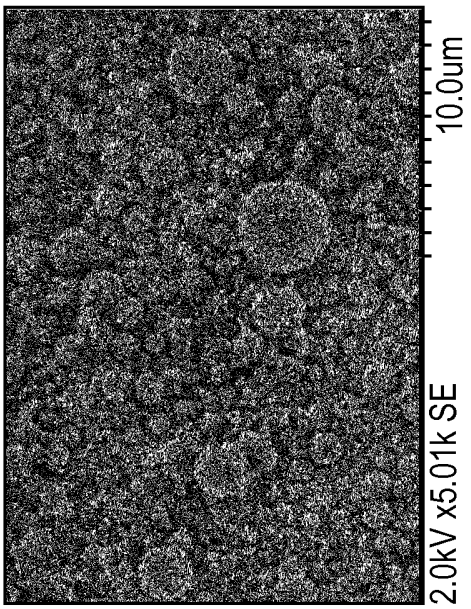

FIG. 20A

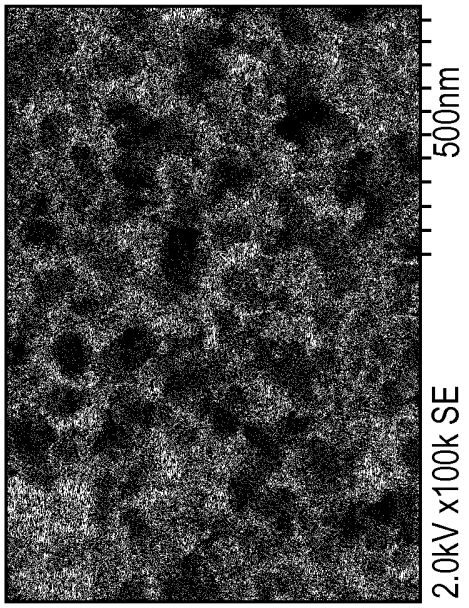

FIG. 20D

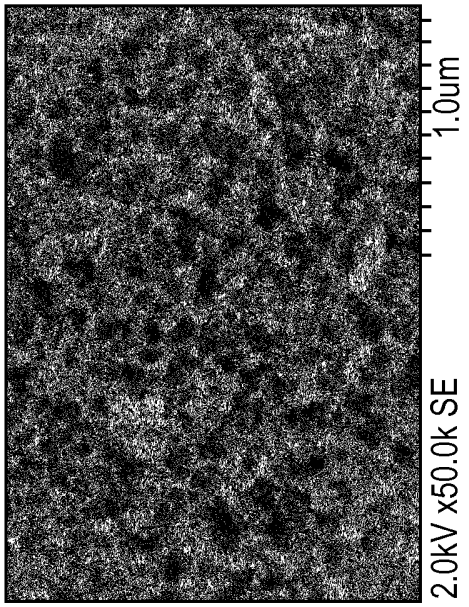

FIG. 20C

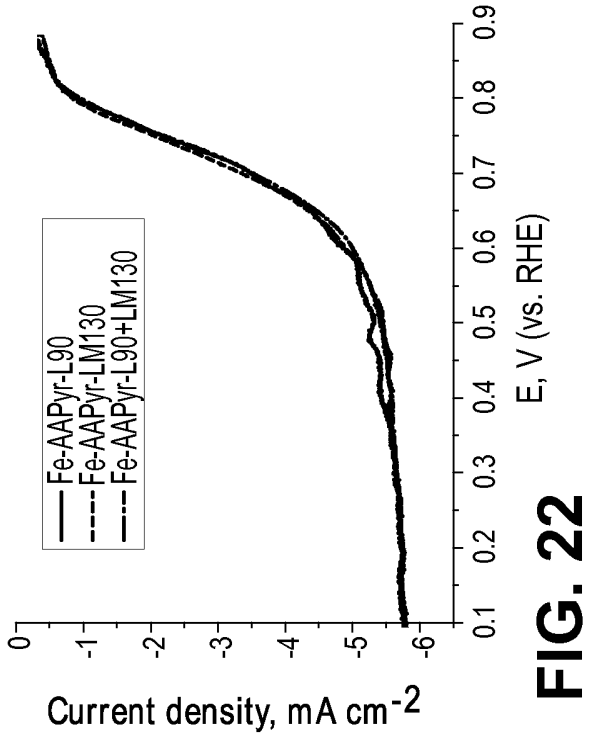

FIG. 22

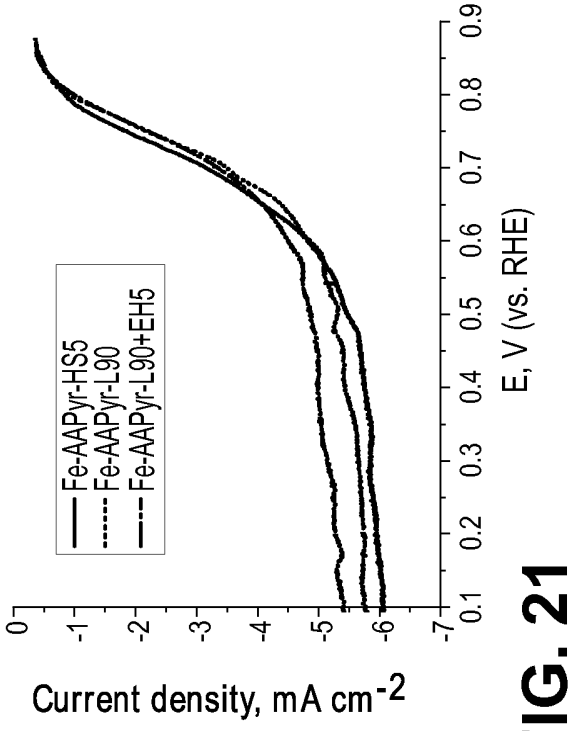

FIG. 21

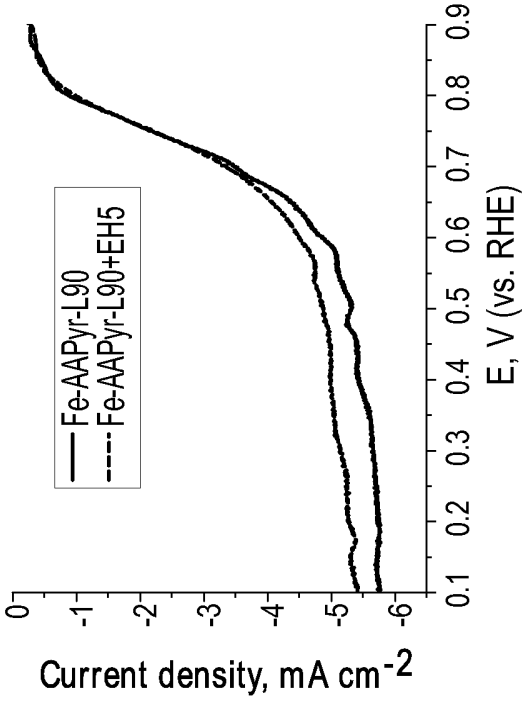

FIG. 24

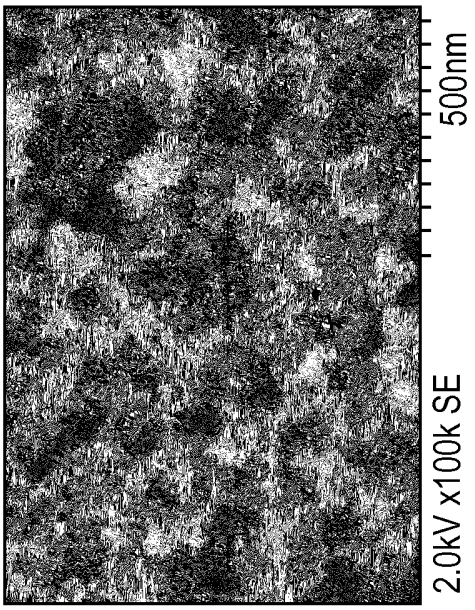

FIG. 26

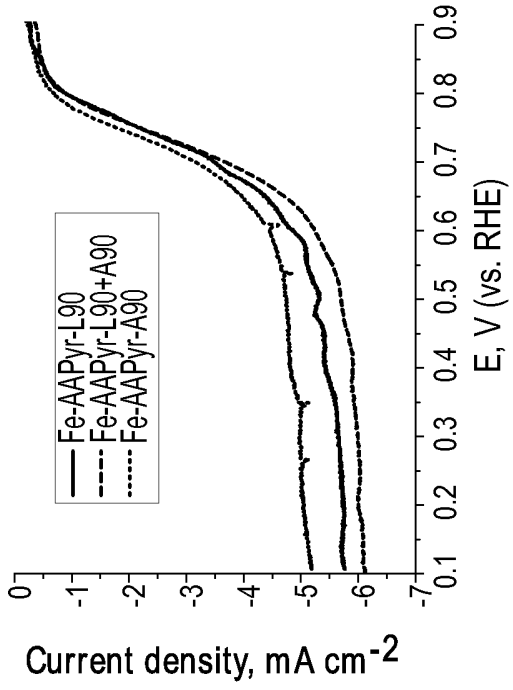

FIG. 23

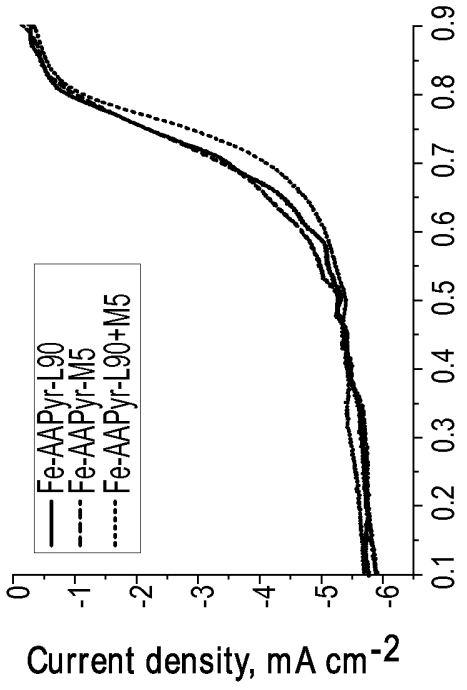

FIG. 25

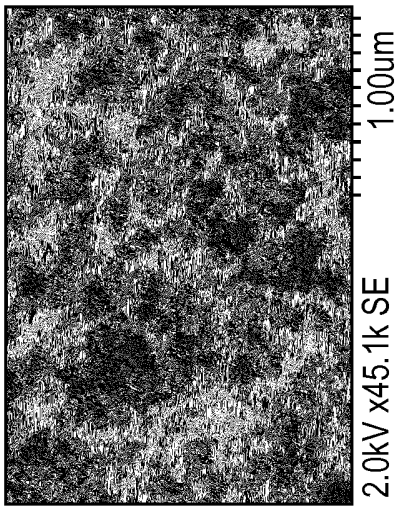

FIG. 29A

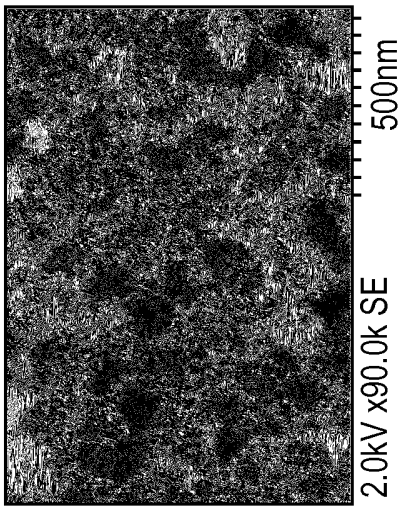

FIG. 30B

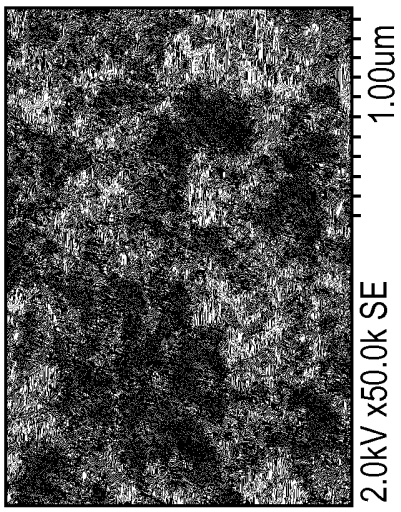

FIG. 28

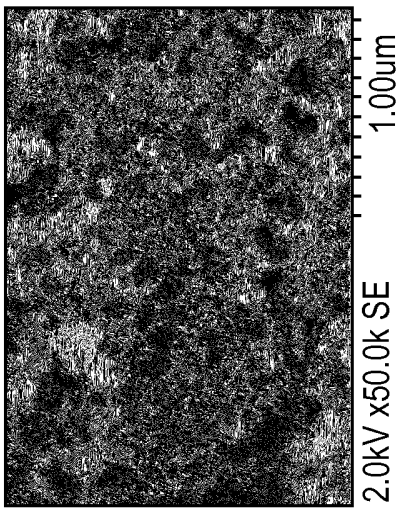

FIG. 30A

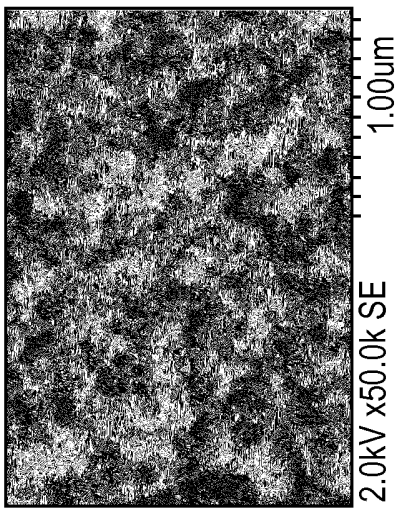

FIG. 27

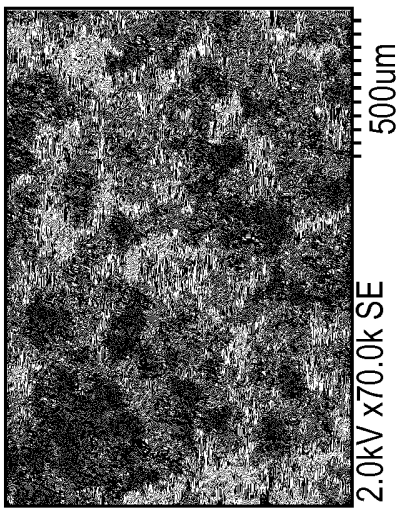

FIG. 29B

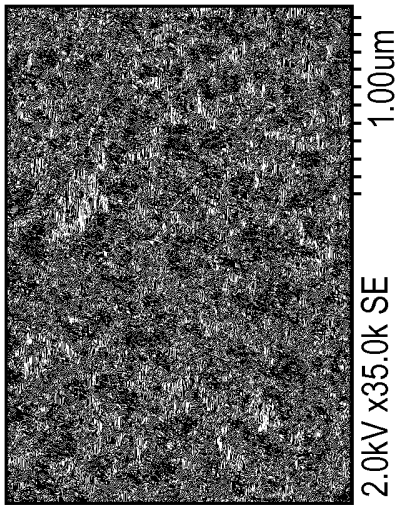

FIG. 32A

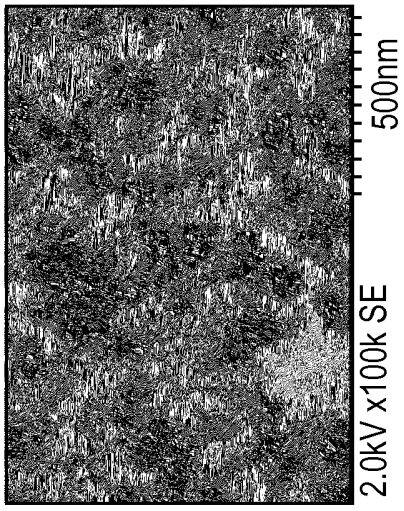

FIG. 33B

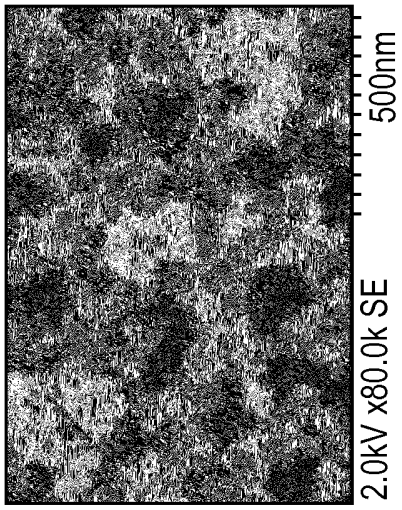

FIG. 31B

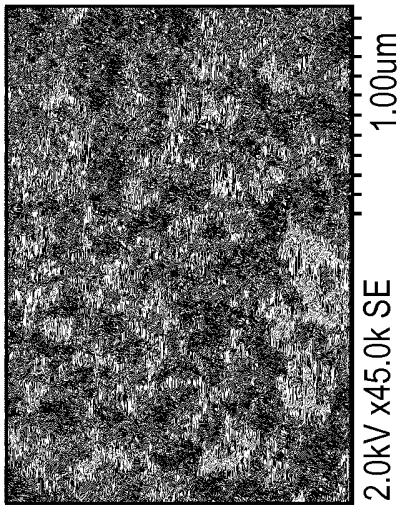

FIG. 33A

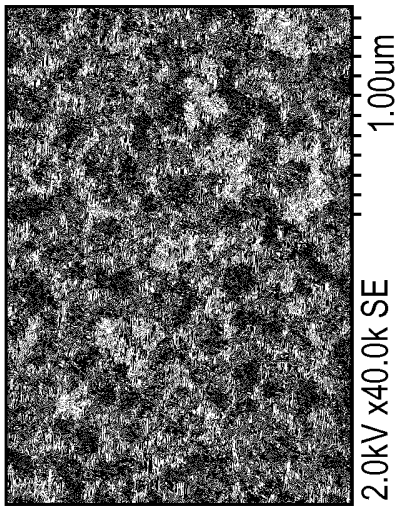

FIG. 31A

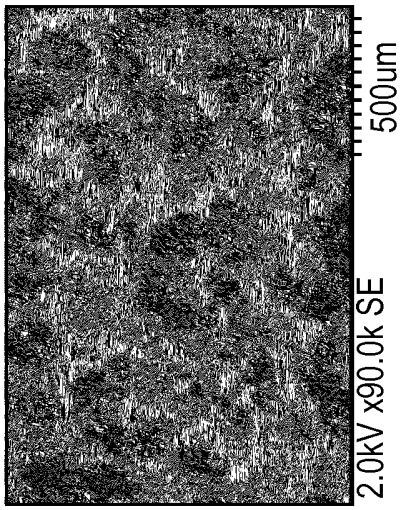

FIG. 32B

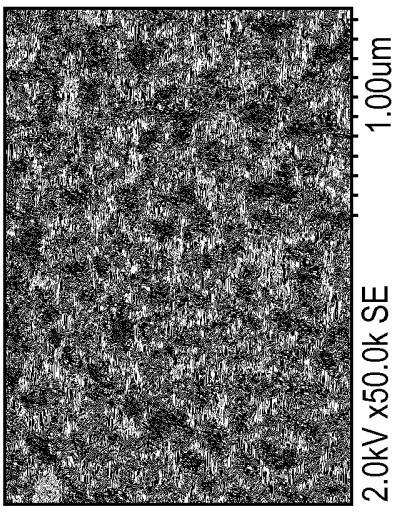

FIG. 34A

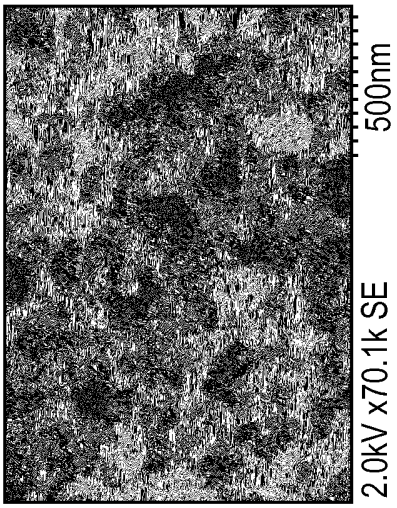

FIG. 34B

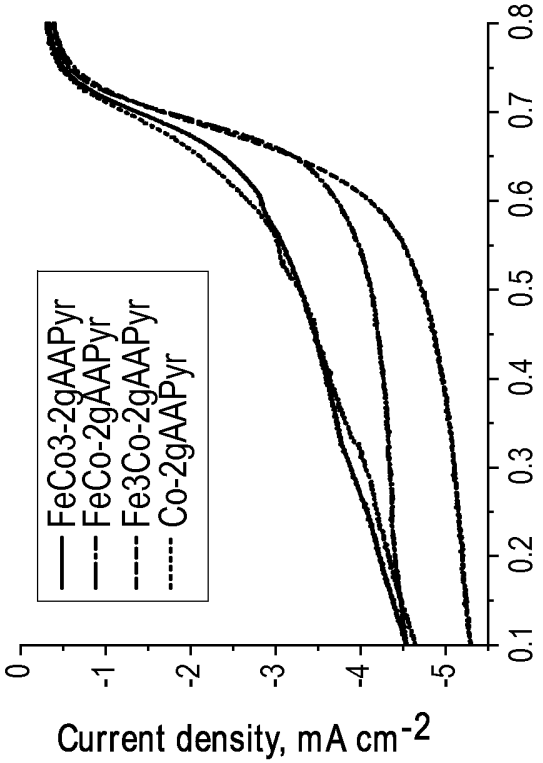

FIG. 35

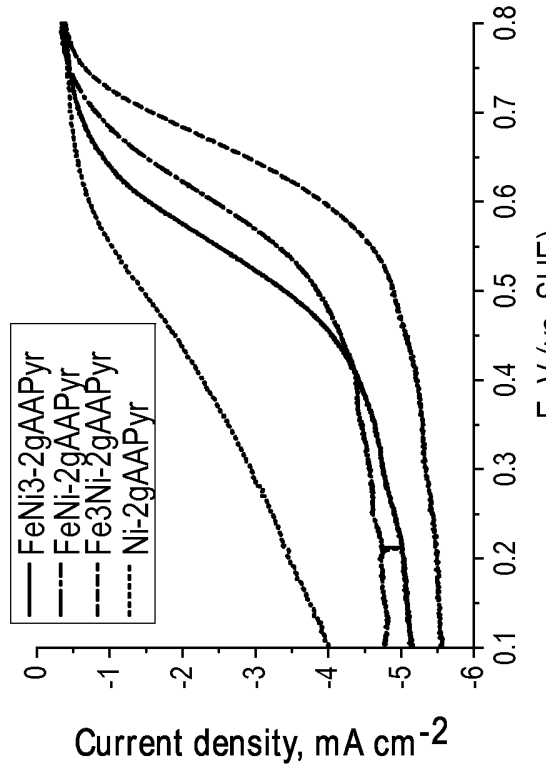

FIG. 36

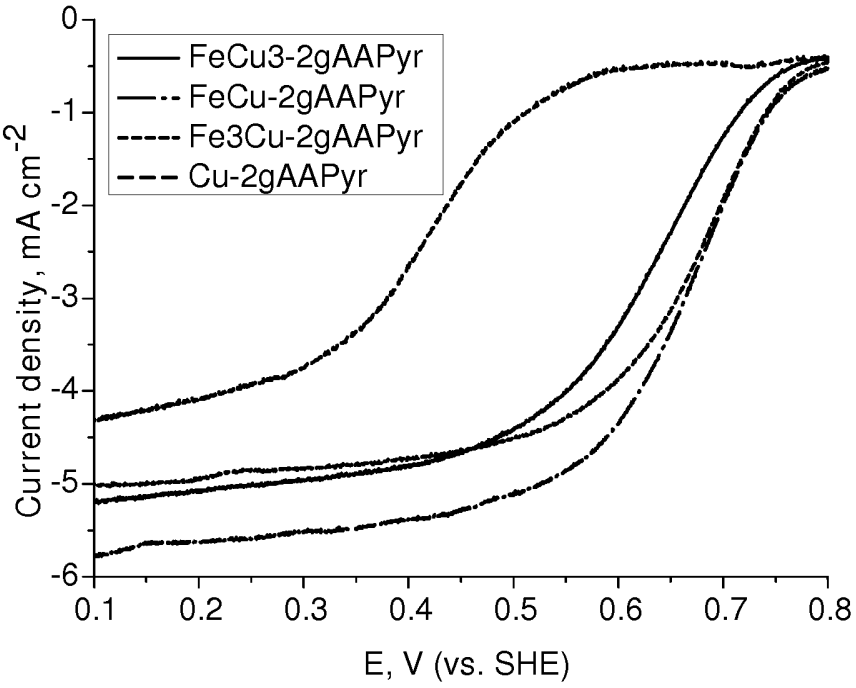
FeCu3-2gAAPyr
FeCu-2gAAPyr
Fe3Cu-2gAAPyr
Cu-2gAAPyr
Current density, mA cm-2
E, V (vs. SHE)
0
-1
-2
-3
-4
-5
-6
0.1
0.2
0.3
0.4
0.5
0.6
0.7
0.8

FIG. 37

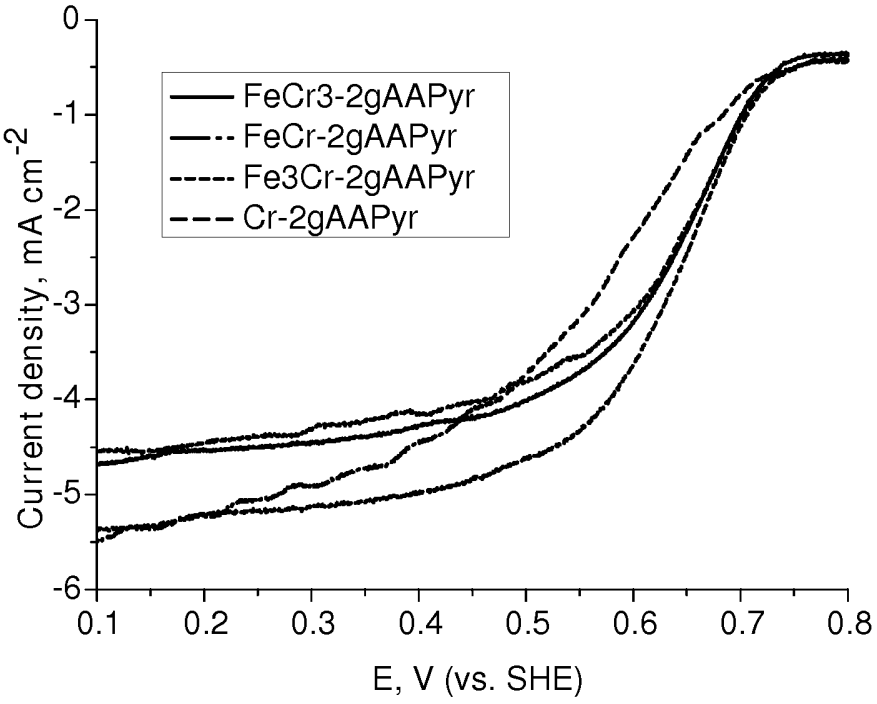
FeCr3-2gAAPyr
FeCr-2gAAPyr
Fe3Cr-2gAAPyr
Cr-2gAAPyr
Current density, mA cm-2
E, V (vs. SHE)
0
-1
-2
-3
-4
-5
-6
0.1
0.2
0.3
0.4
0.5
0.6
0.7
0.8

FIG. 38

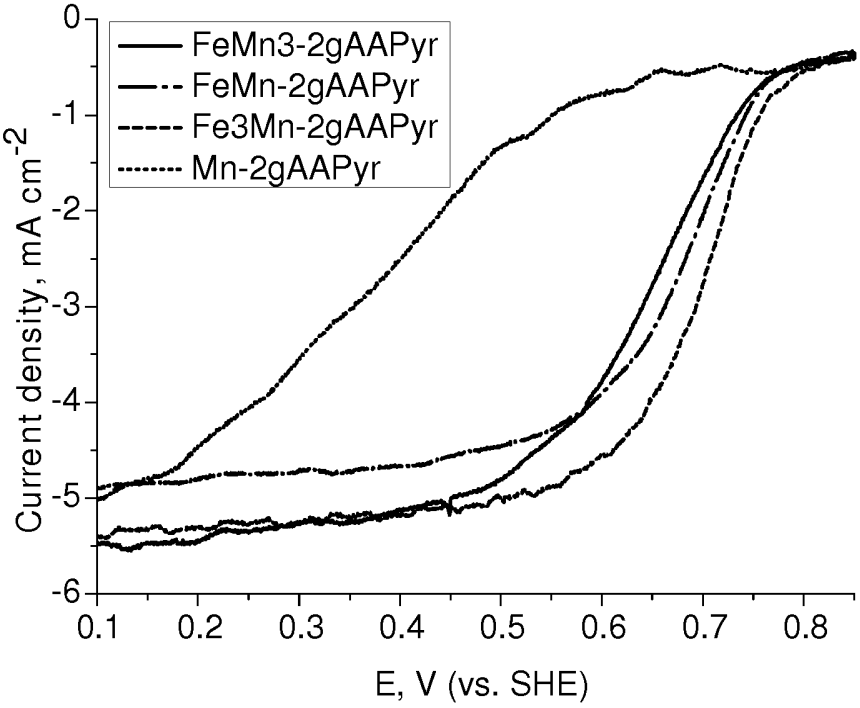
FeMn3-2gAAPyr
FeMn-2gAAPyr
Fe3Mn-2gAAPyr
Mn-2gAAPyr
Current density, mA cm-2
0
-1
-2
-3
-4
-5
-6
0.1
0.2
0.3
0.4
0.5
0.6
0.7
0.8
E, V (vs. SHE)

FIG. 39

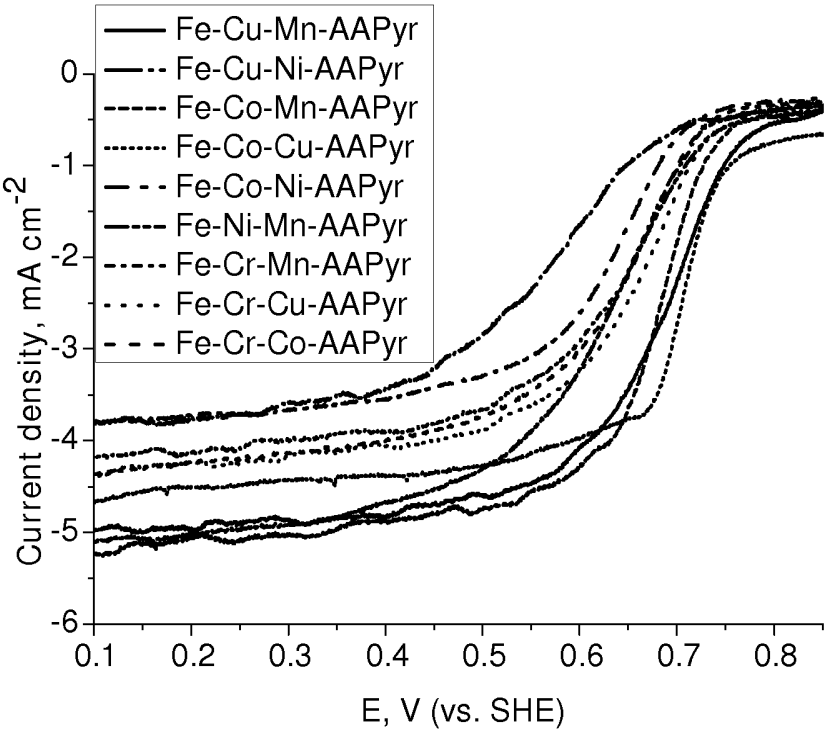
Fe-Cu-Mn-AAPyr
Fe-Cu-Ni-AAPyr
Fe-Co-Mn-AAPyr
Fe-Co-Cu-AAPyr
Fe-Co-Ni-AAPyr
Fe-Ni-Mn-AAPyr
Fe-Cr-Mn-AAPyr
Fe-Cr-Cu-AAPyr
Fe-Cr-Co-AAPyr
Current density, mA cm-2
0
-1
-2
-3
-4
-5
-6
0.1
0.2
0.3
0.4
0.5
0.6
0.7
0.8
E, V (vs. SHE)

FIG. 40

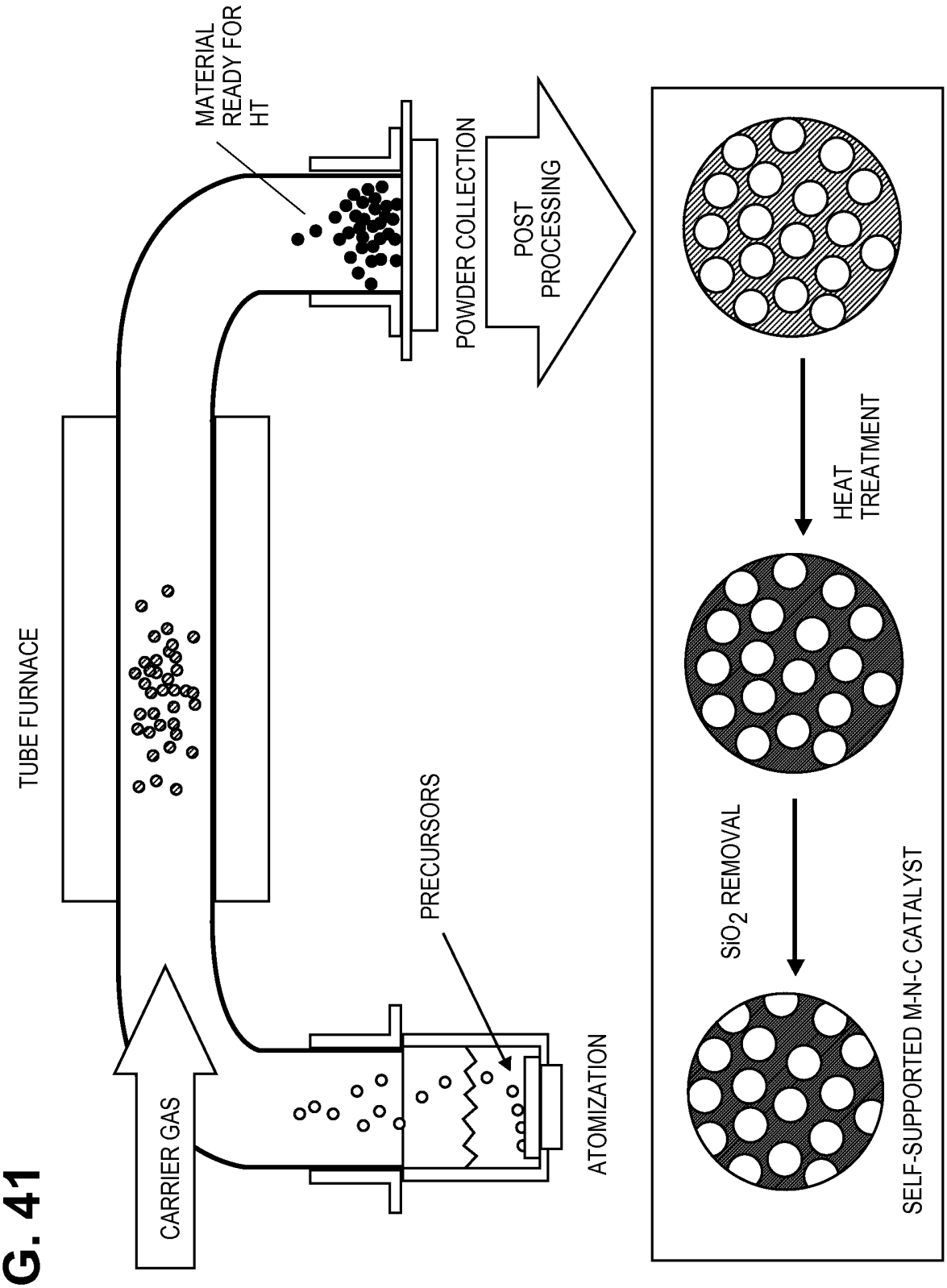
MATERIAL READY FOR HT
POWDER COLLECTION
POST PROCESSING
TUBE FURNACE
PRECURSORS
CARRIER GAS
ATOMIZATION
HEAT TREATMENT
SiO_2 REMOVAL
SELF-SUPPORTED M-N-C CATALYST

FIG. 41

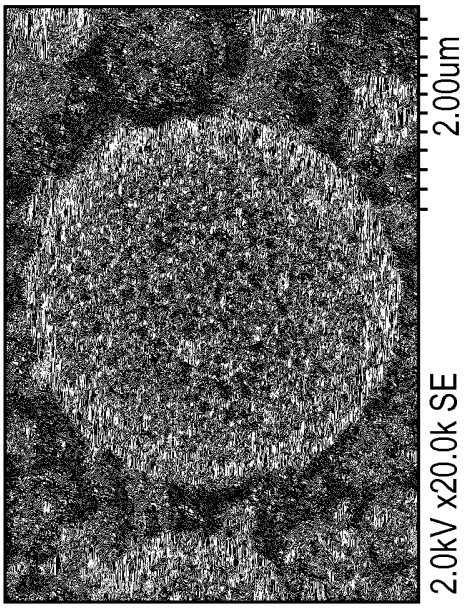

FIG. 42B

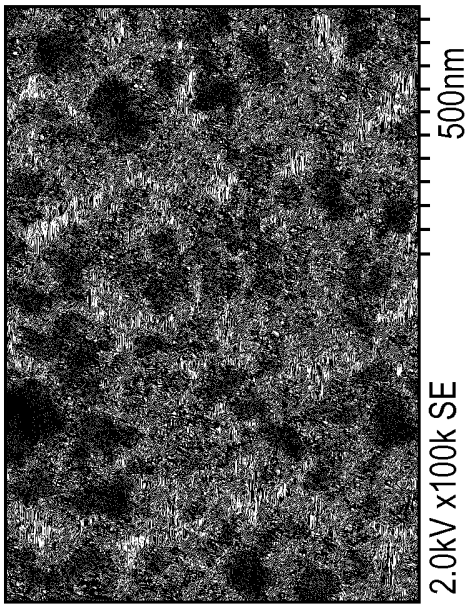

FIG. 42D

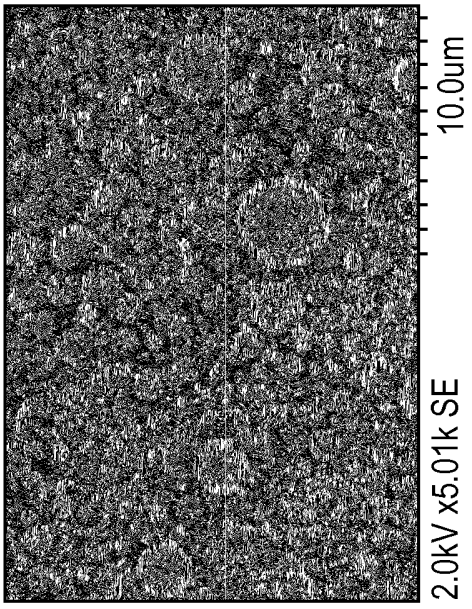

FIG. 42A

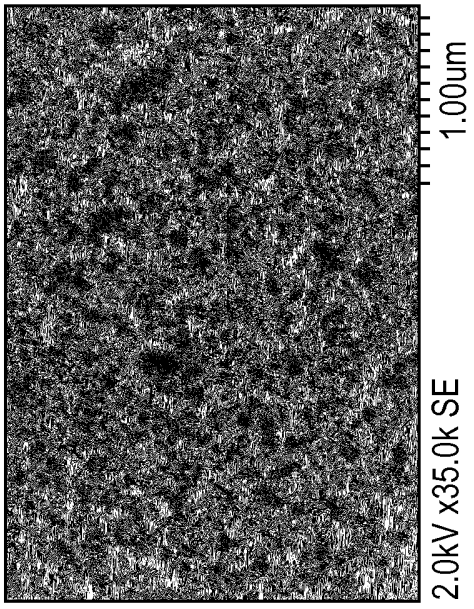

FIG. 42C

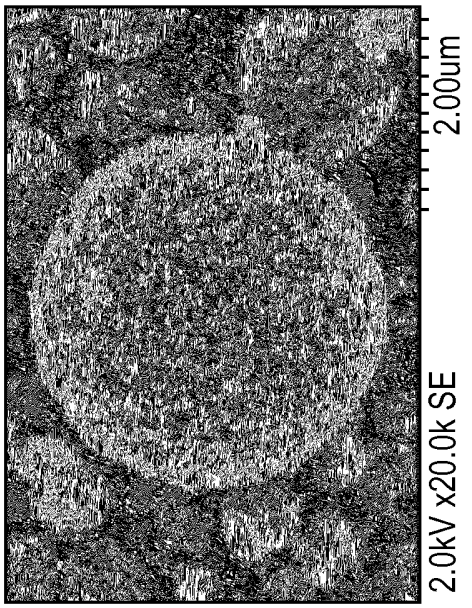

FIG. 43B

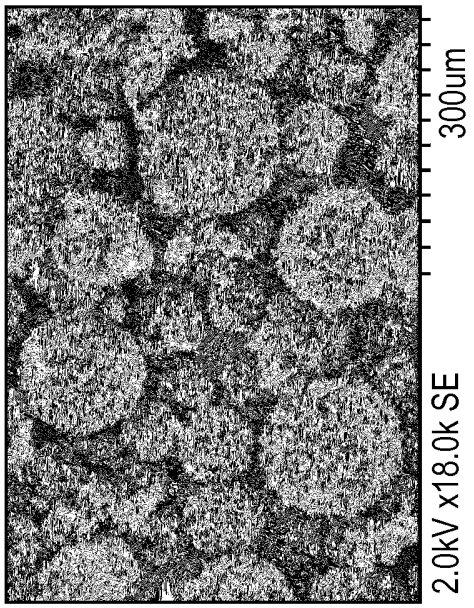

FIG. 44A

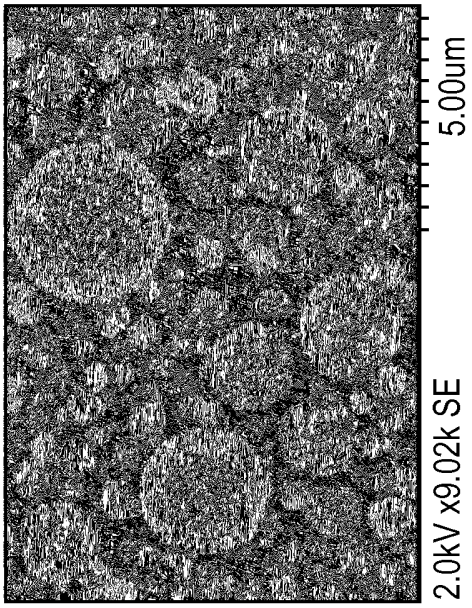

FIG. 43A

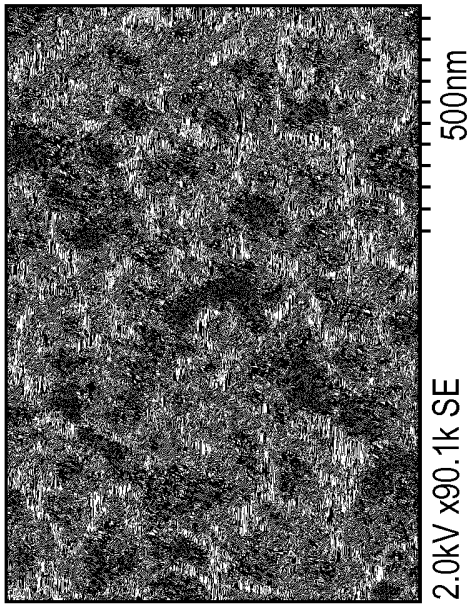

FIG. 43C

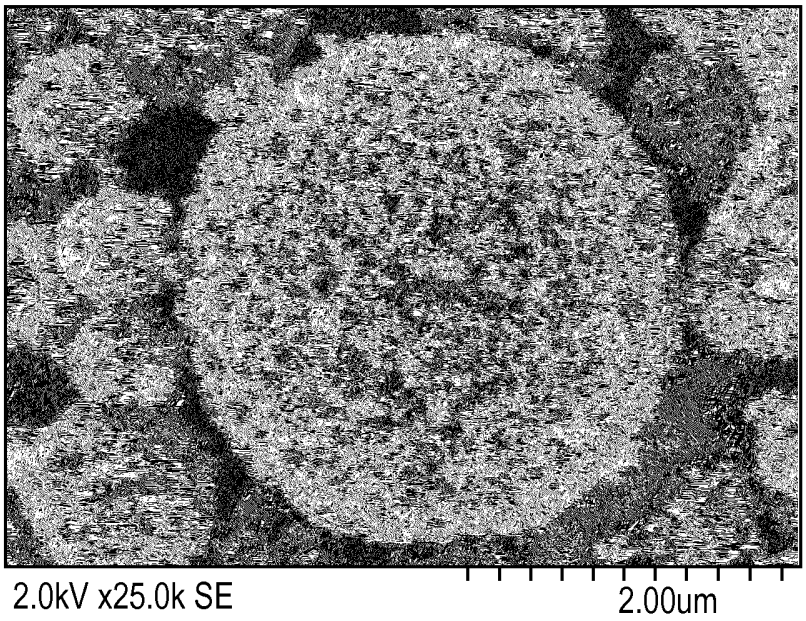

FIG. 44B

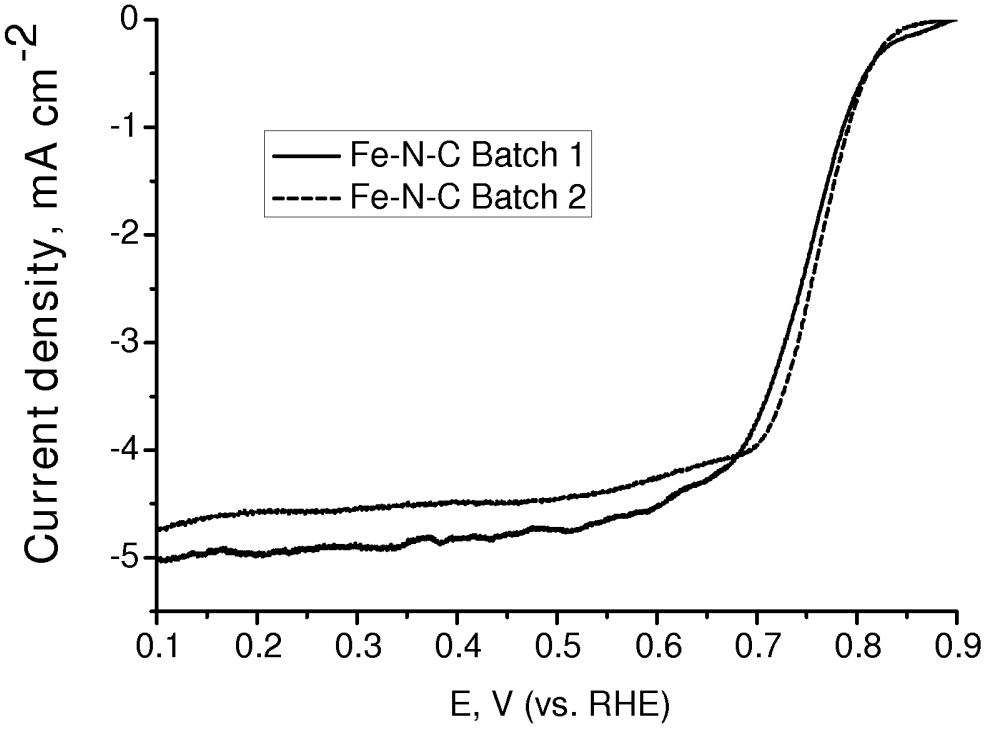

FIG. 45

(19)中华人民共和国国家知识产权局

(12)发明专利申请

(10)申请公布号 CN 103998131 A
(43)申请公布日 2014.08.20

(21)申请号 201280039823.4
(22)申请日 2012.06.15
(30)优先权数据
61/497444 2011.06.15 US
61/606109 2012.03.02 US
61/621084 2012.04.06 US
61/621095 2012.04.06 US
(85)PCT国际申请进入国家阶段日
2014.02.14
(86)PCT国际申请的申请数据
PCT/US2012/042609 2012.06.15
(87)PCT国际申请的公布数据
WO2012/174344 EN 2012.12.20
(71)申请人 STC.UNM 公司
地址 美国新墨西哥州
(72)发明人 A. 塞罗夫 B. 哈列维
K. 阿特于什科瓦 P.B. 阿塔纳索夫
U.A. 马丁内斯
(74)专利代理机构 中国专利代理(香港)有限公司 72001
代理人 周李军 林森
(51)Int.Cl.
B01J 31/12(2006.01)
B01J 38/02(2006.01)
H01M 4/90(2006.01)

权利要求书1页 说明书12页 附图66页

(54)发明名称

从热处理的杂原子胺前体衍生的用于燃料电池应用的非-PGM阴极催化剂

(57)摘要

公开一种利用牺牲性载体方法和廉价易得的聚合物前体作为氮和碳的来源制备M-N-C催化剂的方法。示例性聚合物前体包括不具有初始催化活性的非卟啉前体。适合的非催化非卟啉前体的实例包括但不必限于与铁形成络合物的低分子量前体,例如4-氨基安替比林、苯二胺、羟基琥珀酰亚胺、乙醇胺等。

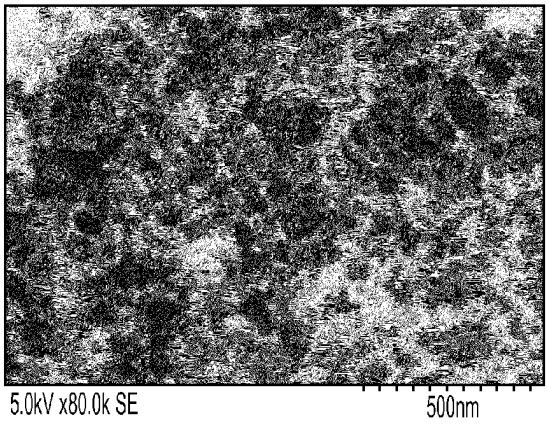

CN 103998131 A

1. 一种制备适用于燃料电池的金属 - 氮 - 碳催化剂的方法，所述方法包括：

提供牺牲性模板颗粒；

使一种或多种过渡金属前体和不具有初始催化活性的非卟啉前体沉淀到所述牺牲性模板颗粒上，以产生分散的前体；

使所述分散的前体热解；并且

去除所述牺牲性模板颗粒，以产生高分散、自担载、高表面积电催化材料。

2. 权利要求 1 的方法，其中所述非卟啉前体与铁形成络合物。

3. 权利要求 1 的方法，其中所述非卟啉前体为 4- 氨基安替比林。

4. 权利要求 1 的方法，其中所述过渡金属前体为铁前体。

5. 权利要求 1 的方法，其中所述一种或多种过渡金属前体选自 Ce、Cr、Cu、Mo、Ni、Ru、Ta、Ti、V、W 和 Zr 的前体。

6. 权利要求 1 的方法，其中使用所述至少两种不同的金属前体，得到多金属催化剂。

7. 权利要求 1 的方法，其中其中选择使用所述牺牲性模板颗粒和非卟啉前体，以使所述电催化材料的反应机制向 4e- 途径转换。

8. 权利要求 1 的方法，其中所述牺牲性模板颗粒包含至少两个颗粒群，其中每个群具有不同于其它群的平均粒径，得到具有多峰孔分布的电催化材料。

9. 权利要求 8 的方法，其中所述电催化材料包含具有 20-60nm 平均直径的孔群和具有 100-200nm 平均直径的第二孔群。

10. 权利要求 9 的方法，其中所述牺牲性模板颗粒由二氧化硅形成。

11. 权利要求 10 的方法，其中每个二氧化硅颗粒群由不同类型的二氧化硅形成。

12. 权利要求 11 的方法，其中形成每个群中的颗粒的二氧化硅选自 HS5、M4、LM130、A90、L90、A200 和 A380 二氧化硅。

13. 权利要求 1 的方法，所述方法进一步包括：

使所述过渡金属和非卟啉前体与所述牺牲性模板颗粒混合；

使所述混合物雾化，以形成粉末；

收集所述粉末；并且

热处所述理粉末。

14. 一种高度分散的非担载催化材料，所述催化材料基本由以下组成：来自不具有初始催化活性的非卟啉前体的氮和碳和来自用权利要求 1 的方法制备的经热解金属前体的至少一种过渡金属。

15. 一种高度分散的非负载催化材料，所述催化材料基本由以下组成：来自不具有初始催化活性的非卟啉前体的氮和碳和来自经热解金属前体的至少一种过渡金属。

16. 权利要求 15 的材料，所述材料进一步包括多峰孔分布。

17. 权利要求 16 的材料，其中所述材料包含具有 20-60nm 平均直径的第一孔群和具有 100-200nm 平均直径的第二孔群。

18. 权利要求 16 的材料，所述材料进一步包括三峰孔分布，其中所述材料包含具有小于或约等于 20nm 平均直径的第一孔群、具有约 40-60nm 平均直径的第二孔群和具有 150-200nm 平均直径的第三孔群。

19. 权利要求 15 的材料，所述材料包含多种过渡金属。

从热处理的杂原子胺前体衍生的用于燃料电池应用的非 -PGM 阴极催化剂

[0001] 相关申请的交叉引用

以下申请要求 2011 年 6 月 15 日提交的美国临时申请 61/497,444、2012 年 3 月 2 日提交的 61/606,109、2012 年 4 月 6 日提交的 61/621084 和 2012 年 4 月 6 日提交的 61/621,095 的权益，各申请通过引用以其全文结合到本文中。

[0002] 背景

燃料电池作为可行的替代能量，正受到越来越多的关注。通常，燃料电池使电化学能量以环境清洁和有效的方式转化成电能。预期燃料电池作为各种物品的潜在能源，由小电子器件到汽车和家居。为了满足不同的能量需求，现今已有一些不同类型的燃料电池，各自具有不同的化学组成、需要和用途。

[0003] 作为一个实例，直接甲醇燃料电池 (DMFC) 依赖甲醇在电催化剂层上氧化生成二氧化碳。水在阳极消耗并在阴极产生。正离子 (H+) 跨质子交换膜输送到阴极，在此与氧反应产生水。然后，电子可通过外电路从阳极输送到阴极，为外源提供电力。

[0004] 作为另一个实例，聚合物电解质膜 (PEM) 燃料电池（也称为质子交换膜燃料电池）用纯氢（一般由氢罐提供）作为燃料。氢流输送到膜 - 电极组件 (MEA) 的阳极侧，在此催化分解成质子和电子。与 DMFC 一样，正离子跨质子交换膜输送到阴极，在此与氧反应产生水。

[0005] 目前，在 PEM 和 DMFC 燃料电池大规模商业化中的限制因素之一是与贵金属相关的成本。DMFC 和 PEM 两种燃料电池一般用铂作为电催化剂。在阴极催化缓慢的氧还原反应 (ORR) 需要贵金属，例如铂。克服这一限制的主要途径之一是增加贵金属基电催化剂中的铂利用率。另一种可行途径是使用较大量较廉价然而仍有足够活性的催化剂。已被确定为具有足够的氧还原活性几类非铂电催化剂被认为是工业燃料电池应用中的潜在电催化剂。

[0006] 通常，已知的非铂电催化剂担载于高表面积碳黑上。这样做是为了增加催化层的分散、活性表面积和电导率。合成步骤通常包括在担载基底上沉淀前体分子和使担载的前体热解。

[0007] 已发现 M-N-C 催化剂很有希望在燃料电池膜电极组件 (MEA)、堆和燃料电池系统中用于电化学氧还原应用。材料的关键方面包括存在金属颗粒、共轭碳 - 氮 - 氧化物 - 金属网络和结合氮的碳。金属相包括金属的氧化物、碳化物、氮化物和这些状态的混合物。N/C/M 网络和 N/C 网络的化学状态和结合影响性能，例如，增加的总氮含量提高 ORR 性能。然而，这些系统仍遭受几个显著缺陷，包括 :在酸性环境中的低稳定性、在酸和碱性环境中的低耐久性、氮前体的高成本和与铂比较在 ORR 中的低活性。在酸中的低稳定性问题与从碳 - 氮网络流失金属相关。在酸和碱性溶液中的低耐久性由在这些环境中释放显著量 H_2O_2 所解释，H_2O_2 对金属和碳 - 氮网络二者均为腐蚀性。低活性可能是由于低金属负载，并由于使用外部碳源（高表面碳，例如 Vulcan、KetjenBlack 等）在这些催化剂中产生低浓度活性位点。

[0008] 用于合成克服以上确定的一些问题的非担载 M-N-C 催化剂的前述基于热解的方法包括 :使已知具有一定初始催化活性的含氮和碳的卟啉模在牺牲性载体（例如，二氧化

硅）上板化，使模板化载体热解，然后例如通过浸蚀去除载体。参见，例如 2010 年 3 月 15 日颁布的美国专利 7,678,728 号，所述专利通过引用结合到本文中。

[0009] 概述

M-N-C 体系是用于氧还原反应 (ORR) 的已知催化剂。然而，它们有一些显著的缺点，包括：在酸介质中的低稳定性，与常规 ORR 催化剂（铂）比较的低活性，和高前体成本。在本公开中描述一种利用牺牲性载体方法并使用廉价易得的聚合物前体制备 M-N-C 催化剂的方法。用这种方法制备的合成催化剂表现量好，在碱性和酸介质中高度耐用，并且制备廉价。

[0010] 附图简述

图 1 为如本文所述制备的 Fe-M-C 催化剂的 X- 射线衍射图。

[0011] 图 2 为用本文所述方法制备的 Fe-AApyr 催化剂的 SEM 图像。

[0012] 图 3 为图示说明用本文所述方法制备的 Fe-AApyr 催化剂的氧还原的旋转圆盘电极电伏安图。

[0013] 图 4 为图示说明用多种热处理温度制备的 Fe-AAPyr 的氧还原的旋转圆盘电极电伏安图。

[0014] 图 5 为对于如本文所述制备的多种 Fe-AAPyr 催化剂，参与 ORR 的电子数的曲线图。

[0015] 图 6 为对于如本文所述制备的多种 Fe-AAPyr 催化剂的过氧化氢产率的曲线图。

[0016] 图 7 为对于如本文所述制备的 Fe-AAPyr 催化剂，参与 ORR 的电子数的曲线图。

[0017] 图 8 为对于如本文所述制备的多种 Fe-AAPyr 催化剂的过氧化氢产率的曲线图。

[0018] 图 9 为如本文所述制备具有多峰孔径分布的催化剂的方法的示意图。

[0019] 图 10A 为具有 500nm 标度的从 Fe-AAPyr 和 HS5 二氧化硅得到的单峰催化剂的 SEM 图像。

[0020] 图 10B 为具有 300nm 标度的从 Fe-AAPyr 和 HS5 二氧化硅得到的单峰催化剂的 SEM 图像。

[0021] 图 11A 为具有 500nm 标度的从 Fe-AAPyr 和 M5 二氧化硅得到的双峰催化剂的 SEM 图像。

[0022] 图 11B 为具有 300nm 标度的从 Fe-AAPyr 和 M5 二氧化硅得到的双峰催化剂的 SEM 图像。

[0023] 图 12A 为具有 500nm 标度的从 Fe-AAPyr 和 LM130 二氧化硅得到的双峰催化剂的 SEM 图像。

[0024] 图 12B 为具有 300nm 标度的从 Fe-AAPyr 和 LM130 二氧化硅得到的双峰催化剂的 SEM 图像。

[0025] 图 13A 为具有 500nm 标度的从 Fe-AAPyr 和 A90 二氧化硅得到的催化剂的 SEM 图像。

[0026] 图 13B 为具有 300nm 标度的从 Fe-AAPyr 和 A90 二氧化硅得到的催化剂的 SEM 图像。

[0027] 图 14 为从 Fe-AAPyr 和 L90 与 A90 二氧化硅的混合物得到的双峰催化剂的 SEM 图像。

[0028] 图 15A 为具有 500nm 标度的从 Fe-AAPyr 和 L90 与 EH5 二氧化硅的混合物得到的

三峰催化剂的 SEM 图像。

[0029] 图 15B 为具有 400nm 标度的从 Fe-AAPyr 和 L90 与 EH5 二氧化硅的混合物得到的三峰催化剂的 SEM 图像。

[0030] 图 15C 为具有 300nm 标度的从 Fe-AAPyr 和 L90 与 EH5 二氧化硅的混合物得到的三峰催化剂的 SEM 图像。

[0031] 图 16 为具有 500nm 标度的从 Fe-AAPyr 和 L90 与 M5 二氧化硅的混合物得到的双峰催化剂的 SEM 图像。

[0032] 图 17 为具有 500nm 标度的从 Fe-AAPyr 和 L90 与 LM130 二氧化硅的混合物得到的双峰催化剂的 SEM 图像。

[0033] 图 18 为从 Fe-AAPyr 和 L90 与 A200 二氧化硅的混合物得到的双峰催化剂的 SEM 图像。

[0034] 图 19 为从 Fe-AAPy 和 L90 与 A380 二氧化硅的混合物得到的双峰催化剂的 SEM 图像。

[0035] 图 20A 为从 Fe-AAPyr 和 M5 二氧化硅得到的球形催化剂的 SEM 图像。

[0036] 图 20B 为从 Fe-AAPyr 和 M5 二氧化硅得到的球形催化剂的另一个 SEM 图像。

[0037] 图 20C 为从 Fe-AAPyr 和 M5 二氧化硅得到的球形催化剂的另一个 SEM 图像。

[0038] 图 20E 为从 Fe-AAPyr 和 M5 二氧化硅得到的球形催化剂的另一个 SEM 图像。

[0039] 图 21 为图示说明从 Fe-AAPyr 和 HS5、L90 和 L90+EH5 二氧化硅制备的催化剂的 RDE 数据的氧还原的旋转圆盘电极电伏安图。

[0040] 图 22 为图示说明从 Fe-AAPyr 和 L90、LM130 和 L90+LM130 二氧化硅制备的催化剂的 RDE 数据的氧还原的旋转圆盘电极电伏安图。

[0041] 图 23 为图示说明从 Fe-AAPyr 和 L90、L90+A90 和 A90 二氧化硅制备的催化剂的 RDE 数据的氧还原的旋转圆盘电极电伏安图。

[0042] 图 24 为图示说明从 Fe-AAPyr 和 L90 和 L90+EH5 二氧化硅制备的催化剂的 RDE 数据的氧还原的旋转圆盘电极电伏安图。

[0043] 图 25 为图示说明从 Fe-AAPyr 和 L90、M5 和 L90+M5 二氧化硅制备的催化剂的 RDE 数据的氧还原的旋转圆盘电极电伏安图。

[0044] 图 26 为用本文所述方法制备的 Fe_3Co-AAPyr 催化剂的 SEM 图像。

[0045] 图 27 为用本文所述方法制备的 FeCo-AAPyr 催化剂的 SEM 图像。

[0046] 图 28 为用本文所述方法制备的 $FeCo_3$-AAPyr 催化剂的 SEM 图像。

[0047] 图 29A 为用本文所述方法制备的 $FeCu_3$-AAPyr 双金属催化剂的 SEM 图像。

[0048] 图 29B 为用本文所述方法制备的 $FeCu_3$-AAPyr 双金属催化剂的另一个 SEM 图像。

[0049] 图 30A 为用本文所述方法制备的 $FeMn_3$-AAPyr 双金属催化剂的 SEM 图像。

[0050] 图 30B 为用本文所述方法制备的 $FeMn_3$-AAPyr 双金属催化剂的另一个 SEM 图像。

[0051] 图 31A 为用本文所述方法制备的 $FeNi_3$-AAPyr 双金属催化剂的 SEM 图像。

[0052] 图 31B 为用本文所述方法制备的 $FeNi_3$-AAPyr 双金属催化剂的另一个 SEM 图像。

[0053] 图 32A 为用本文所述方法制备的 FeCoCu-AAPyr 三金属催化剂的 SEM 图像。

[0054] 图 32B 为用本文所述方法制备的 FeCoCu-AAPyr 三金属催化剂的另一个 SEM 图像。

[0055] 图 33A 为用本文所述方法制备的 FeCoMn-AAPyr 三金属催化剂的 SEM 图像。

[0056] 图 33B 为用本文所述方法制备的 FeCoMn-AAPyr 三金属催化剂的另一个 SEM 图像。

[0057] 图 34A 为用本文所述方法制备的 FeCuMn-AAPyr 三金属催化剂的 SEM 图像。

[0058] 图 34B 为用本文所述方法制备的 FeCuMn-AAPyr 三金属催化剂的另一个 SEM 图像。

[0059] 图 35 为图示说明 Fe_xCo_y-AAPyr 双金属催化剂与 Co-AAPyr 比较的氧还原的旋转圆盘电极电伏安图。

[0060] 图 36 为图示说明 Fe_xNi_y-AAPyr 双金属催化剂与 Ni-AAPyr 比较的氧还原的旋转圆盘电极电伏安图。

[0061] 图 37 为图示说明 Fe_xCu_y-AAPyr 双金属催化剂与 Cu-AAPyr 比较的氧还原的旋转圆盘电极电伏安图。

[0062] 图 38 为图示说明 Fe_xCr_y-AAPyr 双金属催化剂与 Cr-AAPyr 比较的氧还原的旋转圆盘电极电伏安图。

[0063] 图 39 为图示说明 Fe_xMn_y-AAPyr 双金属催化剂与 Mn-AAPyr 比较的氧还原的旋转圆盘电极电伏安图。

[0064] 图 40 为图示说明 FeM^IM^{II}-AAPyr 三金属催化剂的氧还原的旋转圆盘电极电伏安图。

[0065] 图 41 为根据本公开制备 M-N-C 催化剂的分批方法的示意图。

[0066] 图 42A 为具有 10μm 标度的在低表面积二氧化硅上制备的球形高度多孔 Fe-N-C 催化剂的 SEM 图像。

[0067] 图 42B 为具有 2μm 标度的在低表面积二氧化硅上制备的球形高度多孔 Fe-N-C 催化剂的 SEM 图像。

[0068] 图 42C 为具有 1μm 标度的在低表面积二氧化硅上制备的球形高度多孔 Fe-N-C 催化剂的 SEM 图像。

[0069] 图 42D 为具有 500nm 标度的在低表面积二氧化硅上制备的球形高度多孔 Fe-N-C 催化剂的 SEM 图像。

[0070] 图 43A 为具有 5μm 标度的在高表面积二氧化硅上制备的第一批球形高度多孔 Fe-N-C 催化剂的 SEM 图像。

[0071] 图 43B 为具有 2μm 标度的在高表面积二氧化硅上制备的第一批球形高度多孔 Fe-N-C 催化剂的 SEM 图像。

[0072] 图 43C 为具有 500nm 标度的在高表面积二氧化硅上制备的第一批球形高度多孔 Fe-N-C 催化剂的 SEM 图像。

[0073] 图 44A 为具有 3μm 标度的在高表面积二氧化硅上制备的第二批球形高度多孔 Fe-N-C 催化剂的 SEM 图像。

[0074] 图 44B 为具有 2μm 标度的在高表面积二氧化硅上制备的第二批球形高度多孔 Fe-N-C 催化剂的 SEM 图像。

[0075] 图 45 为图示说明球形 F-N-C 催化剂的 RDE 数据的氧还原的旋转圆盘电极电伏安图，所述催化剂通过当前所述方法在用 O_2 饱和的 0.5M H_2SO_4 中制备（催化剂负载：600 μ g cm^{-2}，1200RPM，5mV s^{-1}）。

[0076] 详述

根据一个实施方案，本公开提供新的催化剂及其制备方法。在形成 M-N-C 催化剂的先

前所述方法中，氮和碳源一般为具有初始催化活性的卟啉前体。然后通过用金属颗粒络合提高该初始催化活性。本公开依赖于意外和意料之外地发现能够通过用不具有初始催化活性的非卟啉前体作为氮和碳源合成 M-N-C 催化剂。适合的非催化非卟啉前体的实例包括但不必限于与铁形成络合物的低分子量前体，例如 4- 氨基安替比林 (4-aminoantipirine)、苯二胺、羟基琥珀酰亚胺、乙醇胺等。根据一些实施方案，由于其与铁络合的能力，可选择这种非催化前体。根据另外的其它实施方案，由于它们包含与具有初始催化活性的前体中的活性位点相同或相似的部分，可选择非催化前体，然后通过高温处理使其结晶结构稳定化。

[0077] 根据一个实施方案，本公开的 M-N-C 催化剂可通过以下制备 :将硝酸铁形式的铁前体和 4- 氨基安替比林 (AAPyr) 形式的 C-N 前体湿浸渍于热解法二氧化硅的牺牲性载体表面上。其它适合的铁前体包括但不限于硫酸铁、乙酸铁、氯化铁等。

[0078] 应了解，其它过渡金属可代替铁，例如 Ce、Cr、Cu、Mo、Ni、Ru、Ta、Ti、V、W 和 Zr，通过简单地使用那些替代金属的前体。示例性过渡金属前体包括但不限于硝酸铈、硝酸铬、硝酸铜、钼酸铵、硝酸镍、氯化钌、异丙醇钽、乙醇钛、硫酸钒、钨酸铵和硝酸锆。另外，根据一些实施方案并且如以下更详细描述，当前所述方法可用两种或更多种金属的前体制备多金属催化剂。

[0079] 适合的牺牲性载体包括但不限于二氧化硅、沸石、氧化铝等。载体可以为以下形式 :球体、颗粒或其它二维或三维的规则、不规则或无定形形状。球体、颗粒或其它形状可以为单分散，或者不规则尺寸。球体、颗粒或其它形状可有或者可没有孔，这些孔可以为相同或不同的尺寸和形状。

[0080] 应了解并且如以下更详细地描述，可根据电催化剂材料内空隙的期望形状和大小选择二氧化硅颗粒的尺寸和形状。因此，通过选择二氧化硅颗粒的具体粒径和形状，可制备具有可预测尺寸和形状的空隙的电催化剂。例如，如果二氧化硅颗粒为球体，则电催化剂将包含多个球状空隙。本领域的技术人员应熟悉电催化剂 Pt-Ru 黑，其由多个铂 - 钌合金球体组成。利用上述方法由使用二氧化硅球体形成的电催化剂看起来像 Pt-Ru 黑的负像，在 Pt-Ru 黑中作为空隙存在的空间被金属电催化剂填充，在 Pt-Ru 黑中作为金属电催化剂存在的空间是空隙。

[0081] 如上所述，根据一些实施方案，可使用任何直径的二氧化硅球体。在一些优选的实施方案中，可使用具有 1nm-100nm 特征长度的二氧化硅颗粒，在更优选的实施方案中，可使用具有 100nm-1000nm 特征长度的二氧化硅颗粒，在其它优选的实施方案中，可使用具有 1mm-10mm 特征长度的二氧化硅颗粒。也可在模板化合成方法中使用其它中孔二氧化硅。在此情况下，模板化包括插入材料的中孔，产生具有 2-20nm 范围孔隙性的自担载电催化剂。在一个具体实施方案中，二氧化硅模板为 Cabosil 无定形热解法二氧化硅 ($325m^2/g$)。如上所述，由于球体用作形成电催化剂的模板，在使用具有 20nm 平均直径的二氧化硅颗粒的实施方案中，电催化剂中的球状空隙一般具有约 20nm 的直径。本领域的技术人员应熟悉多种市售可得的二氧化硅颗粒，并且可使用这些颗粒。或者，为了得到期望形状和 / 或尺寸的颗粒，可利用形成二氧化硅颗粒的已知方法。

[0082] 在牺牲性载体上沉积和 / 或浸渍 C-N 和金属前体后，将催化剂在惰性气氛例如 N_2、Ar 或 He 中热处理，或者在反应性气氛例如 NH_3 或乙腈中热处理。在 C-N 前体富氮时，一般使用惰性气氛，因为惰性气氛使得能够产生具有 Fe(或其它金属)N4 中心的大量活性位

点。然而，如果 C-N 前体富碳且贫氮，则可能期望使用富氮气氛，因为富氮气氛使得能够产生 Fe（或其它金属）N4 中心。

[0083] 根据一个实施方案，热处理的最佳温度为 500-1100℃。根据一些实施方案，在 800-900℃热处理是优选的，因为此温度高得足以使材料热解，但一般不高到足以破坏活性位点。

[0084] 在热处理后，用适合方法去除牺牲性载体。例如，可通过化学浸蚀去除牺牲性载体。适合的浸蚀剂的实例包括 NaOH、KOH 和 HF。根据一些实施方案，可优选使用 KOH，因为它使所有的金属和金属氧化物保持在催化剂中，并且如果这些物类为催化活性，则使用 KOH 可实际提高催化活性。或者，在一些实施方案中，HF 可能是优选的，因为它很具侵蚀性，并且可用来从催化剂表面去除一些毒性物类。因此，本领域的技术人员应能够根据要形成的具体催化材料的特定需求选择期望的浸蚀剂。

[0085] 根据一个具体示例性实施方案，通过将铁和氨基安替比林前体湿浸渍于热解法二氧化硅 (Cab-O-Sil™ EH-5，表面积：~400m^2 g^{-1}) 的表面上，制备 Fe-AAPyr 催化剂。首先，用声浴在水中分散 1g 二氧化硅。然后，将 1g AAPyr 在水中的溶液加入到二氧化硅，并超声处理 20 分钟。然后，将 1g 硝酸铁 ($Fe(NO_3)_3 \cdot 9H_2O$, Sigma-Aldrich) 的水溶液加入到 SiO_2-AAPyr 溶液，随后在声浴中超声处理 8 小时。超声处理后，使二氧化硅和 Fe-AApyr 的粘性溶液在 T=85℃干燥过夜。将固体在玛瑙研钵中研磨成细粉，然后经受热处理 (HT)。HT 条件为：UHP N_2 气氛以 100cc min^{-1} 速率流动，HT 温度 800℃，HT 温度坡道速率 10℃ min^{-1}，HT 持续时间 1 小时。

[0086] 图 1-2 图示说明用本文所述方法制备的所选 M-N-C 催化剂的结构和形态数据。

[0087] 图 1 为 X- 射线衍射图，图示说明用硝酸铁作为金属源和用 AAPyr 作为氮和碳源制备的 Fe-M-C 催化剂主要由嵌入碳基质的铁的纳米颗粒（小于 2nm）组成。

[0088] 图 2 为用本文所述方法制备的 Fe-AApyr 催化剂的 SEM 图像，图示说明这种材料具有约 50-70nm 孔径的高度发达多孔结构。相信孔隙性使催化性能向氧还原提高。

[0089] 图 3 和 4 显示氧还原试验的结果，因此证明本文所述材料的效用。

[0090] 图 3 为图示说明 Fe-AApyr 催化剂的氧还原的旋转圆盘电极电伏安图，所述催化剂在用 O_2 饱和的 0.5M H_2SO_4 中用不同量的氨基安替比林前体制备（催化剂负载 160mg cm^{-2}，1600RPM，扫描速率 20mV s^{-1}）。

[0091] 图 4 为图示说明 Fe-AApyr 的氧还原的旋转圆盘电极电伏安图，所述 Fe-AApyr 在用 O_2 饱和的 0.5M H_2SO_4 中以多种热处理温度制备（催化剂负载：160mg cm^{-2}，1600RPM，扫描速率 20mV s^{-1}）。

[0092] 反应试验证明，用廉价杂原子胺前体和本文所述方法制备的 M-N-C 催化剂在碱性和酸介质两者中具有高活性，因此，在中性 pH 也应为活性。

[0093] 图 5-8 图示说明如本文所述制备的催化剂的机理研究，并显示低 H_2O_2 产率，因此表明通过更有效的 4 电子机制进行的反应途径。

[0094] 图 5 为对于 Fe-AAPyr 催化剂，参与 ORR 的电子数的曲线图，在用 O_2 饱和的 0.5M H_2SO_4 中利用不同量的氨基安替比林前体（催化剂负载：160mg cm^{-2}，1600RPM，20mV s^{-1}）。

[0095] 图 6 为 Fe-AAPyr 催化剂的过氧化氢产率的曲线图，所述催化剂在 O_2 饱和的 0.5M H_2SO_4 中用不同量的氨基安替比林前体制备（催化剂负载：160mg cm^{-2}，1600RPM，20mV s^{-1}）。

[0096] 图 7 为对于 Fe-AAPyr 催化剂，参与 ORR 的电子数的曲线图，所述催化剂在用 O_2 饱和的 0.5M H_2SO_4 中利用不同的热处理温度制备（催化剂负载：160mg cm^{-2}，1600RPM，20mV s^{-1}）。

[0097] 图 8 为对于 Fe-AAPyr 的过氧化氢产率的曲线图，所述 Fe-AAPyr 在 O_2 饱和的 0.5M H_2SO_4 中用不同的热处理温度制备（催化剂填负载：160mg cm^{-2}，1600RPM，20mV s^{-1}）。

[0098] 如上所述，氧还原的机制显示氧通过优选的 4 电子途径直接还原成水，从而避免腐蚀性过氧化物产生，因此提高所得催化剂的稳定性和耐久性。

[0099] 如图 3、5 和 6 中所示，通过选择含氮前体用于制备方法的量，可改变所得催化剂的性质。通常，催化剂中氮的浓度越高，在 ORR 中的活性越高。另外，如图 4、7 和 8 中所示，通过改变热处理温度，也可改变催化剂的性质。应了解，期望对过渡金属和 C-N 前体的各组合优化热处理温度，因为太低的温度将不产生活性位点，太高的温度将使材料分解。

[0100] 如上所述，可用当前所述方法由非铁金属制备催化剂，例如 Co、Ni、Cu、Cr、Mn 等。

[0101] 作为一个具体非限制性实例，通过将铁和氨基安替比林前体湿浸渍于热解法二氧化硅 (Cab-O-Sil™ EH-5，表面积：~400m^2 g^{-1}) 的表面上，制备 Fe-AAPyr 催化剂。首先，用声浴在水中分散 1g 二氧化硅。然后，将 1g AAPyr 在水中的溶液加入到二氧化硅，并超声处理 20 分钟。然后，将 1g 硝酸铁 ($Fe(NO_3)_3 \cdot 9H_2O$, Sigma-Aldrich) 的水溶液加入到 SiO_2-AAPyr 溶液，随后在声浴中超声处理 8 小时。超声处理后，使二氧化硅和 Fe-AApyr 的粘性溶液在 T=85℃干燥过夜。将固体在玛瑙研钵中研磨成细粉，然后经受热处理 (HT)。HT 条件为：UHP N_2 气氛以 100cc min^{-1} 速率流动，HT 温度 800℃，HT 温度坡道 10℃ min^{-1}，HT 持续时间 1 小时。

[0102] 根据另一个非限制性实例，通过将铁、锰和氨基安替比林前体湿浸渍于热解法二氧化硅 (Cab-O-Sil™ EH-5，表面积：~400m^2 g^{-1}) 的表面上，制备 Fe-Mn-AAPyr 催化剂。首先，用声浴在水中分散 3g 二氧化硅。然后，将 1.98g AAPyr 在水中的溶液加入到二氧化硅，并超声处理 20 分钟。然后，将 1.4g 硝酸铁 ($Fe(NO_3)_3 \cdot 9H_2O$, Sigma-Aldrich) 和 3.2g 硝酸锰的水溶液加入到 SiO_2-AAPyr 溶液，随后在声浴中超声处理 8 小时。超声处理后，使二氧化硅和 Fe-Mn-AApyr 的粘性溶液在 T=85℃干燥过夜。将固体在玛瑙研钵中研磨成细粉，然后经受热处理 (HT)。HT 条件为：UHP N_2 气氛以 100cc min^{-1} 速率流动，HT 温度 800℃，HT 温度坡道 10℃ min^{-1}，HT 持续时间 1 小时。

[0103] 根据另一个非限制性实施方案，通过将铁和氨基安替比林前体湿浸渍于热解法二氧化硅 (Cab-O-Sil™ EH-5，表面积：~400m^2 g^{-1}) 的表面上，制备 Fe-Cr-AAPyr 催化剂。首先，用声浴在水中分散 2g 二氧化硅。然后，将 3.5g AAPyr 在水中的溶液加入到二氧化硅，并超声处理 20 分钟。然后，将 1g 硝酸铁 ($Fe(NO_3)_3 \cdot 9H_2O$, Sigma-Aldrich) 和 1.25g 硝酸铬的水溶液加入到 SiO_2-AAPyr 溶液，随后在声浴中超声处理 8 小时。超声处理后，使二氧化硅和 Fe-AApyr 的粘性溶液在 T=85℃干燥过夜。将固体在玛瑙研钵中研磨成细粉，然后经受热处理 (HT)。HT 条件为：UHP N_2 气氛以 100cc min^{-1} 速率流动，HT 温度 850℃，HT 温度坡道 10℃ min^{-1}，HT 持续时间 4 小时。

[0104] 根据一个实施方案，可采用促进杂原子原子和载体的电荷转移的方式使本文所述 M-N-C 催化剂沉积于传导性分散载体（碳和非碳两者）上。根据一些实施方案，使用非碳载体，如传导性 Mo 或 W 氧化物，可显著减少过氧化氢产生，提高催化剂在酸和碱性介质中的耐

久性和稳定性。

[0105] 如上所述，不同尺寸和形状的牺牲性载体可一起用于产生具有多种不同形态的催化剂。例如，在一些实施方案中，可期望制备具有多峰孔隙性的催化剂，即，其中催化剂包含两个或更多个不同的孔群，其中各群由具有可与其它群区分的平均直径的孔组成。例如，具有约 10nm 平均直径的一个孔群、具有约 50nm 平均直径的第二孔群和具有 150-200nm 之间平均直径的第三孔群的催化剂被认为具有多峰孔径分布。

[0106] 转向图 9，根据一个实施方案，通过使上述前体在由具有不同直径的球体（或其它形状颗粒）形成的牺牲性载体上模板化，可产生这种多峰孔径分布。如图所示，具有直径 d1 的较大球体 10 和具有直径 d2 的较小球体 12 一起混合形成牺牲性载体，在载体上前体材料沉积并热解。一旦去除载体，得到的催化材料 16 包含对应于不同粒径的不同尺寸的孔 18、20。

[0107] 应了解，为了完全控制所得催化材料的形态，期望使前体模板化到具有已知形状和尺寸的牺牲性载体中。根据从二氧化硅颗粒形成牺牲性载体的一个具体实施方案，通过用不同类型的二氧化硅可靠和可再现地产生不同尺寸的二氧化硅颗粒，可制备不同形状和粒径的牺牲性载体。因此，所得催化剂具有多峰孔分布，其中孔的具体尺寸和形状是已知的。

[0108] 根据一个具体实例，通过将铁和氨基安替比林前体湿浸渍于不同的热解法二氧化硅及其混合物 (Cab-O-Sil™表面积 90-400m^2 g^{-1}) 的表面上，制备本文所述在 EH5 和 LM130 二氧化硅上形成的催化剂。首先，用声浴在水中分散 1g 二氧化硅 EH5 和 1g 二氧化硅 LM130。然后，将 1g AAPyr 在水中的溶液加入到二氧化硅，并超声处理 20 分钟。然后，将 1g 硝酸铁 ($Fe(NO_3)_3 \cdot 9H_2O$, Sigma-Aldrich) 的水溶液加入到 SiO_2-AAPyr 溶液，随后在声浴中超声处理 8 小时。超声处理后，使二氧化硅和 Fe-AApyr 的粘性溶液在 T=85℃干燥过夜。将固体在玛瑙研钵中研磨成细粉，然后经受热处理 (HT)。HT 条件为：UHP N_2 气氛以 100cc min^{-1} 速率流动，HT 温度 800℃，HT 温度坡道 10℃ min^{-1}，HT 持续时间 1 小时。

[0109] 根据另一个具体实例，通过将铁和氨基安替比林前体湿浸渍于不同的热解法二氧化硅及其混合物 (Cab-O-Sil™表面积 90-400m^2 g^{-1}) 的表面上，制备本文所述在 M5D 和 A90 二氧化硅上形成的催化剂。首先，用声浴在水中分散 2g 二氧化硅 M5D 和 0.25g 二氧化硅 A90。然后，将 1.3g AAPyr 在水中的溶液加入到二氧化硅，并超声处理 20 分钟。然后，将 4g 硝酸铁 ($Fe(NO_3)_3 \cdot 9H_2O$, Sigma-Aldrich) 的水溶液加入到 SiO_2-AAPyr 溶液，随后在声浴中超声处理 8 小时。超声处理后，使二氧化硅和 Fe-AApyr 的粘性溶液在 T=85℃干燥过夜。将固体在玛瑙研钵中研磨成细粉，然后经受热处理 (HT)。HT 条件为：UHP N_2 气氛以 100cc min^{-1} 速率流动，HT 温度 800℃，HT 温度坡道 10℃ min^{-1}，HT 持续时间 1 小时。

[0110] 图 10-20 描绘具有多峰孔隙率并且如本文所述制备的不同 M-N-C 催化剂的形态数据。

[0111] 图 10 为从 Fe-AAPyr 和 HS5 二氧化硅得到的单峰催化剂的 SEM 图像。可以看到，孔径在 40-60nm 的范围内。

[0112] 图 11 为从 Fe-AAPyr 和 M5 二氧化硅得到的双峰催化剂的 SEM 图像。可以看到，第一类型的孔具有直径 40-60nm，而第二类型的孔具有直径 <10nm。

[0113] 图 12 为从 Fe-AAPyr 和 LM130 二氧化硅得到的双峰催化剂的 SEM 图像。可以看到，

第一类型的孔具有直径~100nm，而第二类型的孔具有直径~30nm。

[0114] 图13为从Fe-AAPyr和A90二氧化硅得到的催化剂的SEM图像。可以看到，孔具有直径~30nm，同时也有直径40-60nm的纳米通道。

[0115] 图14为从Fe-AAPyr和L90与A90二氧化硅的混合物得到的双峰催化剂的SEM图像。可以看到，第一类型的孔具有直径~150nm，而第二类型的孔具有直径~20nm。

[0116] 图15为从Fe-AAPyr和L90与EH5二氧化硅的混合物得到的三峰催化剂的SEM图像。可以看到，第一类型的孔具有直径~150-200nm，第二类型的孔具有直径~40-60nm，第三类为约20nm。

[0117] 图16为从Fe-AAPyr和L90与M5二氧化硅的混合物得到的双峰催化剂的SEM图像。可以看到，第一类型的孔具有直径~100nm，而第二类型的孔具有直径~25nm。

[0118] 图17为从Fe-AAPyr和L90与LM130二氧化硅的混合物得到的双峰催化剂的SEM图像。可以看到，第一类型的孔具有直径~150-200nm，而第二类型的孔具有直径~30nm。

[0119] 图18为从Fe-AAPyr和L90与A200二氧化硅的混合物得到的双峰催化剂的SEM图像。可以看到，第一类型的孔具有直径~100-200nm，而第二类型的孔具有直径~50nm。

[0120] 图19为从Fe-AAPy和L90与A380二氧化硅的混合物得到的双峰催化剂的SEM图像。可以看到，第一类型的孔具有直径~100nm，而第二类型的孔具有直径<20nm。

[0121] 图20为从Fe-AAPyr和M5二氧化硅得到的球形催化剂的SEM图像。可以看到，催化剂球体在1-3μm的范围内，而孔具有直径约50-70nm。

[0122] 图21-25显示对于选择图10-20中多峰催化剂的氧还原试验的结果，因此证明本文所述材料的效用。

[0123] 图21为图示说明催化剂的RDE数据的氧还原的旋转圆盘电极电伏安图，所述催化剂在用O_2饱和的0.5M H_2SO_4中由Fe-AAPyr和HS5、L90和L90+EH5二氧化硅制备（催化剂负载：600mg cm^{-2}，1200RPM，5mV s^{-1}）。

[0124] 图22为图示说明催化剂的RDE数据的氧还原的旋转圆盘电极电伏安图，所述催化剂在用O_2饱和的0.5M H_2SO_4中由Fe-AAPyr和L90、LM130和L90+LM130二氧化硅制备（催化剂负载：600mg cm^{-2}，1200RPM，5mV s^{-1}）。

[0125] 图23为图示说明催化剂的RDE数据的氧还原的旋转圆盘电极电伏安图，所述催化剂在用O_2饱和的0.5M H_2SO_4中由Fe-AAPyr和L90、L90+A90和A90二氧化硅制备（催化剂负载：600mg cm^{-2}，1200RPM，5mV s^{-1}）。

[0126] 图24为图示说明催化剂的RDE数据的氧还原的旋转圆盘电极电伏安图，所述催化剂在用O_2饱和的0.5M H_2SO_4中由Fe-AAPyr和L90和L90+EH5二氧化硅制备（催化剂负载：600mg cm^{-2}，1200RPM，5mV s^{-1}）。

[0127] 图25为图示说明催化剂的RDE数据的氧还原的旋转圆盘电极电伏安图，所述催化剂在用O_2饱和的0.5M H_2SO_4中由Fe-AAPyr和L90、M5和L90+M5二氧化硅制备（催化剂负载：600mg cm^{-2}，1200RPM，5mV s^{-1}）。

[0128] 应了解，在一些应用中，单金属催化剂可能不够稳定或活性，以至于不能代替传统基于铂或铂合金的催化剂。因此，如上所示，根据一些实施方案，当前所述方法可结合使用多种金属的前体，以达到期望的稳定性和/或活性。

[0129] 根据不同的具体实施方案，通过将铁和第二过渡金属或铁、第二和第三过渡

金属（过渡金属 =Co、Ni、Cu、Cr 和 Mn）和氨基安替比林前体湿浸渍于热解法二氧化硅 (Cab-O-Sil™ EH-5，表面积：~400m^2 g^{-1}) 的表面上，制备 Fe-AAPyr 催化剂。首先，用声浴在水中分散 1g 二氧化硅。然后，将 1g AAPyr 在水中的溶液加入到二氧化硅，并超声处理 20 分钟。然后，将 1g 硝酸铁 ($Fe(NO_3)_3 \cdot 9H_2O$, Sigma-Aldrich) 和 1g 硝酸锰的水溶液加入到 SiO_2-AAPyr 溶液，随后在声浴中超声处理 8 小时。超声处理后，使二氧化硅和 Fe-Mn-AApyr 的粘性溶液在 T=85℃干燥过夜。将固体在玛瑙研钵中研磨成细粉，然后经受热处理 (HT)。HT 条件为：UHP N_2 气氛以 100cc min^{-1} 速率流动，HT 温度 800℃，HT 温度坡道 10℃ min^{-1}，HT 持续时间 1 小时。

[0130] 图 26-34 图示说明用上述方法制备的所选多金属 M-N-C 催化剂的结构和形态数据。

[0131] 图 26-28 分别显示用本文所述方法制备的三种不同催化剂 Fe_3Co-AAPyr、FeCo-AAPyr 和 $FeCo_3$-AAPyr。这些材料具有约 100nm 孔径的高度发达多孔结构。

[0132] 图 29A 和 B 为 $FeCu_3$-AAPyr 双金属催化剂的 SEM 图像，图示说明这种材料具有约 70nm 孔径的高度发达多孔结构。

[0133] 图 30A 和 B 为 $FeMn_3$-AAPyr 双金属催化剂的 SEM 图像，图示说明这种材料具有约 50nm 孔径的高度发达多孔结构。

[0134] 图 31A 和 B 为 $FeNi_3$-AAPyr 双金属催化剂的 SEM 图像，图示说明这种材料具有约 200nm 孔径的高度发达多孔结构。

[0135] 图 32A 和 B 为 FeCoCu-AAPyr 三金属催化剂的 SEM 图像，图示说明这种材料具有约 150nm 孔径的高度发达多孔结构。

[0136] 图 33A 和 B 为 FeCoMn-AAPyr 三金属催化剂的 SEM 图像，图示说明这种材料具有约 100nm 孔径的高度发达多孔结构。

[0137] 图 34A 和 B 为 FeCuMn-AAPyr 三金属催化剂的 SEM 图像，图示说明这种材料具有约 100nm 孔径的高度发达多孔结构。

[0138] 本文所述多金属催化剂的效用由图 35-40 中图示说明的氧还原试验的结果证明。

[0139] 图 35 为图示说明在用 O_2 饱和的 0.5M H_2SO_4 中的 Fe_xCo_y-AAPyr 双金属催化剂与 Co-AAPyr 比较的氧还原的旋转圆盘电极电伏安图（催化剂负载：600mg cm^{-2}，1200RPM，5mV s^{-1}）。

[0140] 图 36 为图示说明在用 O_2 饱和的 0.5M H_2SO_4 中的 Fe_xNi_y-AAPyr 双金属催化剂与 Ni-AAPyr 比较的氧还原的旋转圆盘电极电伏安图（催化剂负载：600mg cm^{-2}，1200RPM，5mV s^{-1}）。

[0141] 图 37 为图示说明在用 O_2 饱和的 0.5M H_2SO_4 中的 Fe_xCu_y-AAPyr 双金属催化剂与 Cu-AAPyr 比较的氧还原的旋转圆盘电极电伏安图（催化剂负载：600mg cm^{-2}，1200RPM，5mV s^{-1}）。

[0142] 图 38 为图示说明在用 O_2 饱和的 0.5M H_2SO_4 中的 Fe_xCr_y-AAPyr 双金属催化剂与 Cr-AAPyr 比较的氧还原的旋转圆盘电极电伏安图（催化剂负载：600mg cm^{-2}，1200RPM，5mV s^{-1}）。

[0143] 图 39 为图示说明在用 O_2 饱和的 0.5M H_2SO_4 中的 Fe_xMn_y-AAPyr 双金属催化剂与 Mn-AAPyr 比较的氧还原的旋转圆盘电极电伏安图（催化剂负载：600mg cm^{-2}，1200RPM，5mV

s^{-1})。

[0144] 图 40 为图示说明在用 O_2 饱和的 0.5M H_2SO_4 中 $FeM^{I}M^{II}$-AAPyr 三金属催化剂的氧还原的旋转圆盘电极电伏安图（催化剂负载：600mg cm^{-2}，1200RPM，5mV s^{-1}）。

[0145] 这些反应试验证明，用本文所述方法从廉价 C-N 前体制备的多金属 M-N-C 催化剂具有显著高于单金属催化剂的活性。这种高活性使这些材料适合作为阴极催化剂用于燃料电池，因为它们在碱性、中性和酸环境具有高 ORR 活性。

[0146] 根据一些实施方案，可期望例如在分批过程中制备大量本文所述的催化剂。因此，本公开还提供一种大规模制备当前所述催化剂的方法。根据一个实施方案，本公开提供将基于牺牲性载体的方法与喷雾热解组合以制备自担载催化剂的方法。根据此方法，喷雾热解方法是一种连续方法，而基于牺牲性载体的方法分批进行。转向图 41，可以看到，使上述前体材料与二氧化硅载体混合，雾化，并在管式炉中干燥。然后，在滤器上收集从该工序得到的粉末。然后，根据催化剂的期望应用，视需要热处理收集的粉末。最后，例如通过用 HF 或 KOH 浸出，去除牺牲性载体。

[0147] 应了解，上述大规模制备方法适用于宽范围前体和材料，因此，不必限于本文公开的催化剂。图 42-44 图示说明用上述方法制备的所选自担载金属－氮－碳 (M-N-C) 催化剂的形态数据。

[0148] 图 42A-D 为在低表面积二氧化硅上制备的球形高度多孔 Fe-N-C 催化剂的 SEM 图像。

[0149] 图 43A-C 为在高表面积二氧化硅上制备的球形高度多孔 Fe-N-C 催化剂的 SEM 图像（批次 1）。

[0150] 图 44 为在高表面积二氧化硅上制备的球形高度多孔 Fe-N-C 催化剂的 SEM 图像（批次 2）。

[0151] 图 45 为图示说明球形 F-N-C 催化剂的 RDE 数据的氧还原的旋转圆盘电极电伏安图，所述催化剂通过当前所述方法在用 O_2 饱和的 0.5M H_2SO_4 中制备（催化剂负载：600 μg cm^{-2}，1200RPM，5mV s^{-1}）。

[0152] 可清楚地看到，材料的形态性质在批次与批次间很一致。这些材料的效用在氧还原试验中证明，其实例显示于图 5 中。

[0153] 本文所述具体方法和组合物为优选实施方案的代表，并且为示例性，而不是旨在作为本发明范围的限制。本领域技术人员在思考本说明书时会想到其它目的、方面和实施方案，这些包含在权利要求范围限定的本发明的精神内。对本领域技术人员显而易见的是，可不脱离本发明的范围和精神地对本文公开的发明作出不同的替代和改进。本文适当地说明性描述的发明可在任何要素或限制不存在下实行，这未在本文作为要点明确公开。本文适当地说明性描述的方法和过程可按不同步骤次序实行，它们不必限于本文或权利要求中指明的步骤次序。如本文和所附权利要求中所用，单数形式“一个”和“该”包括复数对象，除非上下文另作明确指定。因此，例如，提及“一种催化剂”包括多种这些催化剂，等等。

[0154] 在任何情况下均不可将本专利解释成限于本文具体公开的特定实施例或实施方案或方法。在任何情况下均不可将本专利解释为受专利和商标局的任何审查员或任何其它职员或雇员作出的任何声明所限制，除非这些声明明确并且无限制或保留地由申请人在书面回应中采纳。

[0155] 已使用的术语和表达用作说明性而非限制性术语，使用这些术语和表达不旨在排除所显示和描述的特征或其部分的任何等价物，但应认识到，可在要求保护的本发明的范围内有各种改进。因此，应了解，虽然已通过优选实施方案和任选特征明确地公开了本发明，但本领域技术人员可对本文公开的概念采取修改和变化，应将这些修改和变化认为是在由所附权利要求限定的本发明的范围内。

[0156] 以下引用和／或本文提到的所有专利和出版物表示本发明所属领域的技术人员的技术水平，每个这些引用的专利或出版物通过引用结合到本文中，其程度等同于已经通过引用单独以其全文结合，或已经在本文中阐述其全文。申请人保留将任何和所有的材料和信息从任何这些引用的专利或出版物中在实体上引入本说明书的权利。

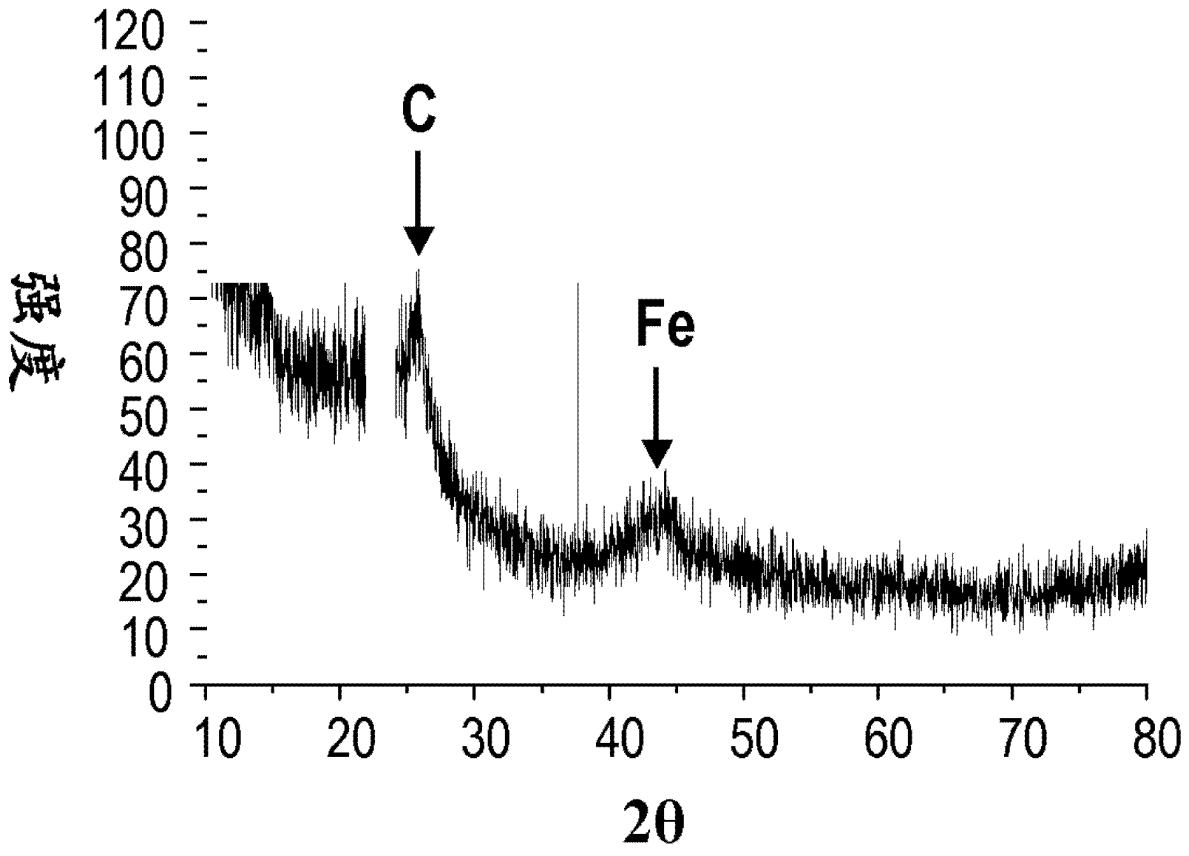
120
110
100
90
80
70
60
50
40
30
20
10
0
强度
C
Fe
10
20
30
40
50
60
70
80
2θ

图 1

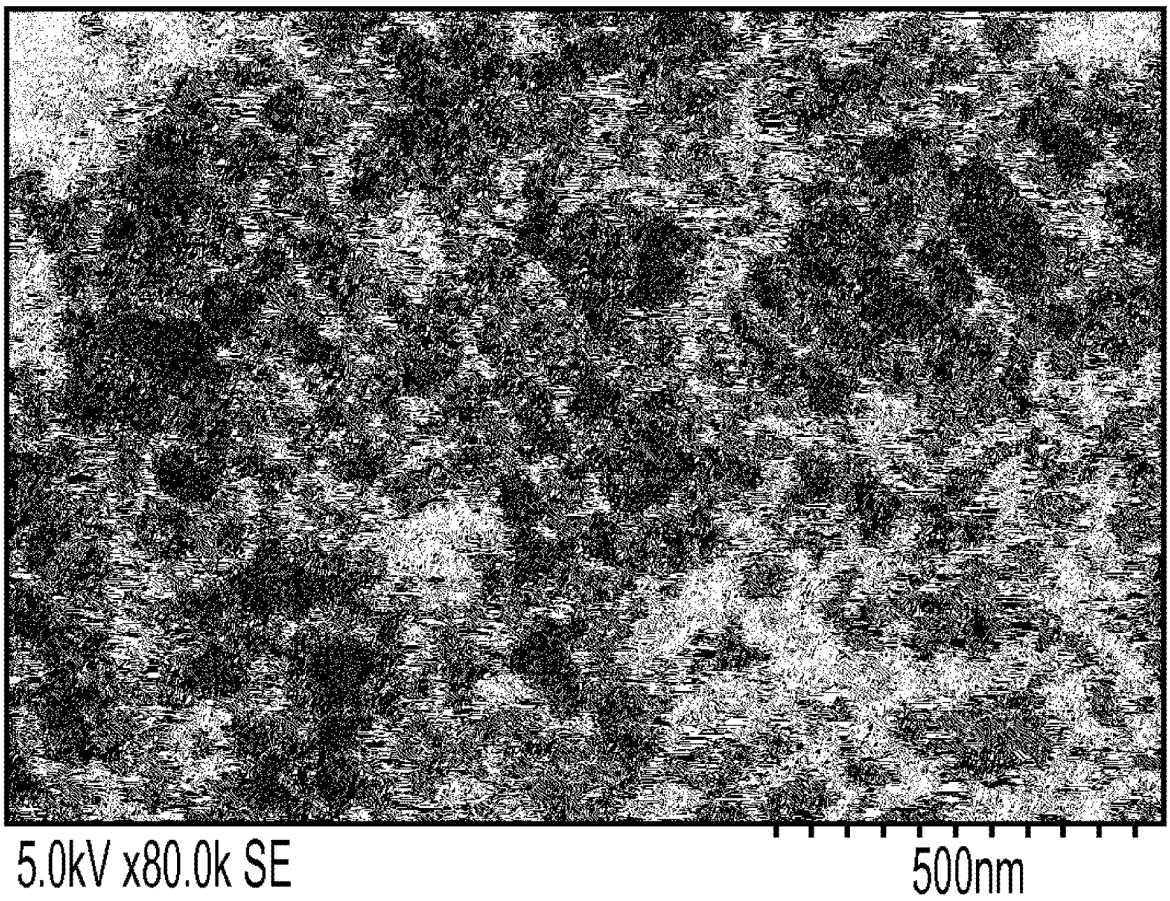

图 2

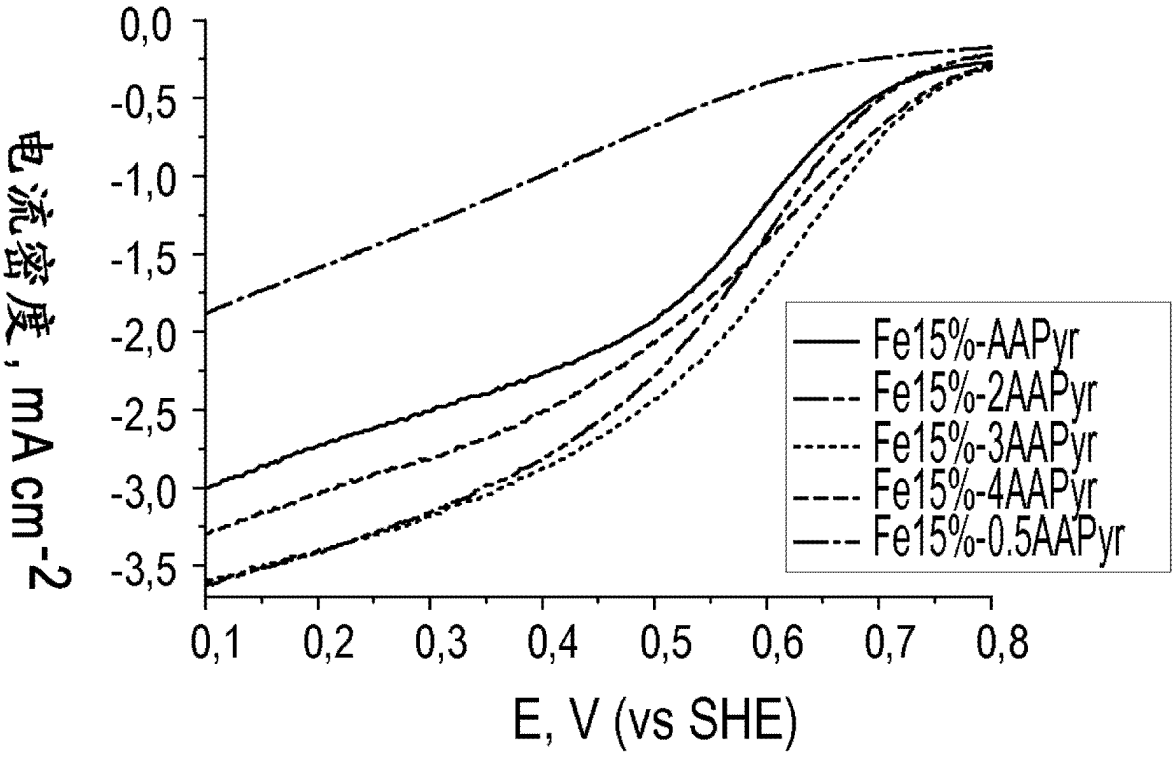
0,0
-0,5
-1,0
-1,5
-2,0
-2,5
-3,0
-3,5
电流密度，mA cm-2
0,1
0,2
0,3
0,4
0,5
0,6
0,7
0,8
E, V (vs SHE)
Fe15%-AAPyr
Fe15%-2AAPyr
Fe15%-3AAPyr
Fe15%-4AAPyr
Fe15%-0.5AAPyr

图 3

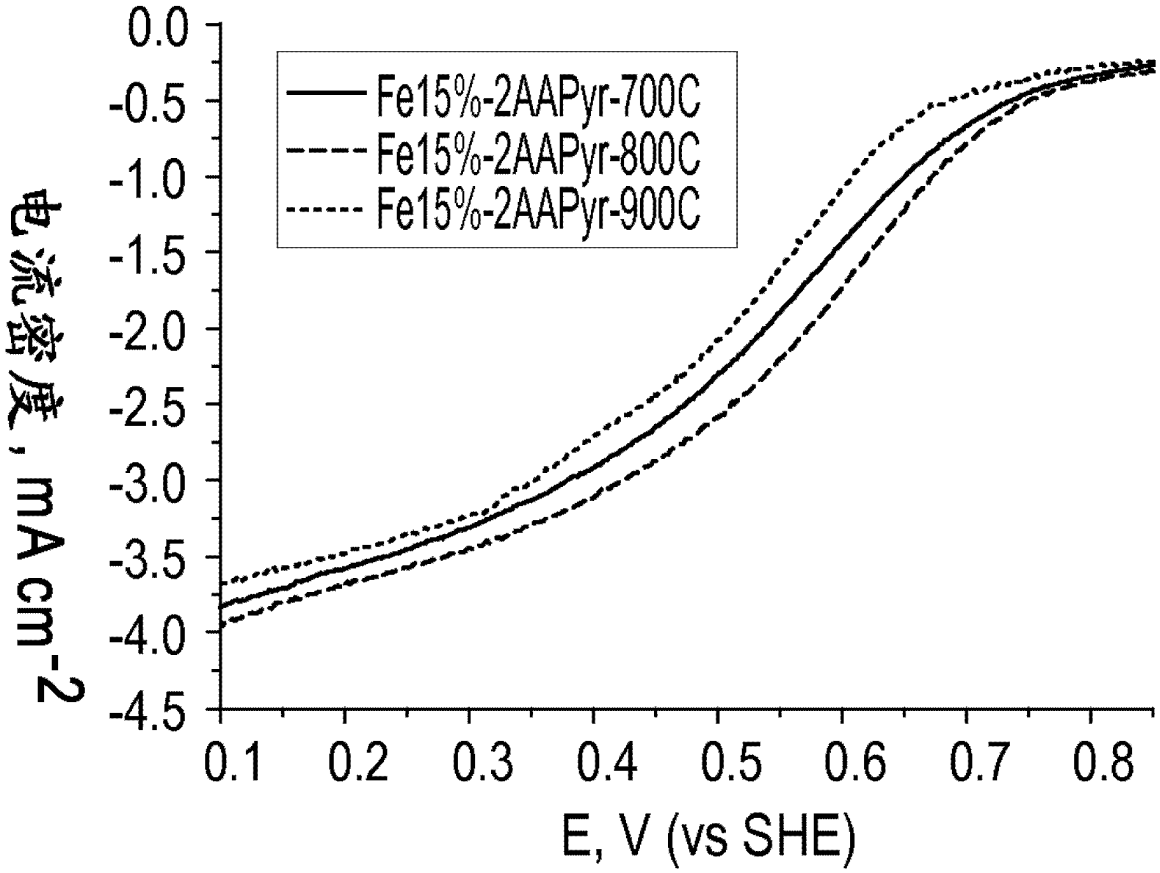
0.0
-0.5
-1.0
-1.5
-2.0
-2.5
-3.0
-3.5
-4.0
-4.5
电流密度，mA cm-2
0.1
0.2
0.3
0.4
0.5
0.6
0.7
0.8
E, V (vs SHE)
Fe15%-2AAPyr-700C
Fe15%-2AAPyr-800C
Fe15%-2AAPyr-900C

图 4

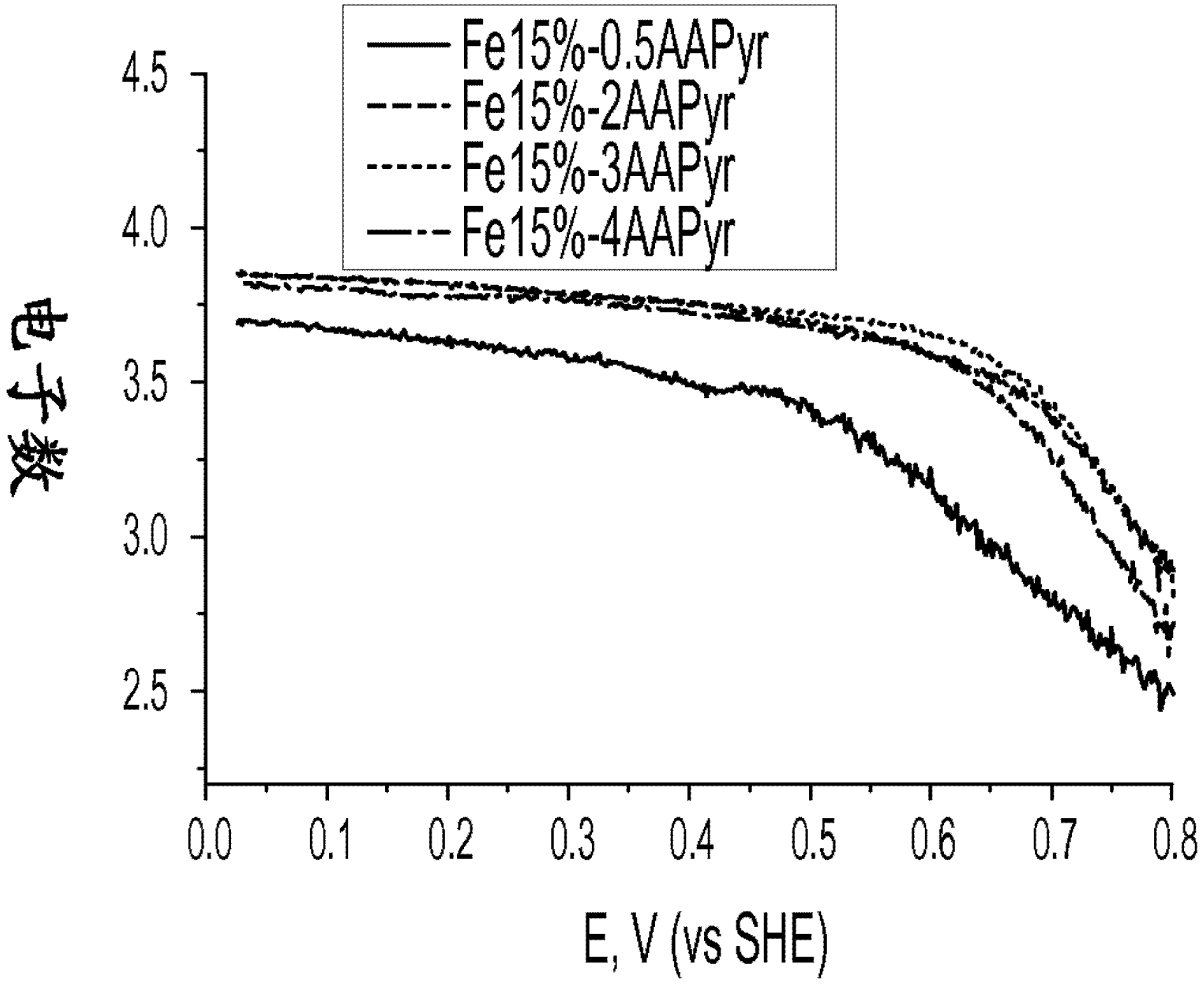
Fe15%-0.5AAPyr
Fe15%-2AAPyr
Fe15%-3AAPyr
Fe15%-4AAPyr
电子数
4.5
4.0
3.5
3.0
2.5
0.0
0.1
0.2
0.3
0.4
0.5
0.6
0.7
0.8
E, V (vs SHE)

图 5

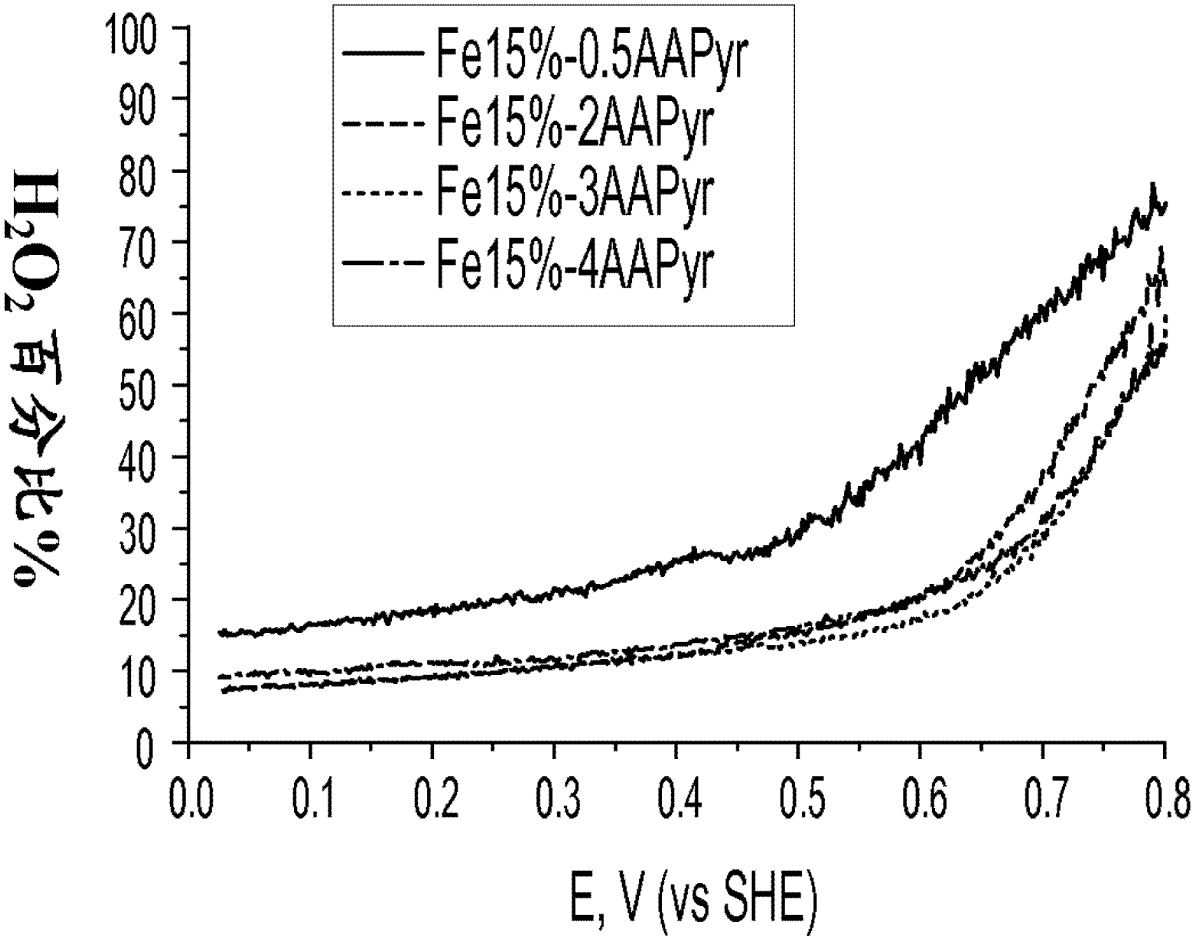
Fe15%-0.5AAPyr
Fe15%-2AAPyr
Fe15%-3AAPyr
Fe15%-4AAPyr
H2O2 百分比%
E, V (vs SHE)
0
10
20
30
40
50
60
70
80
90
100
0.0
0.1
0.2
0.3
0.4
0.5
0.6
0.7
0.8

图 6

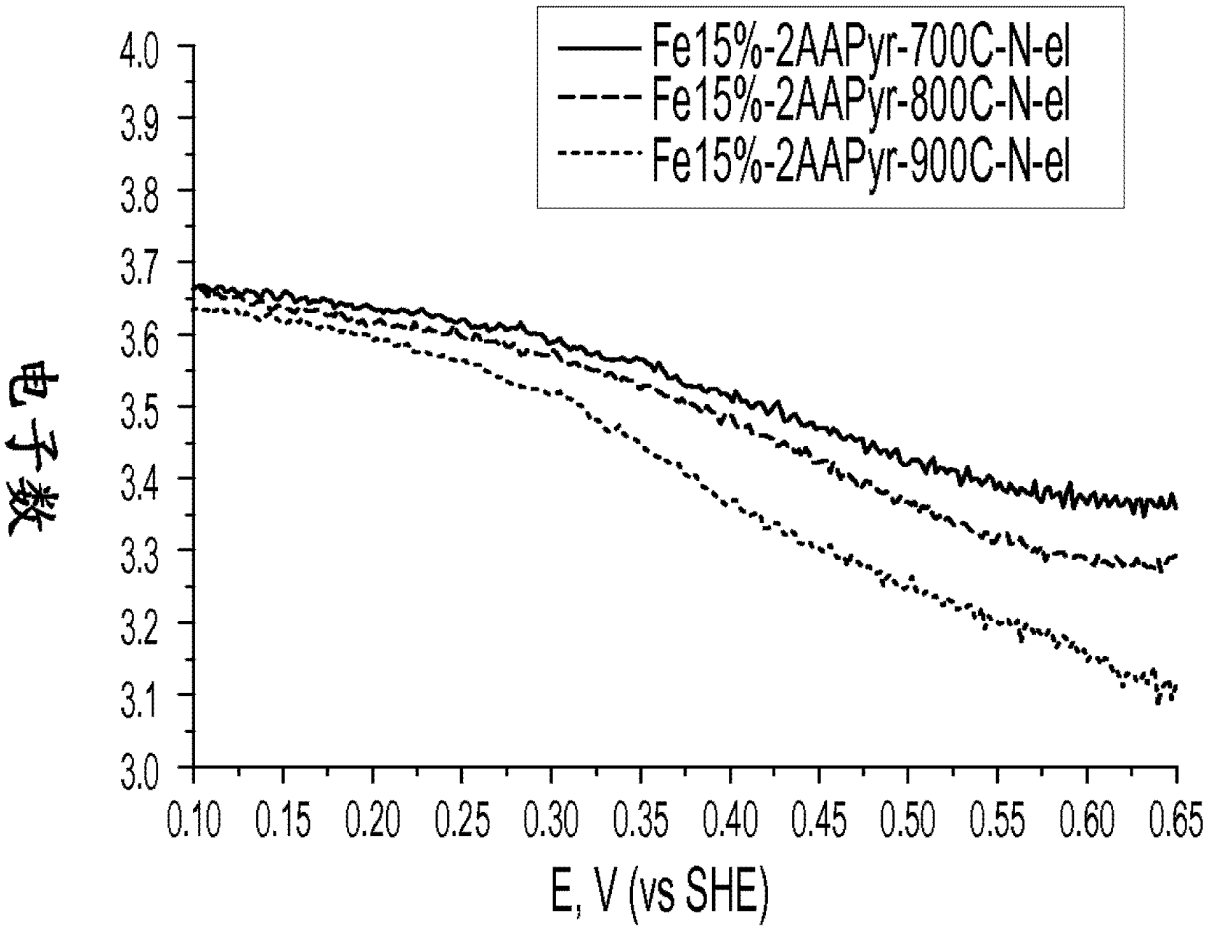
Fe15%-2AAPyr-700C-N-el
Fe15%-2AAPyr-800C-N-el
Fe15%-2AAPyr-900C-N-el
电子数
4.0
3.9
3.8
3.7
3.6
3.5
3.4
3.3
3.2
3.1
3.0
0.10
0.15
0.20
0.25
0.30
0.35
0.40
0.45
0.50
0.55
0.60
0.65
E, V (vs SHE)

图 7

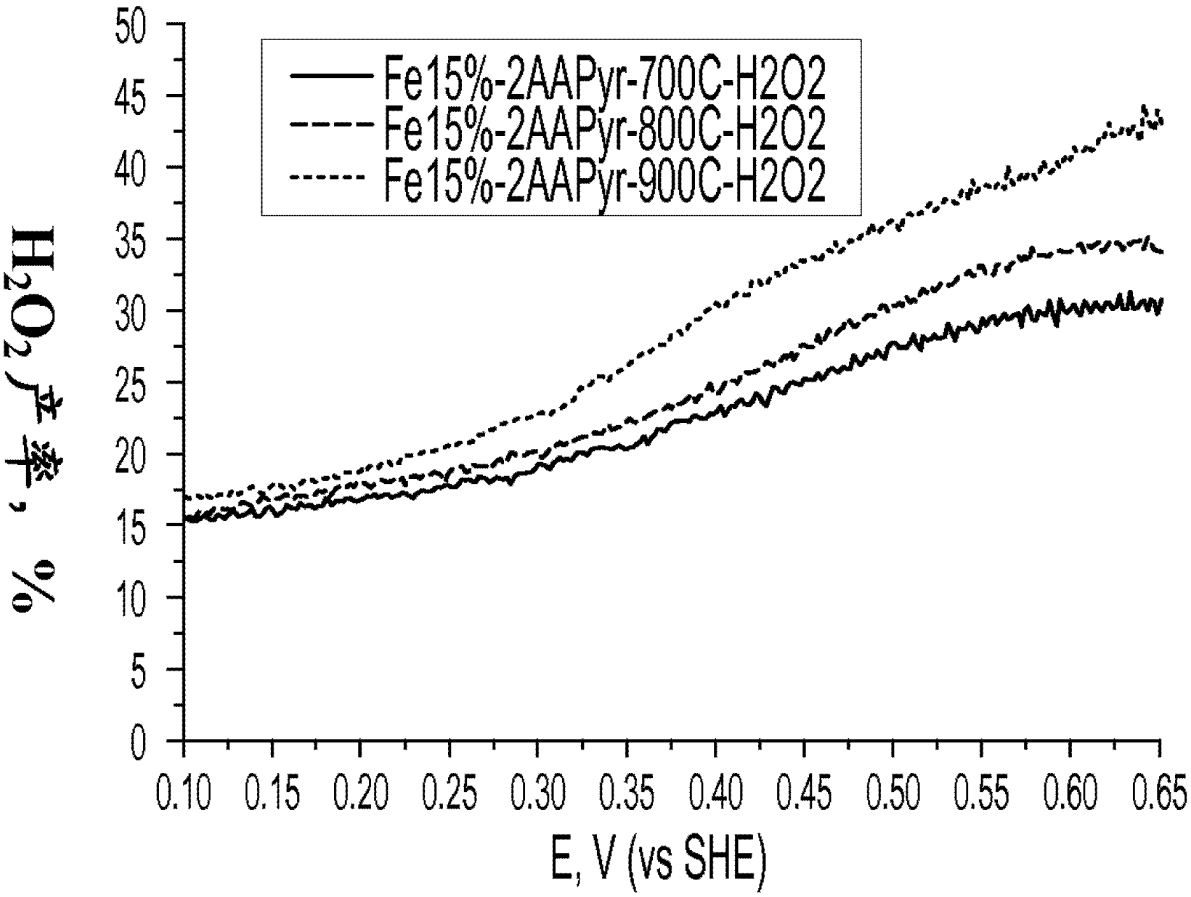
Fe15%-2AAPyr-700C-H2O2
Fe15%-2AAPyr-800C-H2O2
Fe15%-2AAPyr-900C-H2O2
H2O2产率，%
E, V (vs SHE)
0
5
10
15
20
25
30
35
40
45
50
0.10
0.15
0.20
0.25
0.30
0.35
0.40
0.45
0.50
0.55
0.60
0.65

图 8

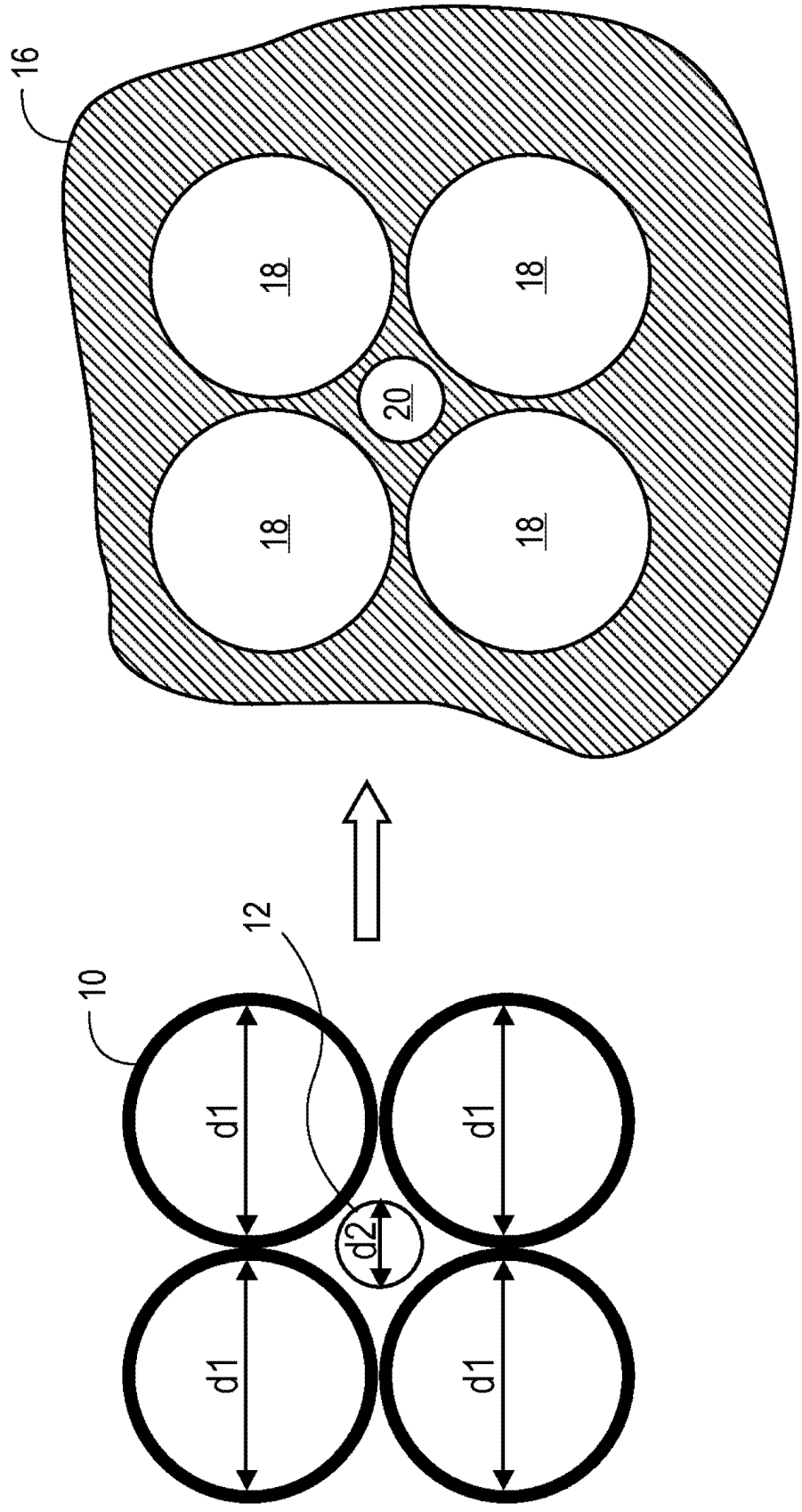

图 9

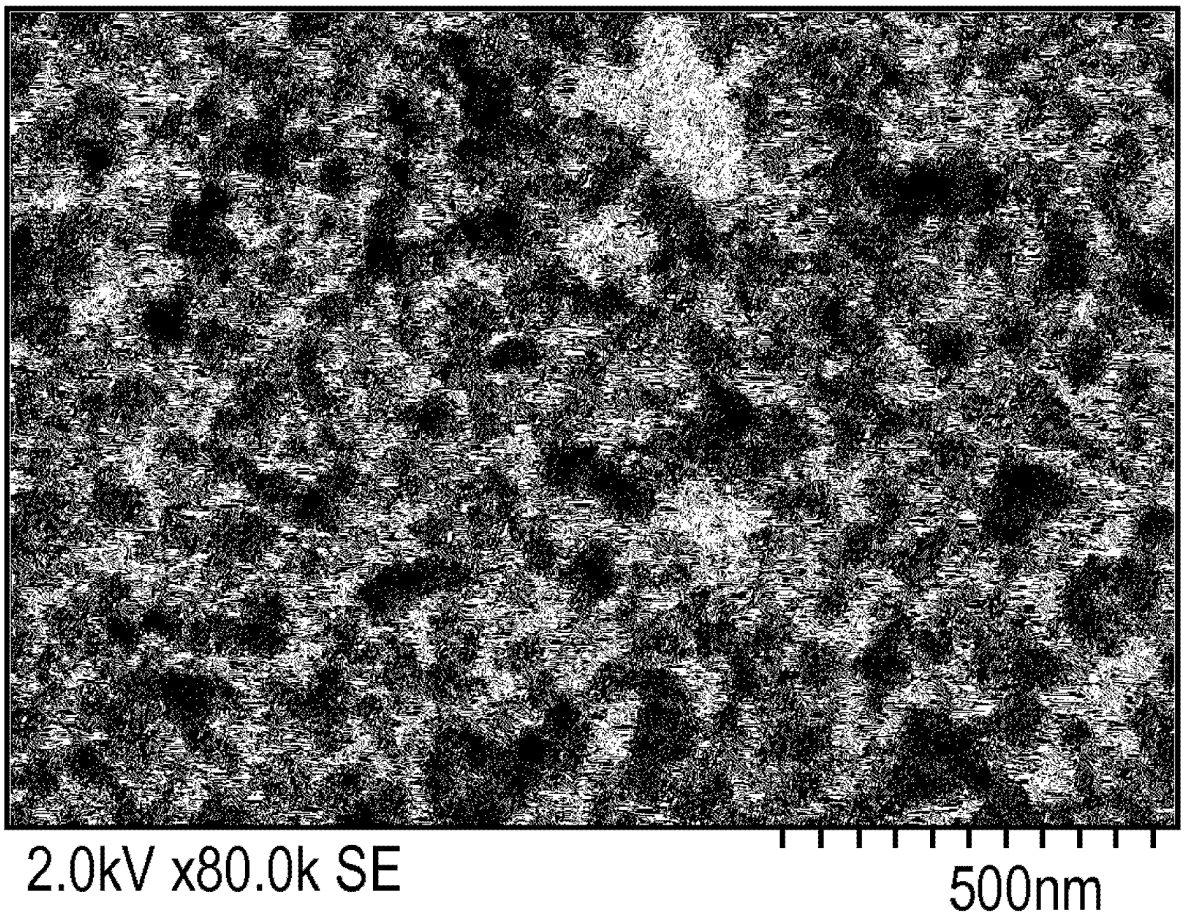

图 10A

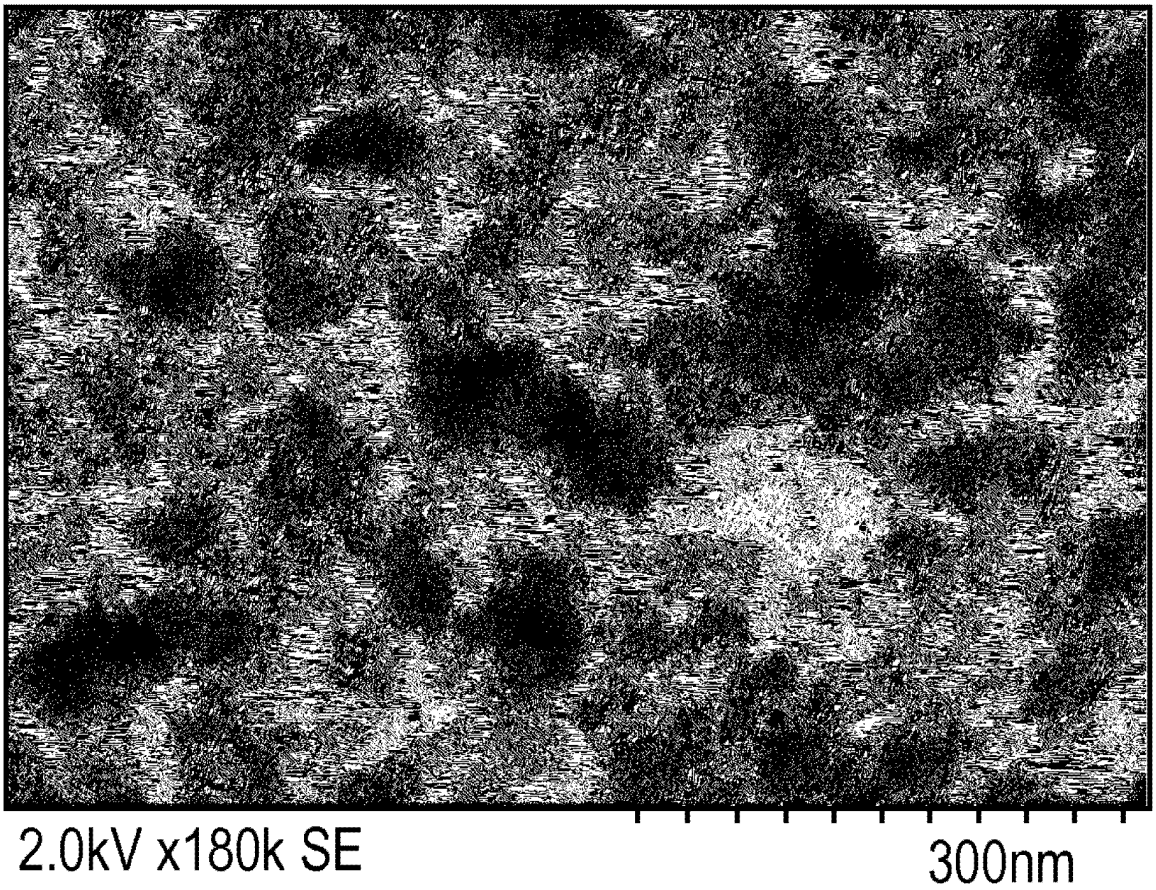

图 10B

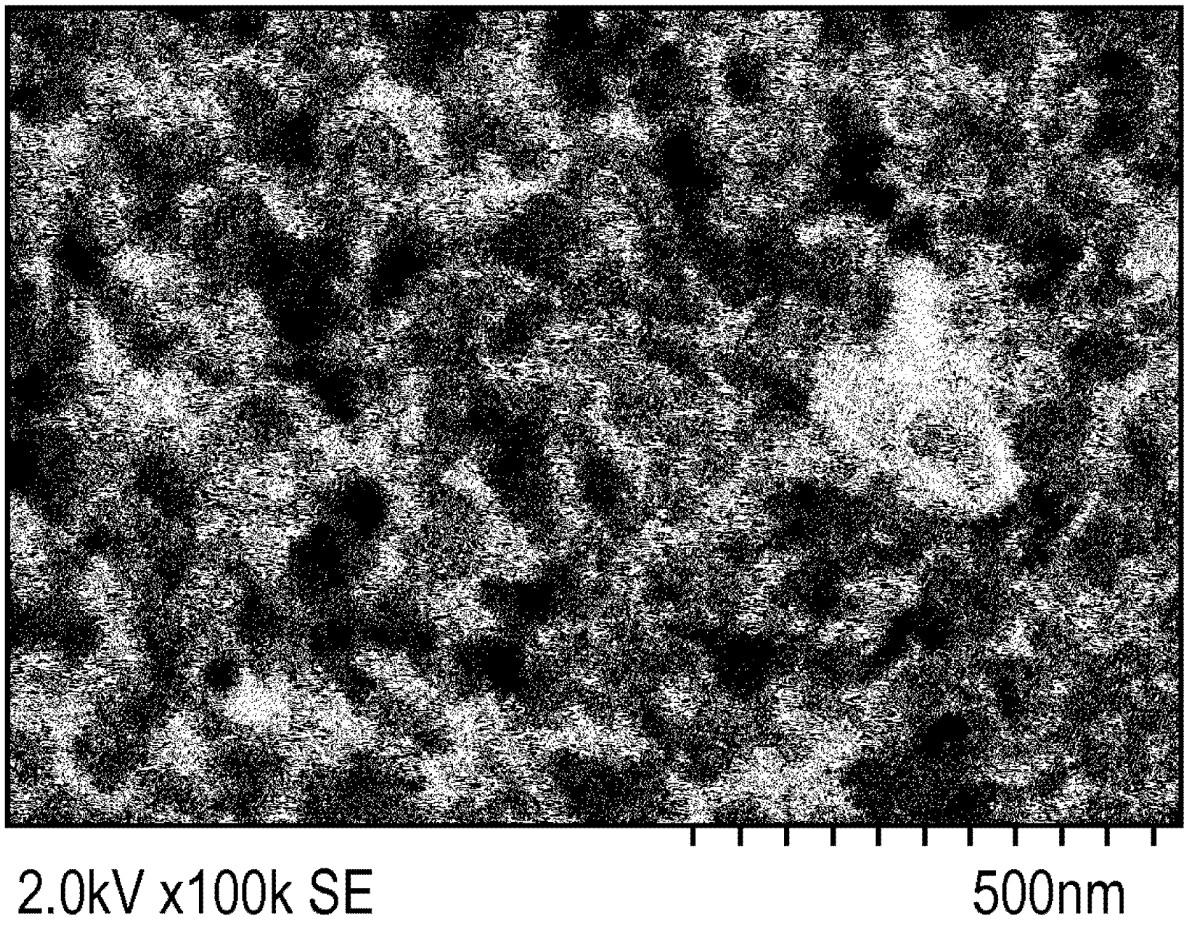

图 11A

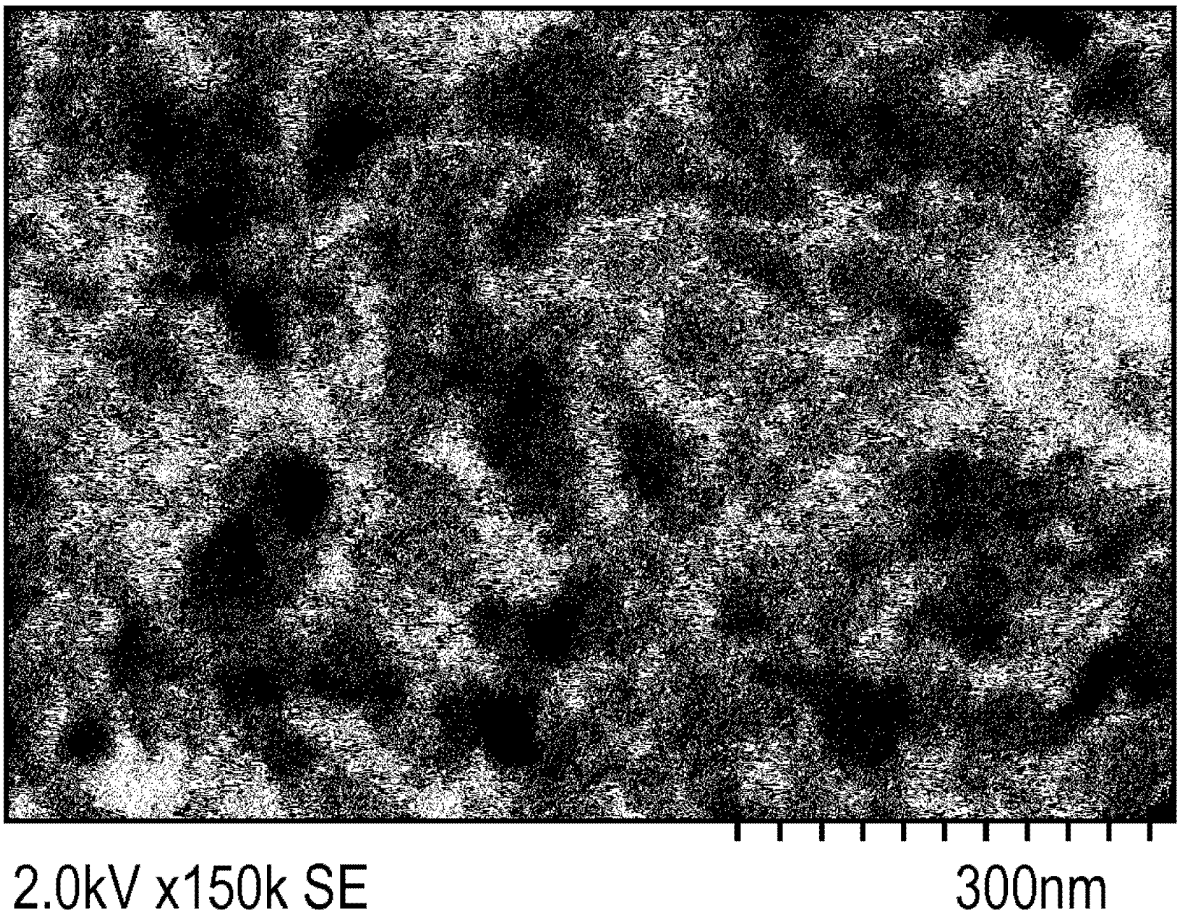

图 11B

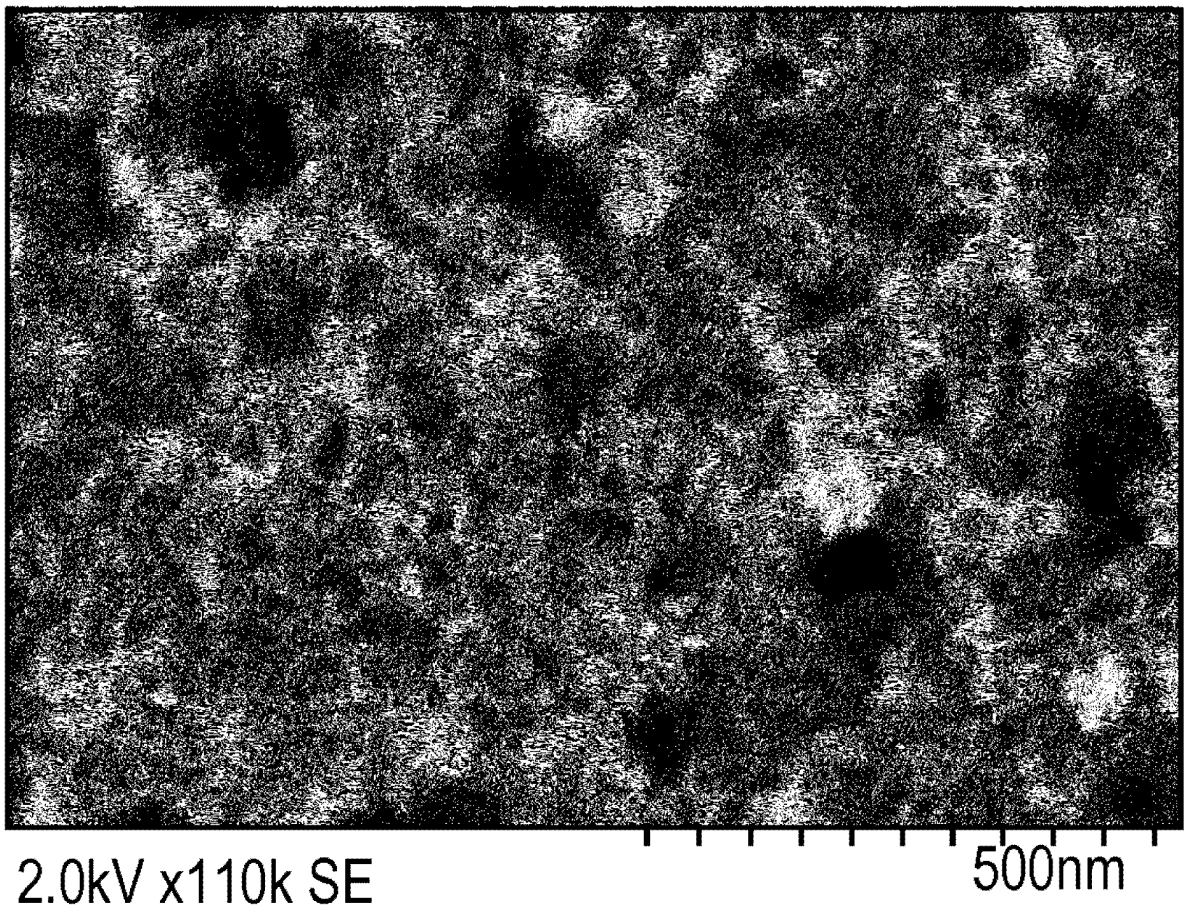

图 12A

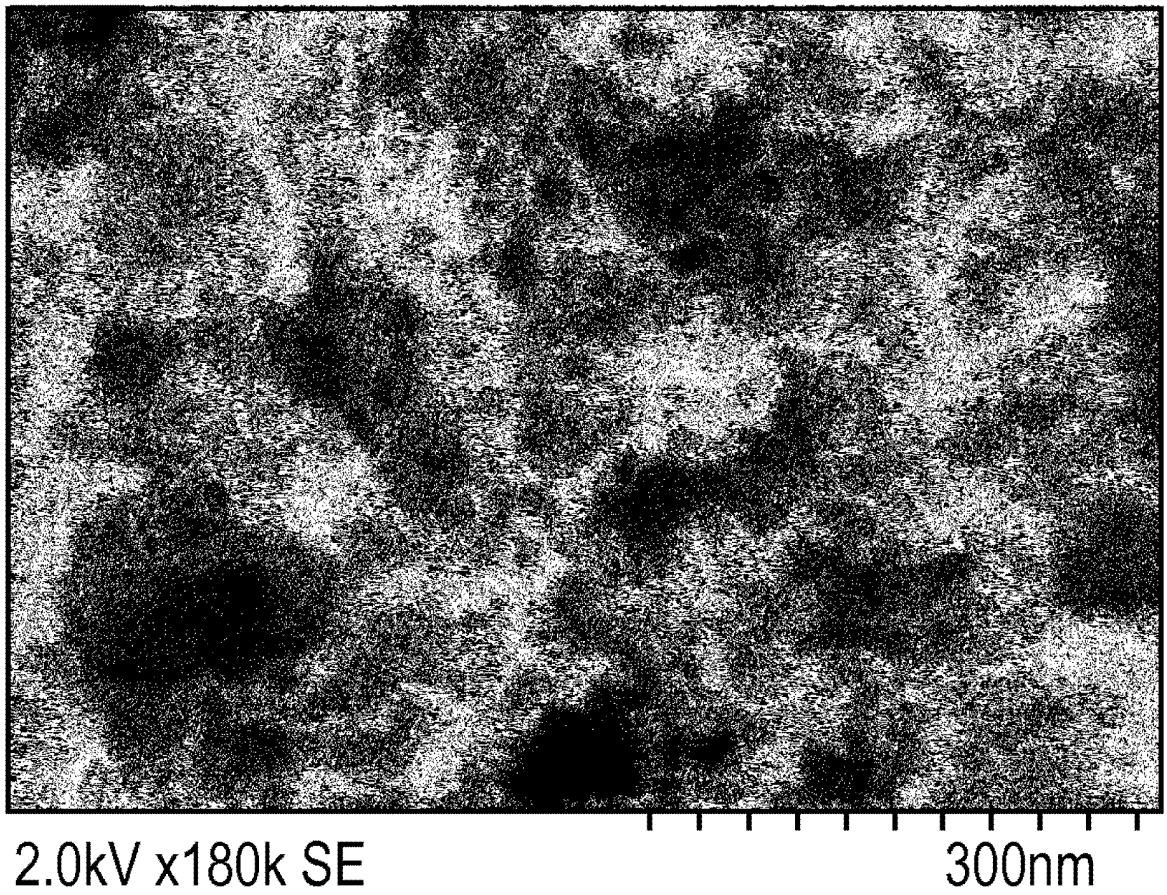

图 12B

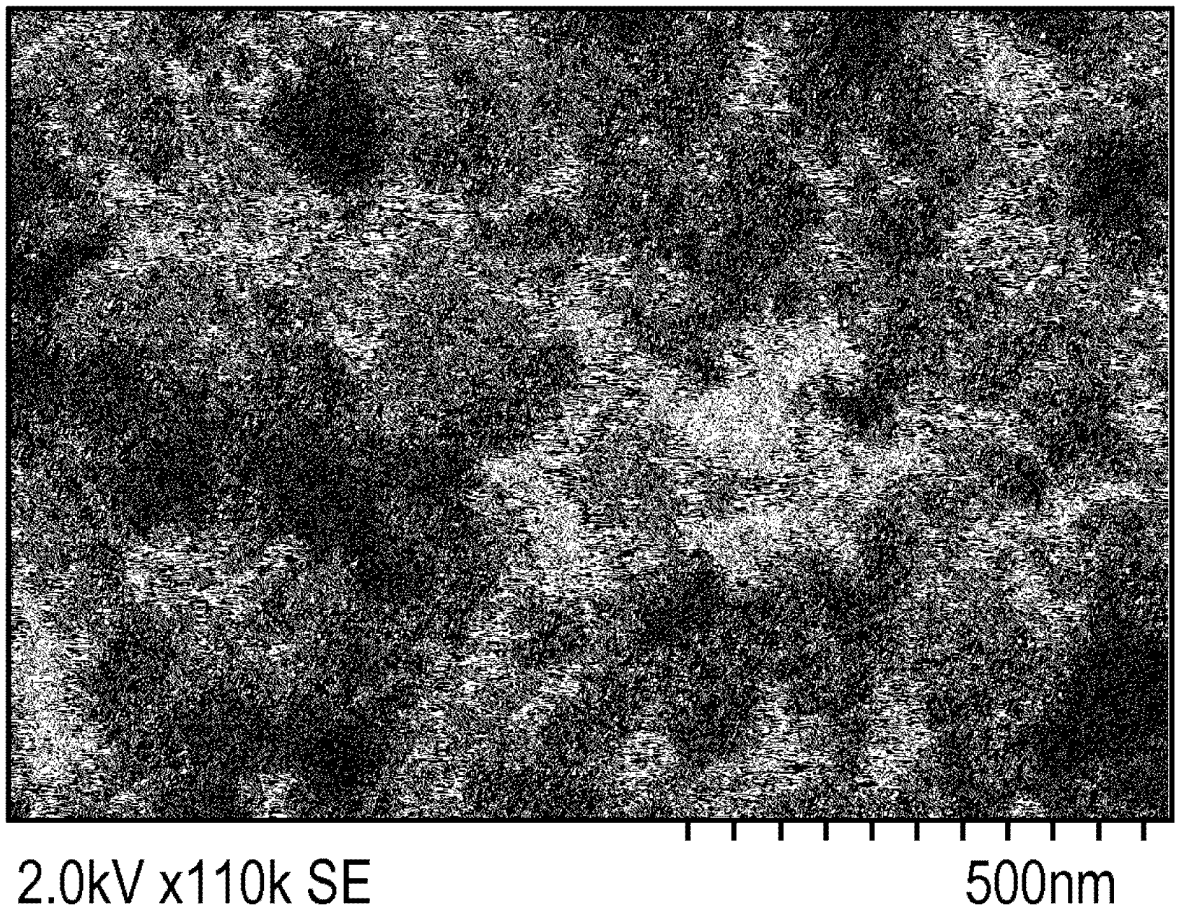

图 13A

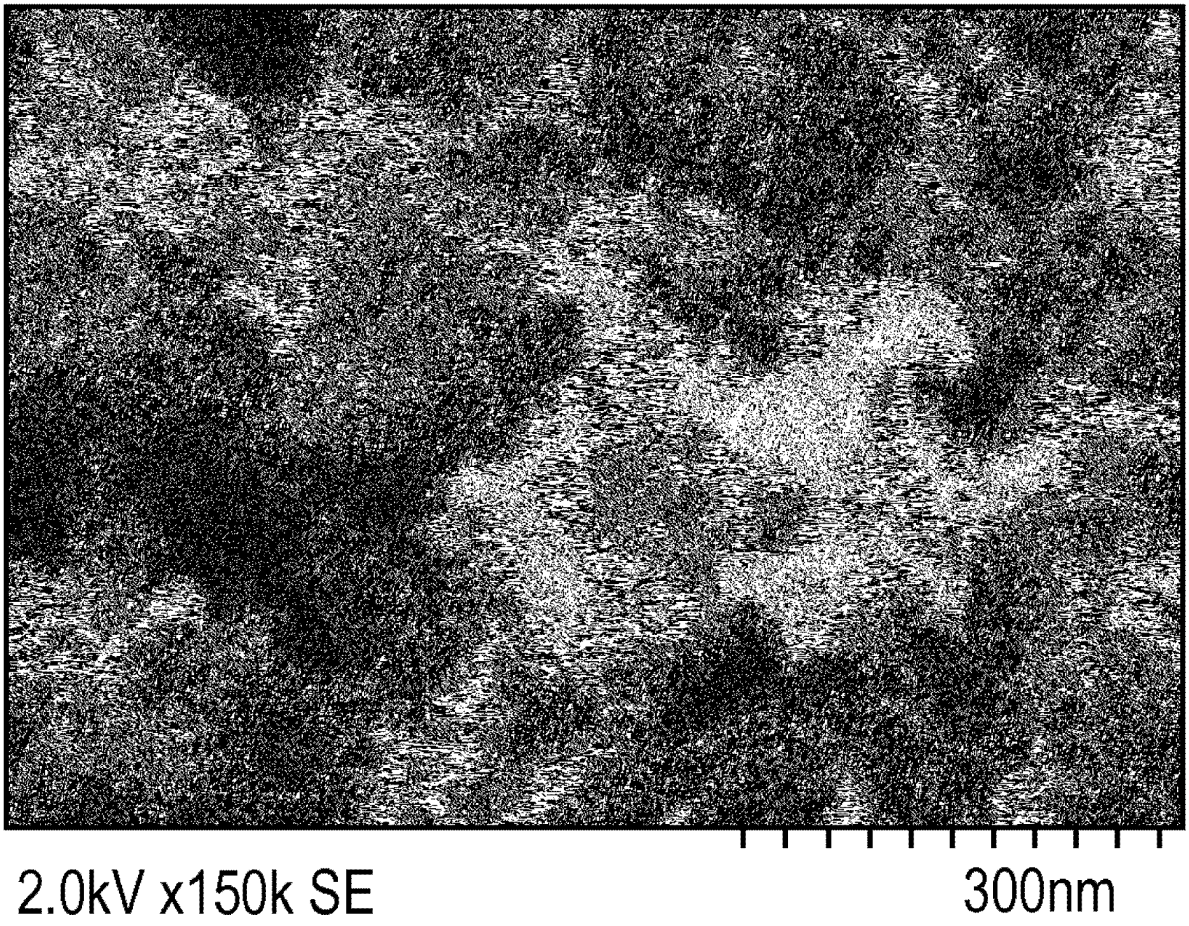

图 13B

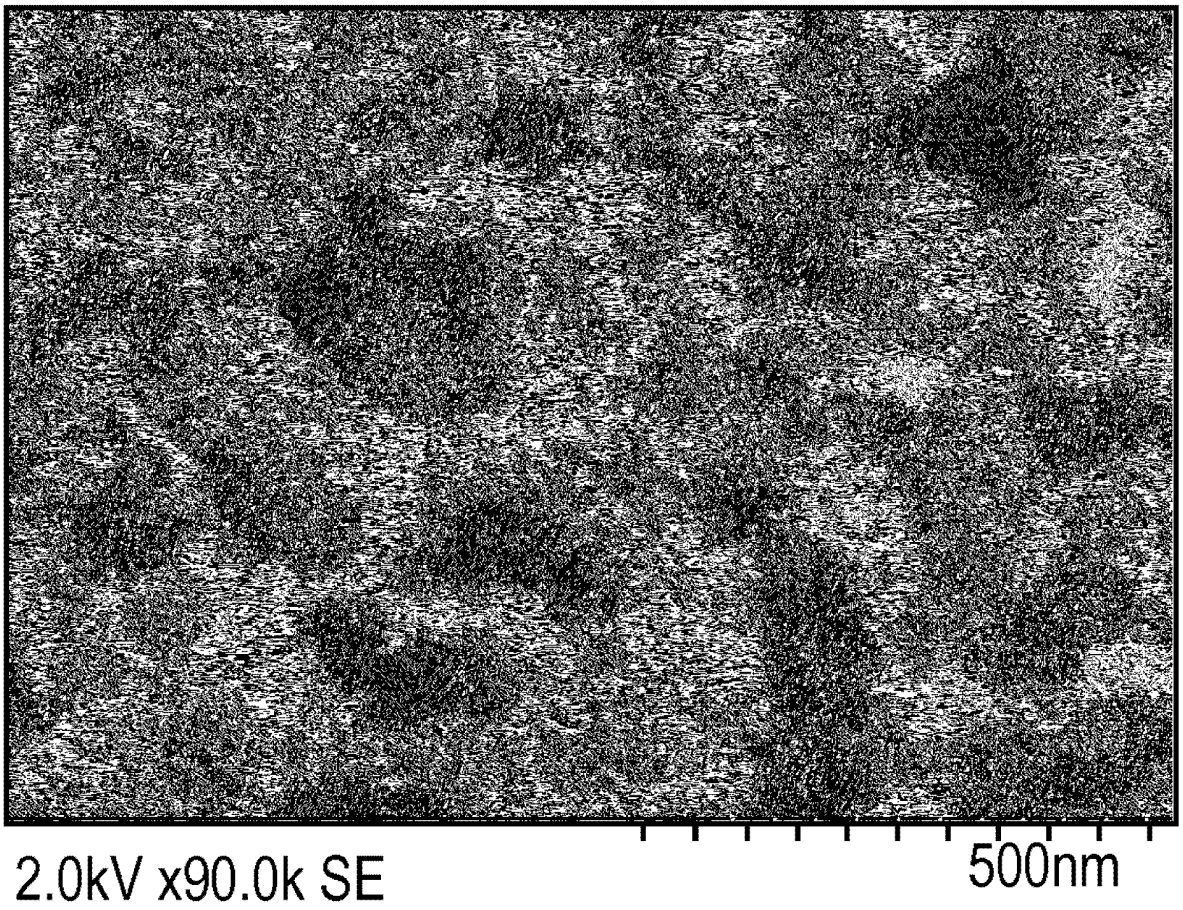

图 14

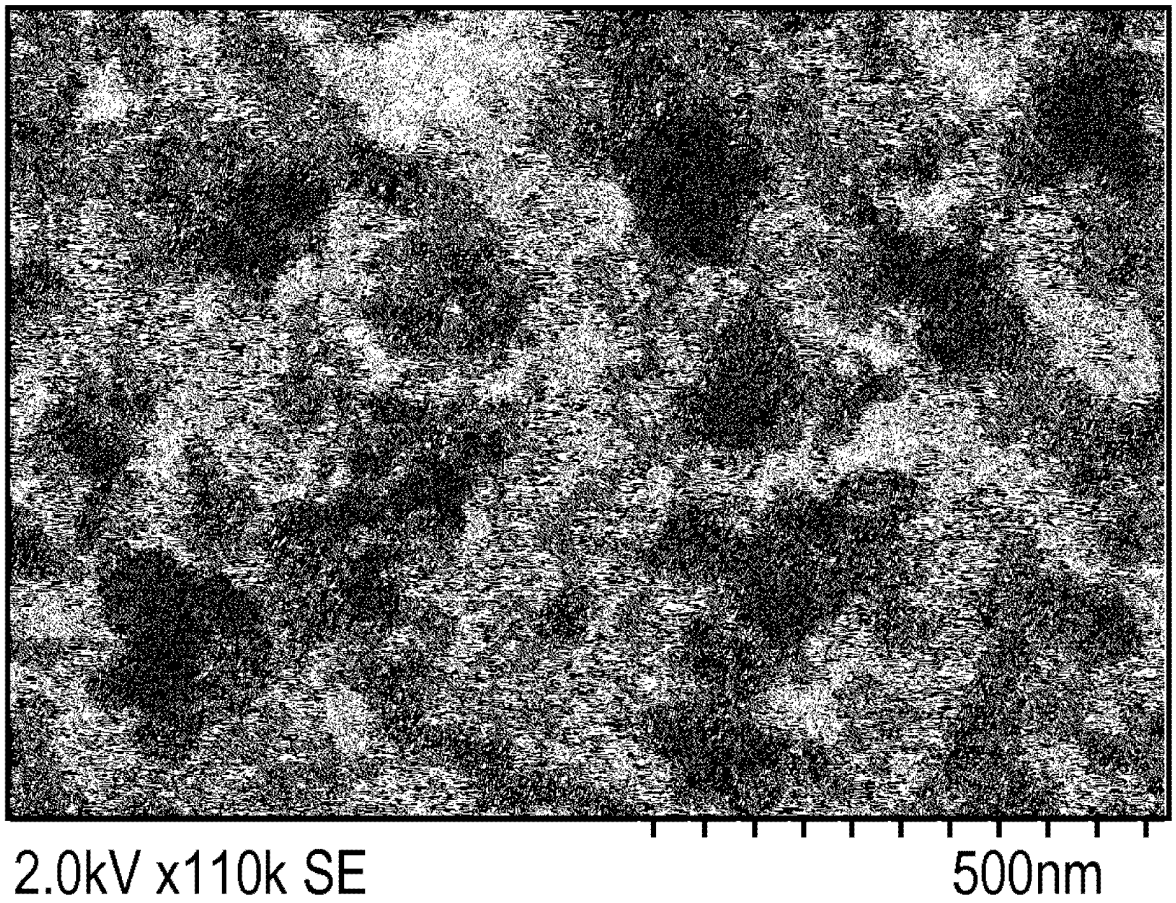

图 15A

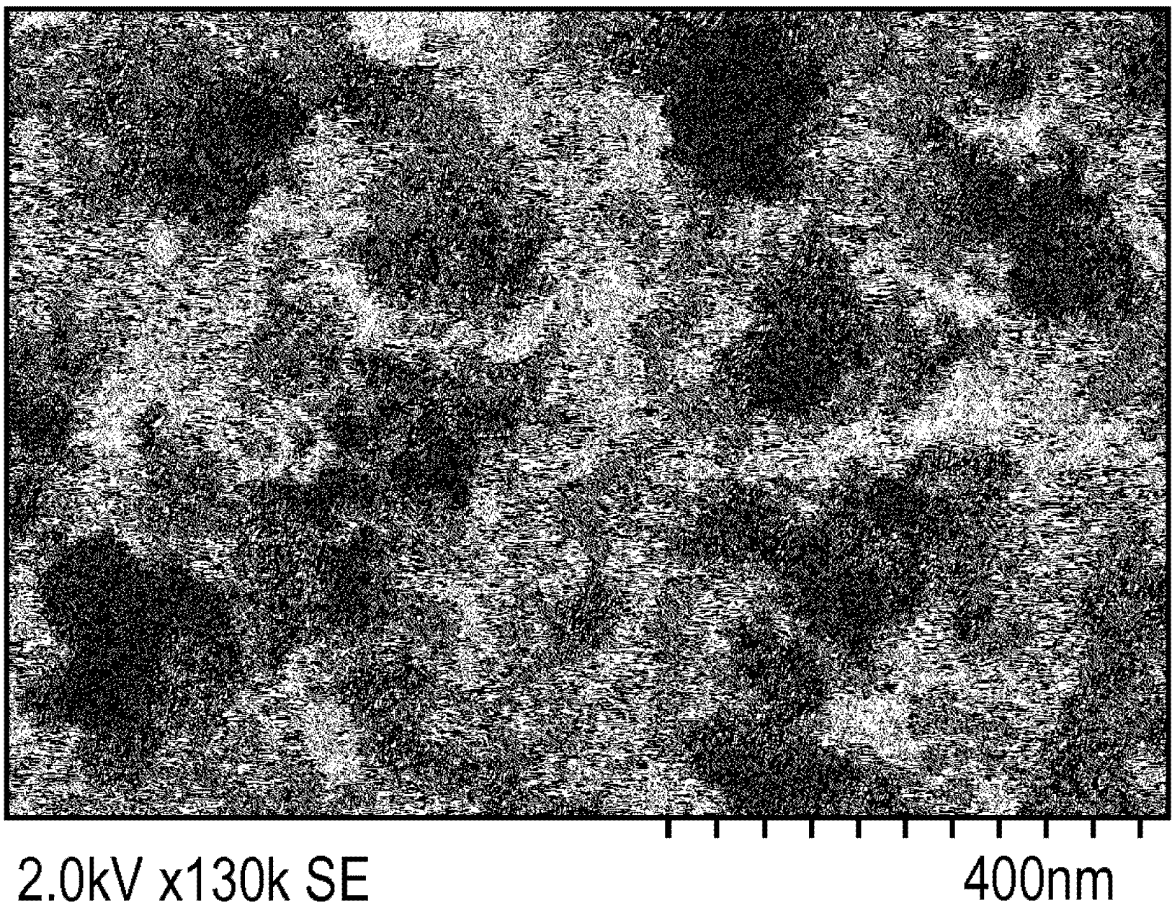

图 15B

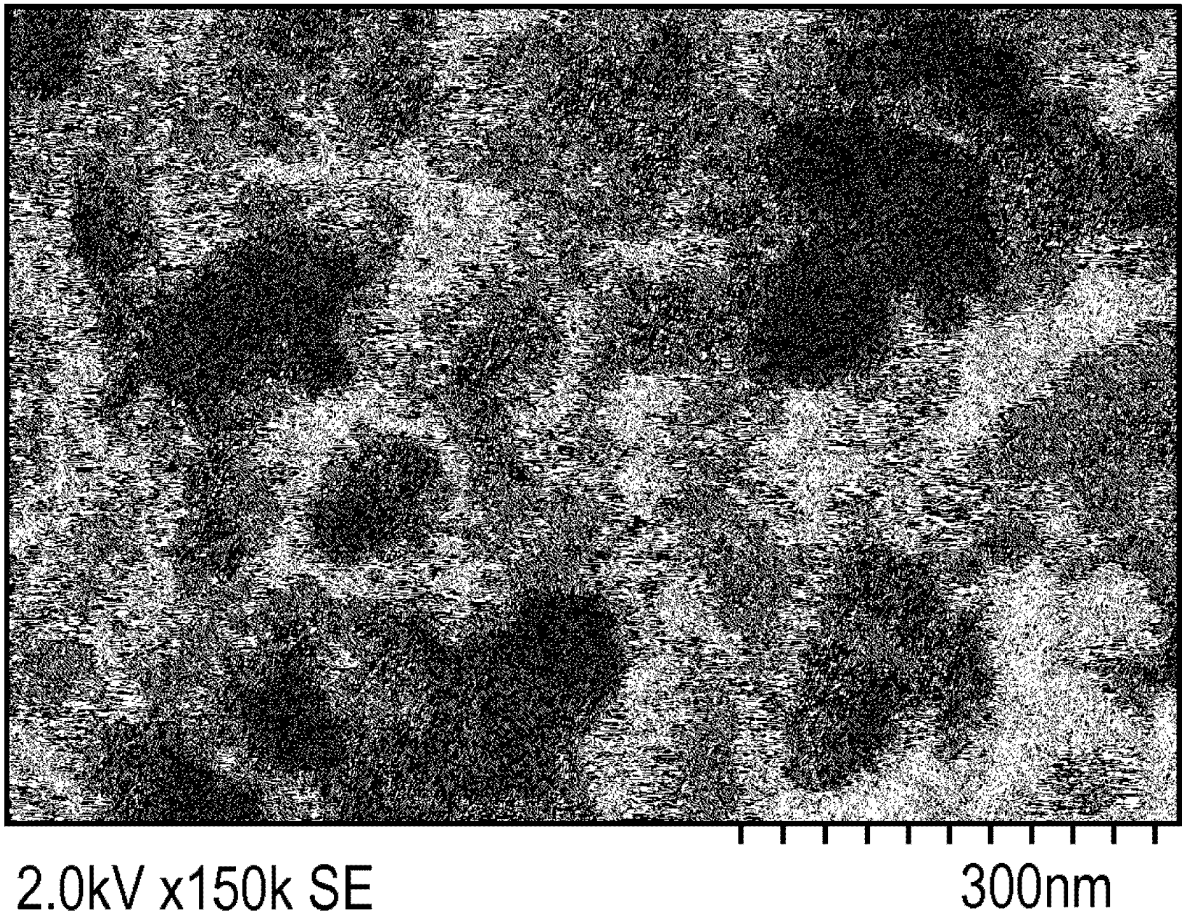

图 15C

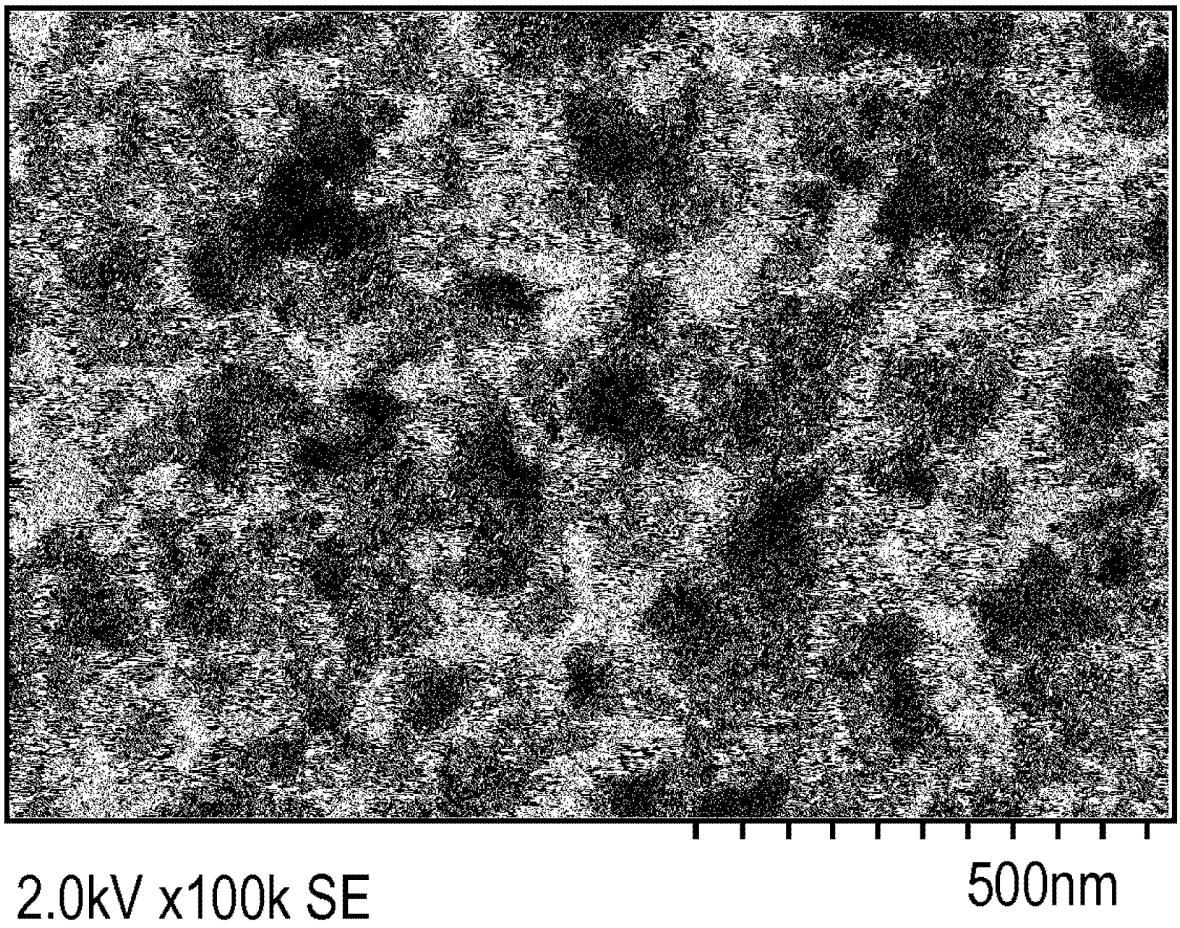

图 16

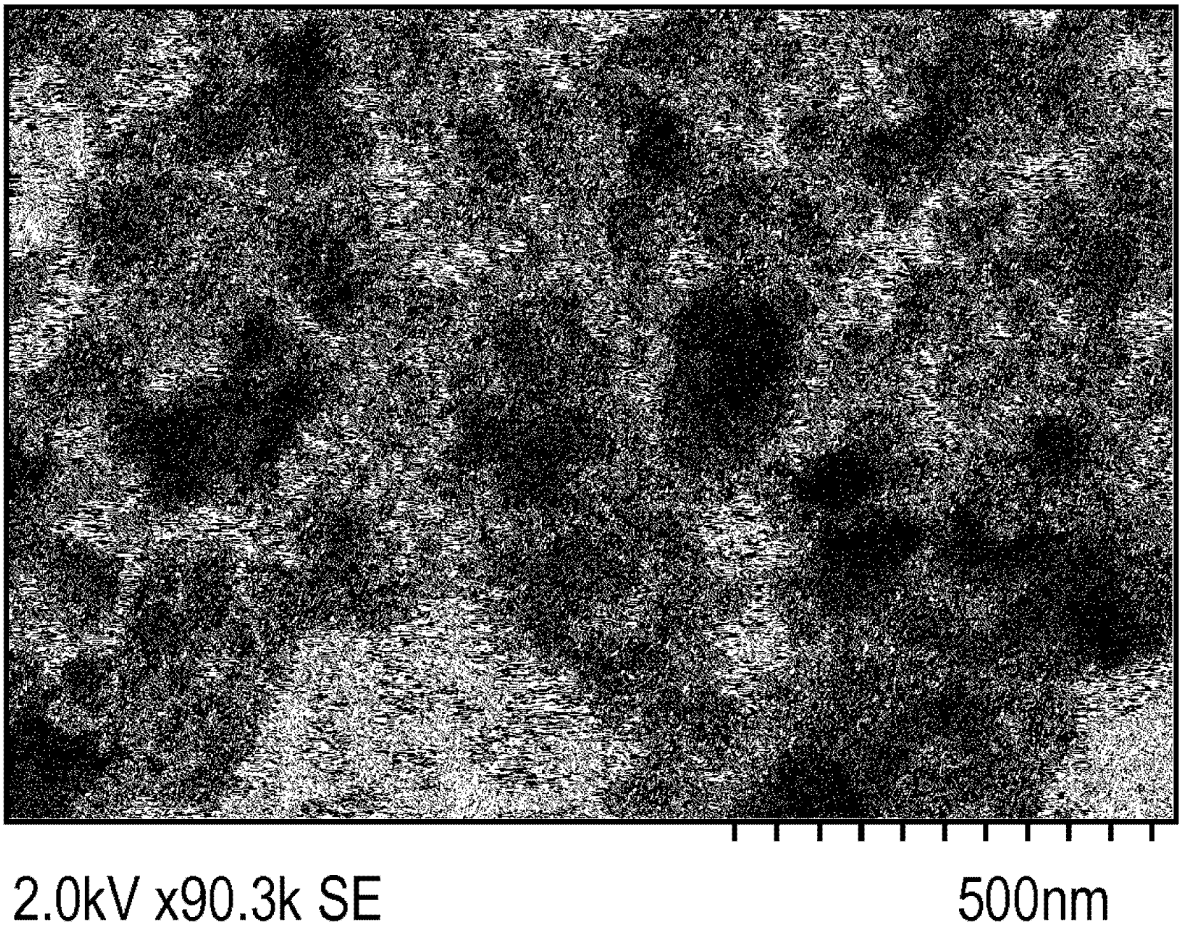

图 17

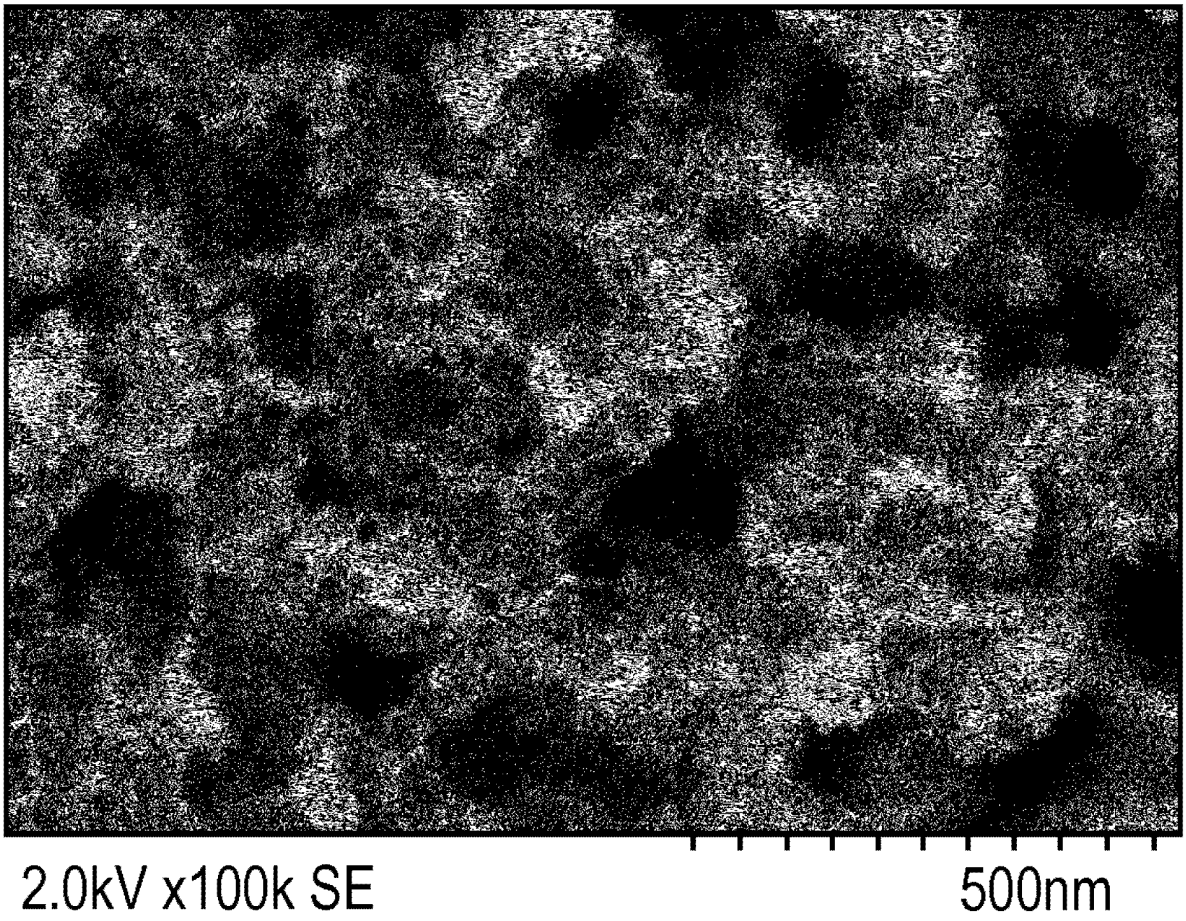

图 18

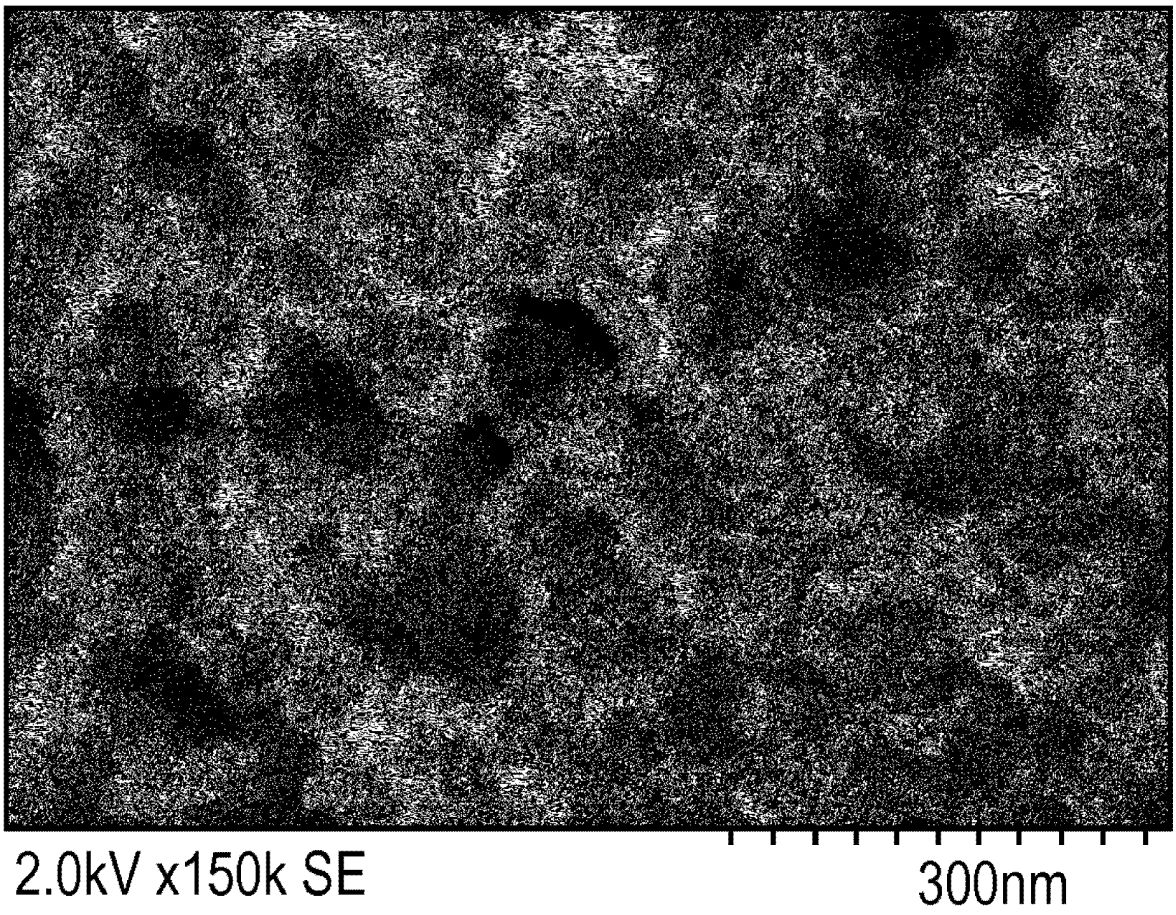

图 19

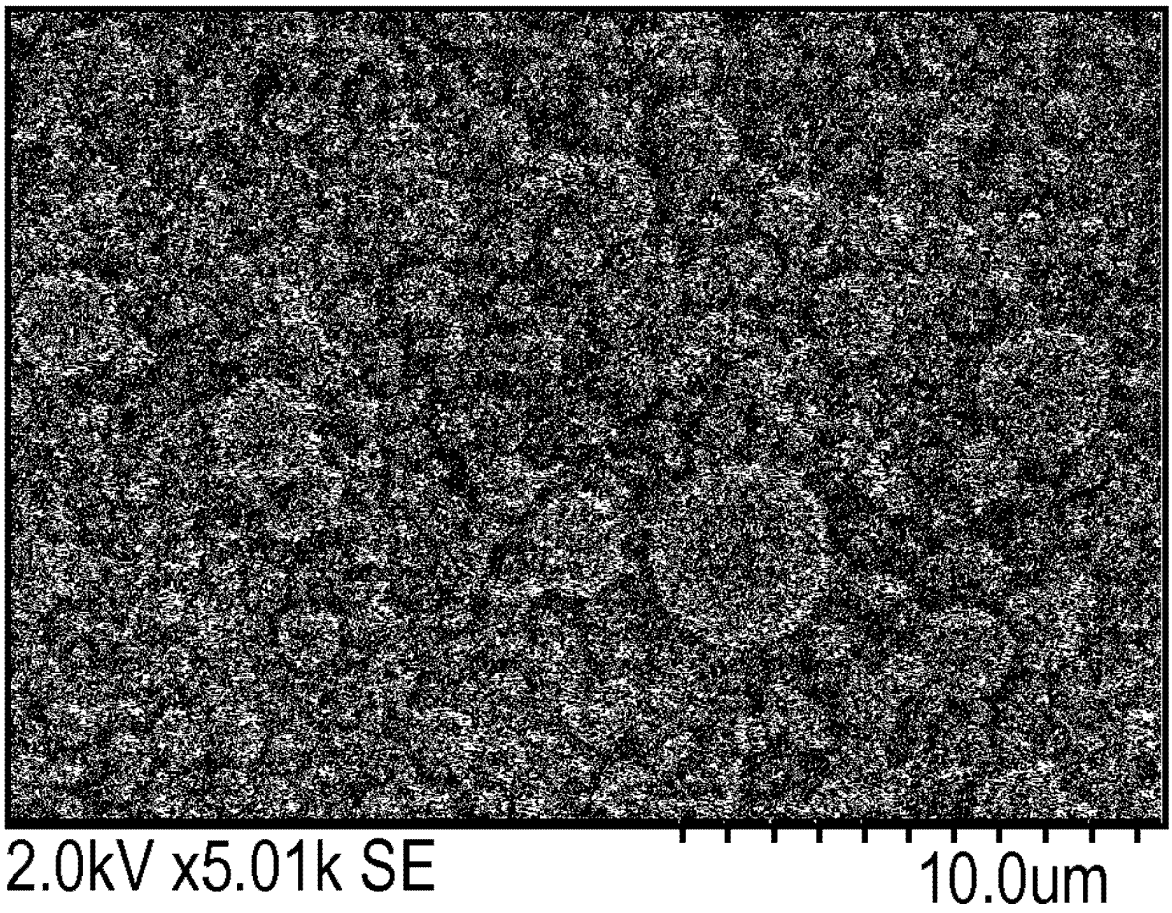

图 20A

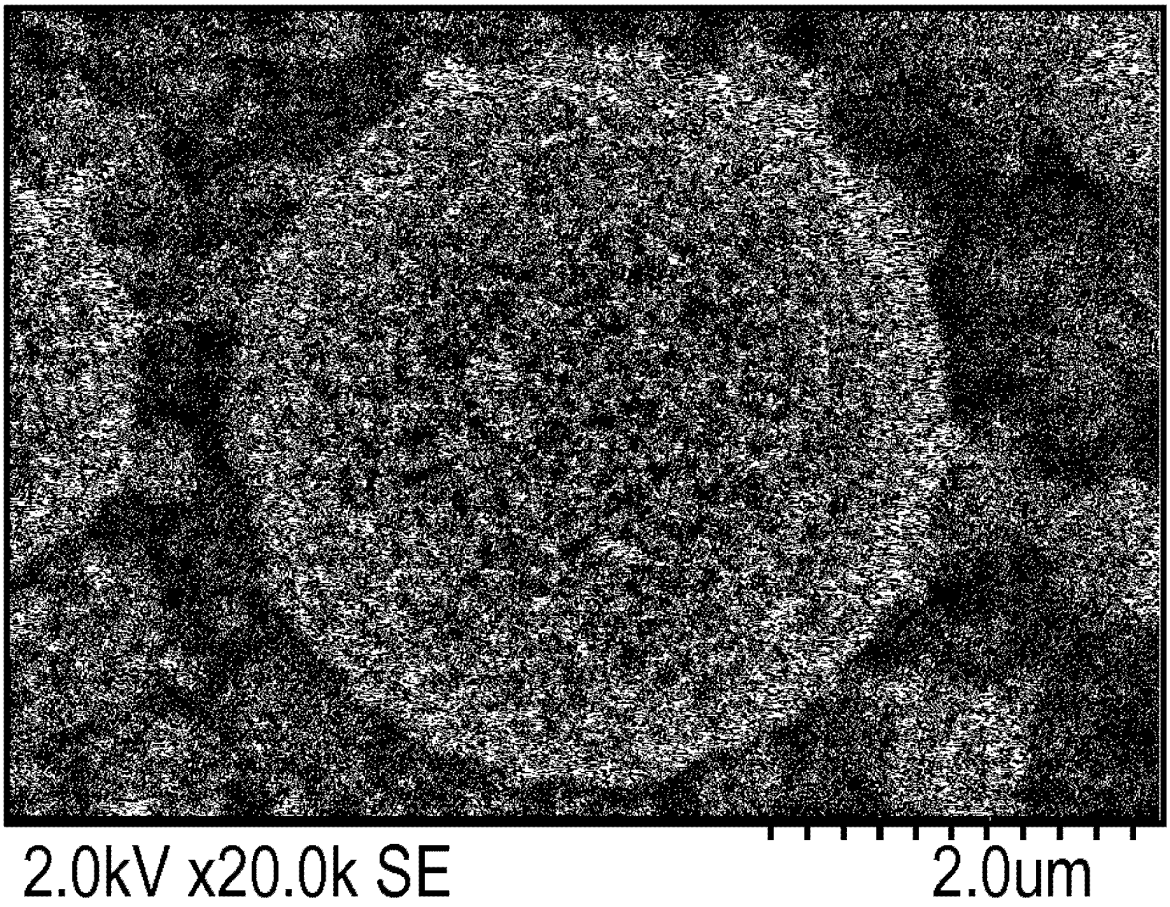

图 20B

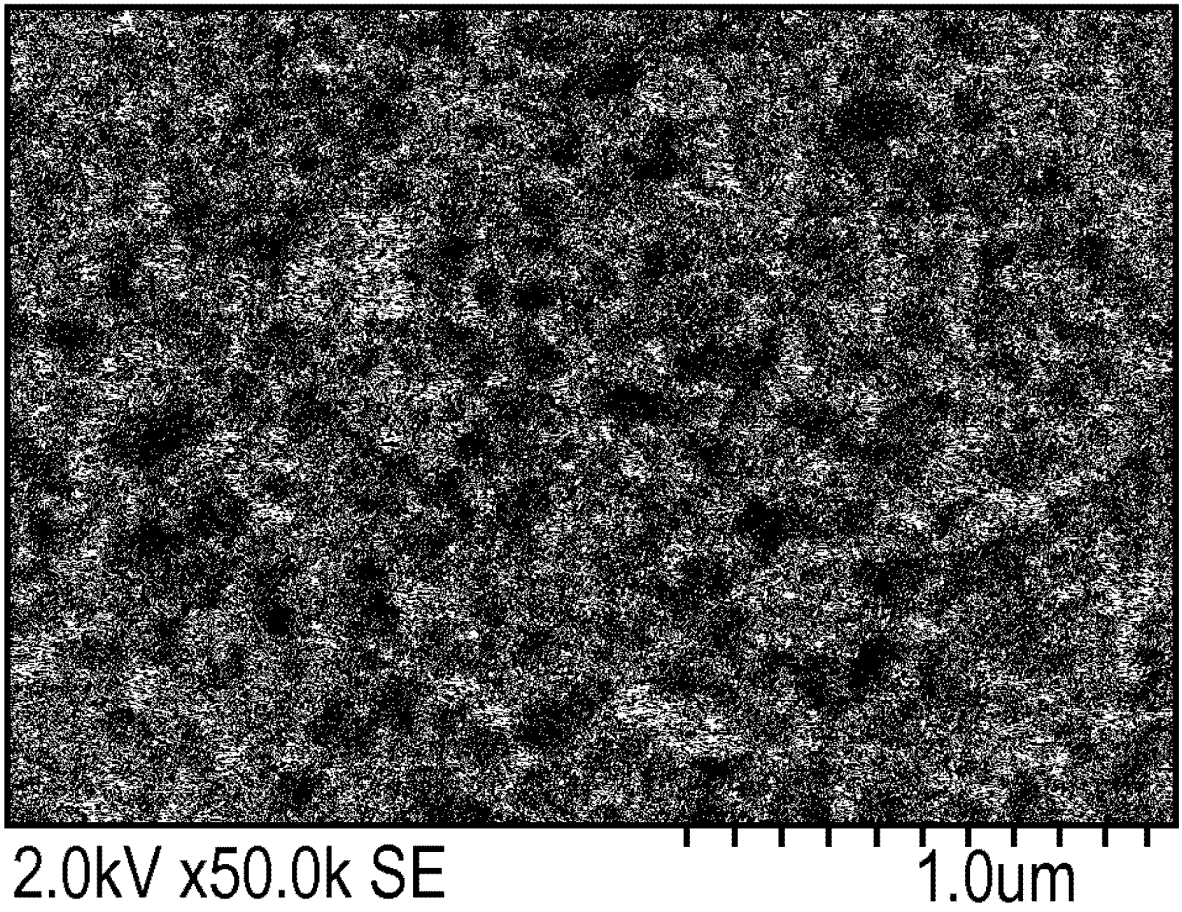

图 20C

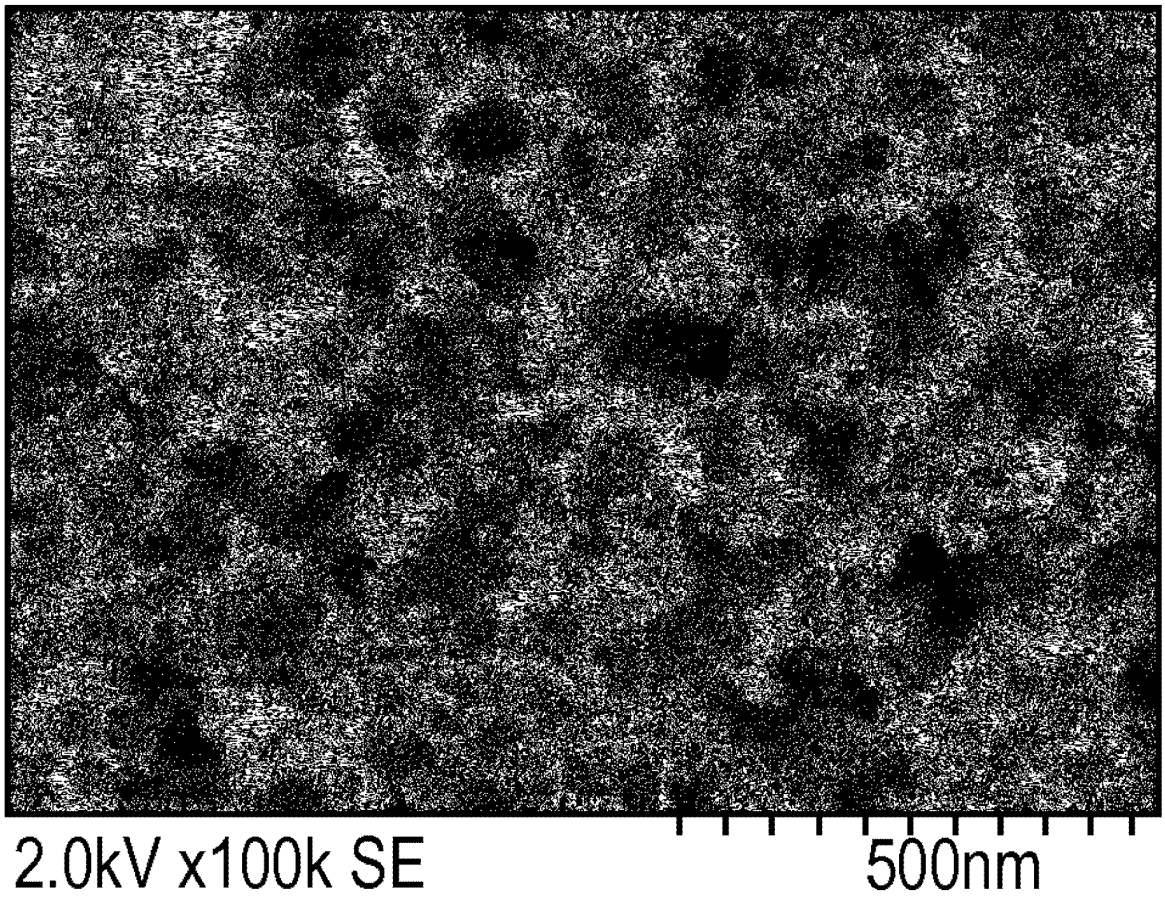

图 20D

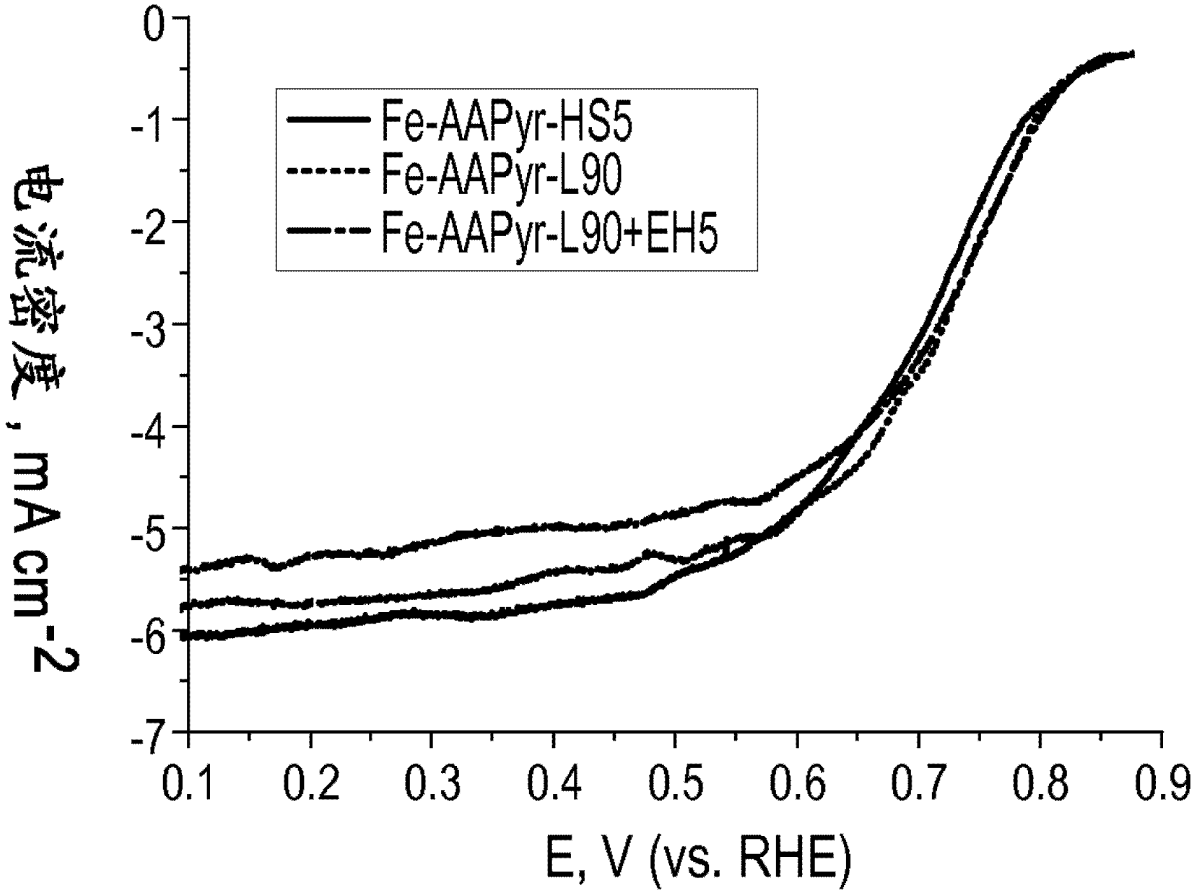
Fe-AAPyr-HS5
Fe-AAPyr-L90
Fe-AAPyr-L90+EH5
电流密度，mA cm-2
0
-1
-2
-3
-4
-5
-6
-7
0.1
0.2
0.3
0.4
0.5
0.6
0.7
0.8
0.9
E, V (vs. RHE)

图 21

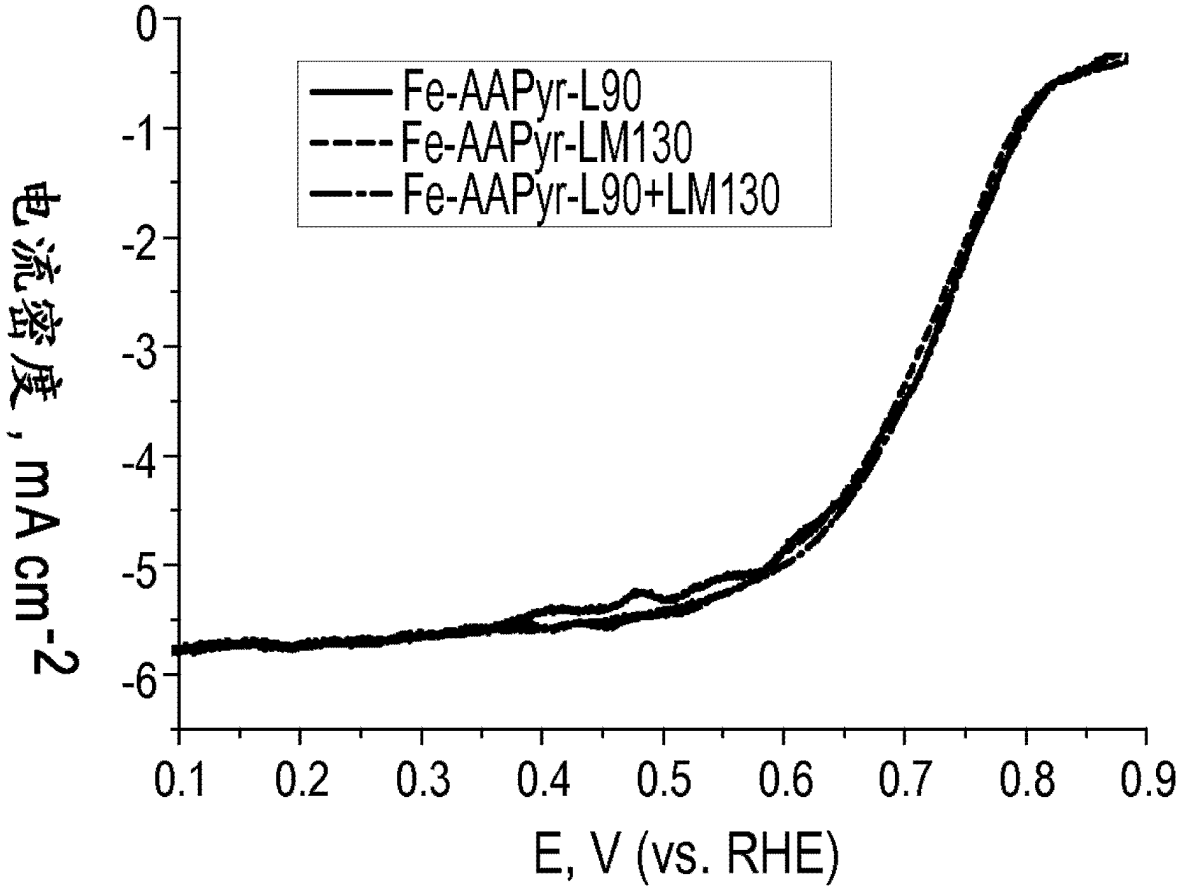
Fe-AAPyr-L90
Fe-AAPyr-LM130
Fe-AAPyr-L90+LM130
电流密度，mA cm-2
0
-1
-2
-3
-4
-5
-6
0.1
0.2
0.3
0.4
0.5
0.6
0.7
0.8
0.9
E, V (vs. RHE)

图 22

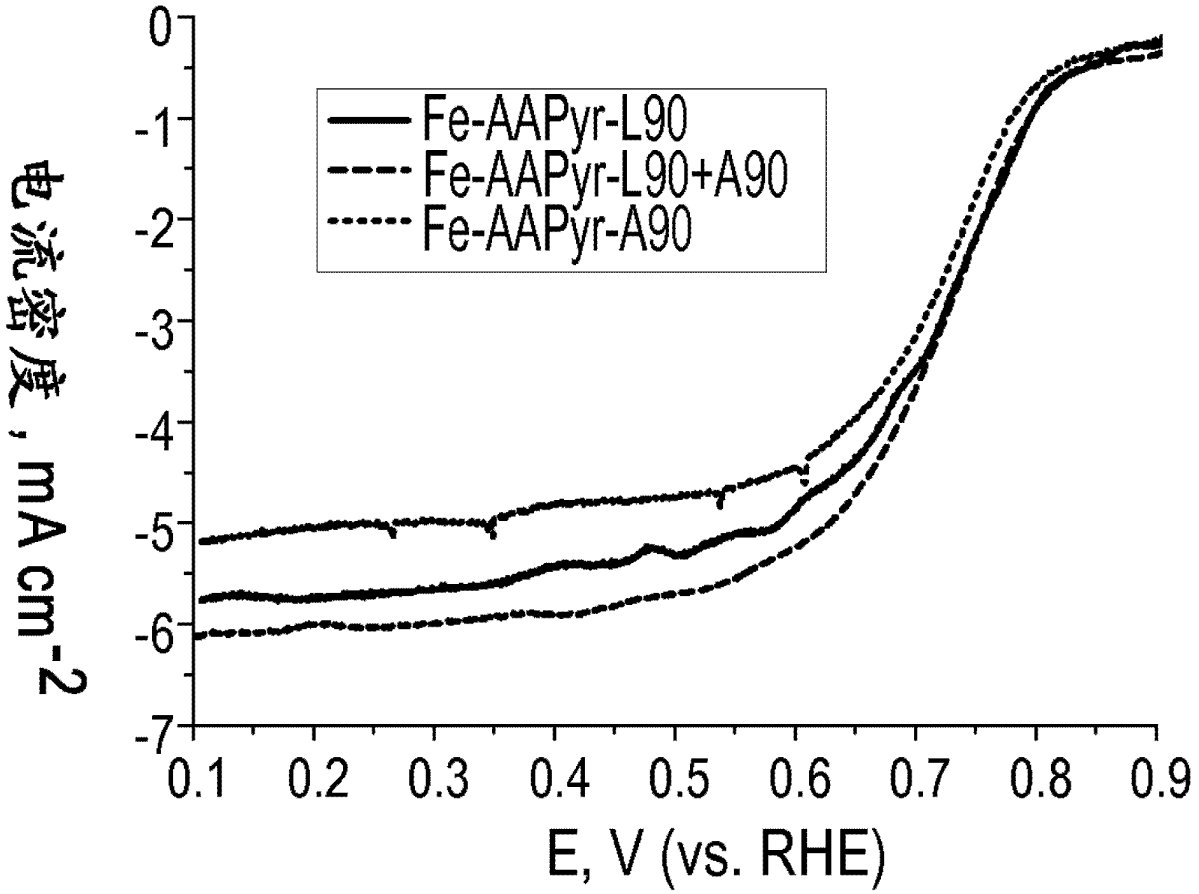
Fe-AAPyr-L90
Fe-AAPyr-L90+A90
Fe-AAPyr-A90
电流密度，mA cm-2
0
-1
-2
-3
-4
-5
-6
-7
0.1
0.2
0.3
0.4
0.5
0.6
0.7
0.8
0.9
E, V (vs. RHE)

图 23

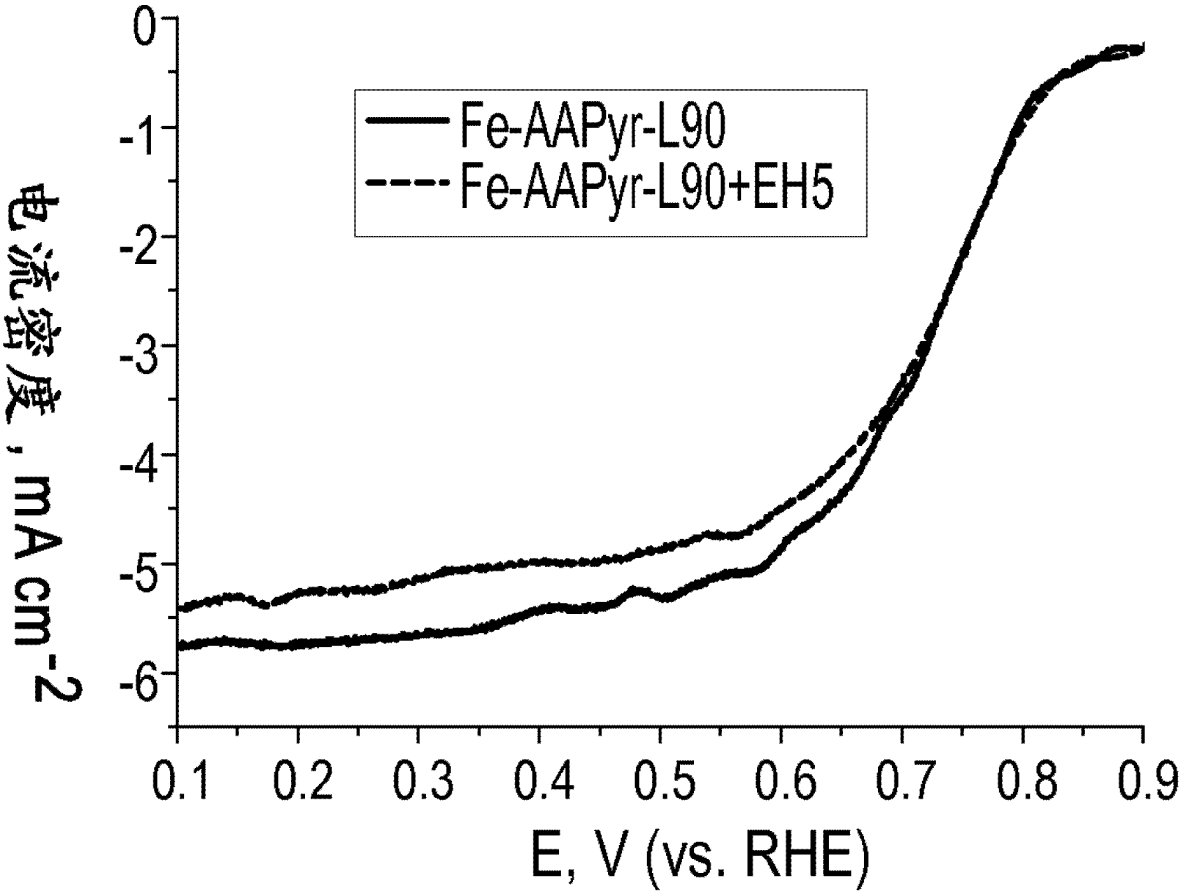
0
-1
-2
-3
-4
-5
-6
电流密度，mA cm-2
Fe-AAPyr-L90
Fe-AAPyr-L90+EH5
0.1
0.2
0.3
0.4
0.5
0.6
0.7
0.8
0.9
E, V (vs. RHE)

图 24

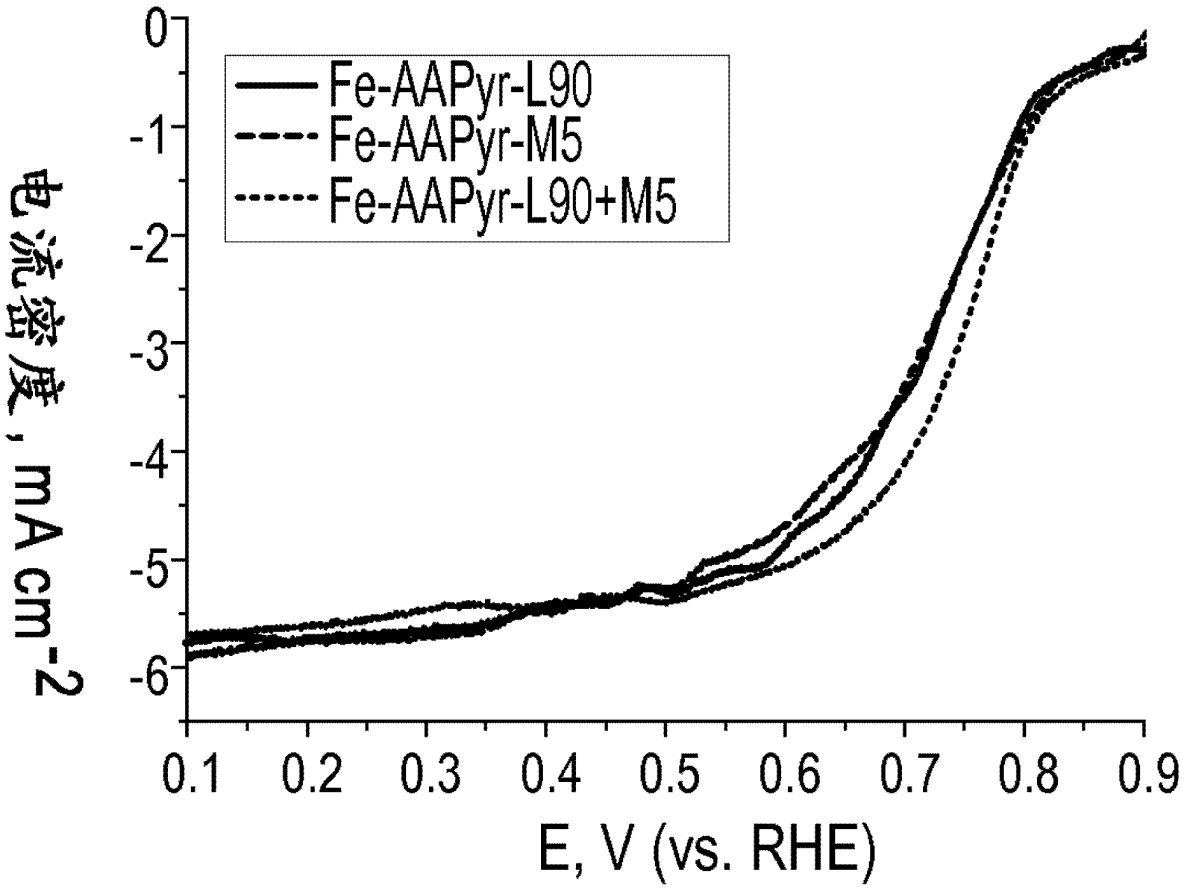
Fe-AAPyr-L90
Fe-AAPyr-M5
Fe-AAPyr-L90+M5
电流密度，mA cm-2
0
-1
-2
-3
-4
-5
-6
0.1
0.2
0.3
0.4
0.5
0.6
0.7
0.8
0.9
E, V (vs. RHE)

图 25

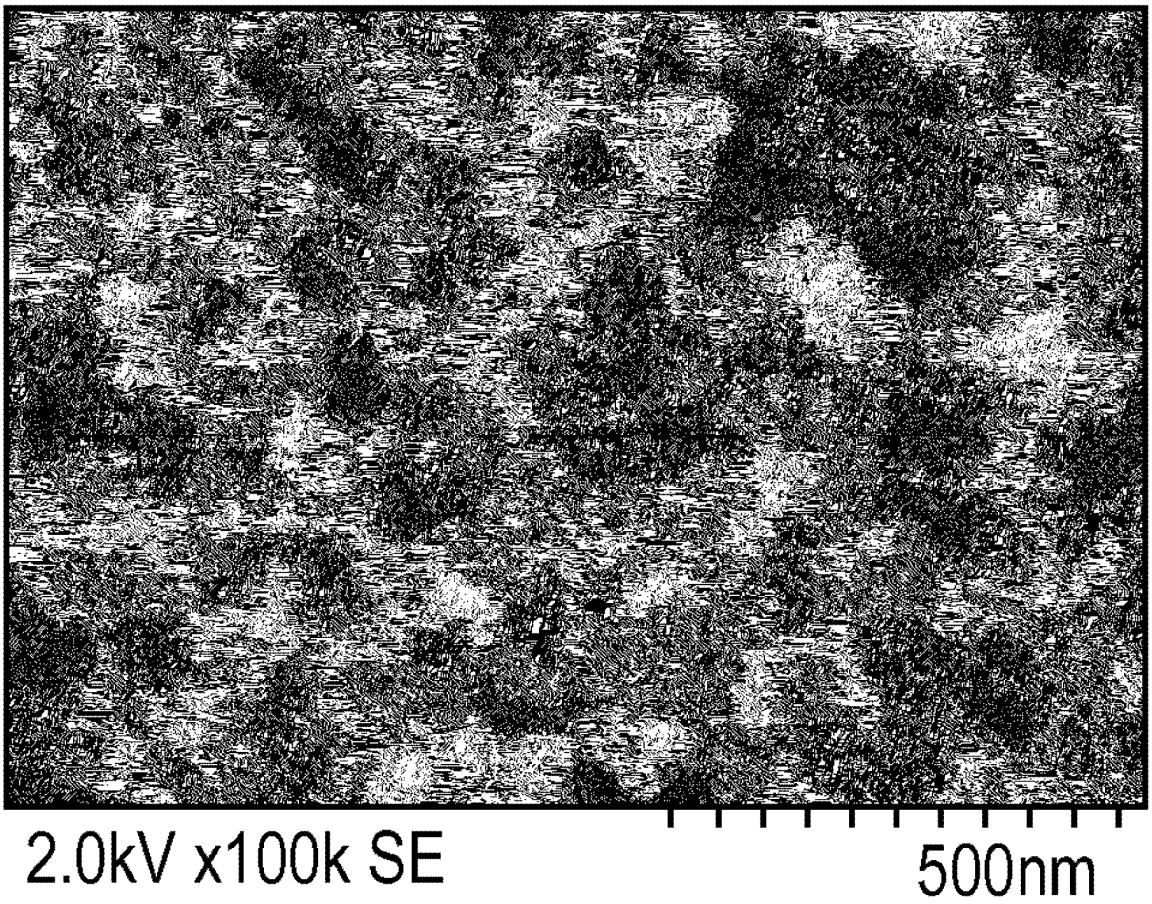

图 26

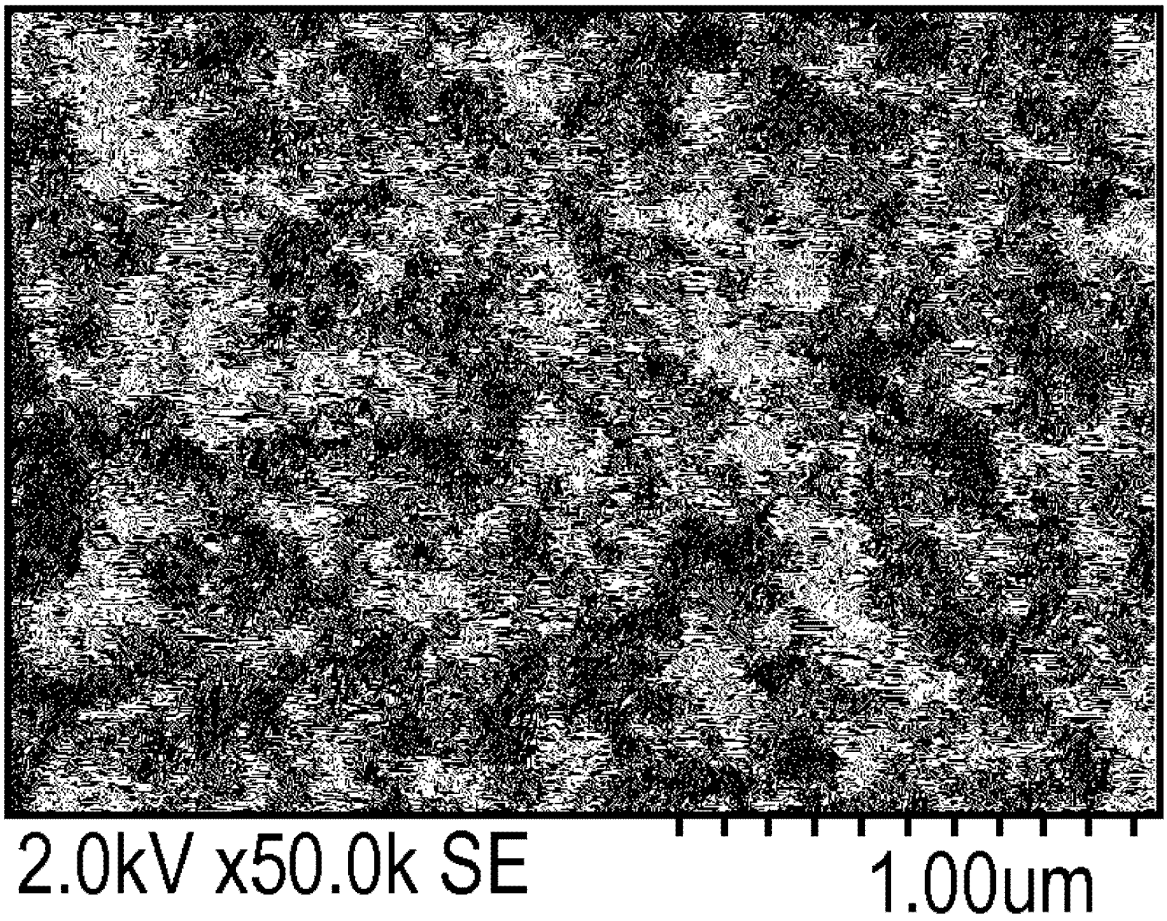

图 27

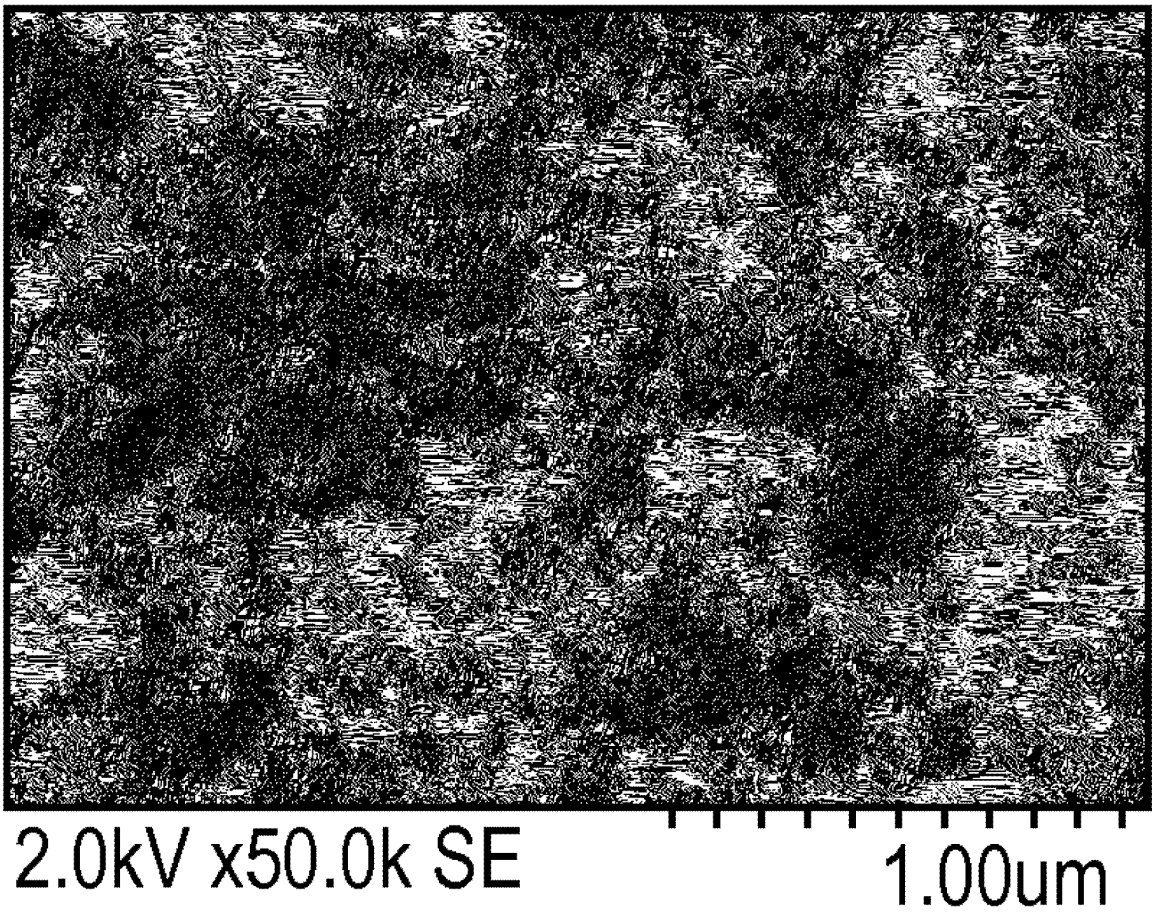

图 28

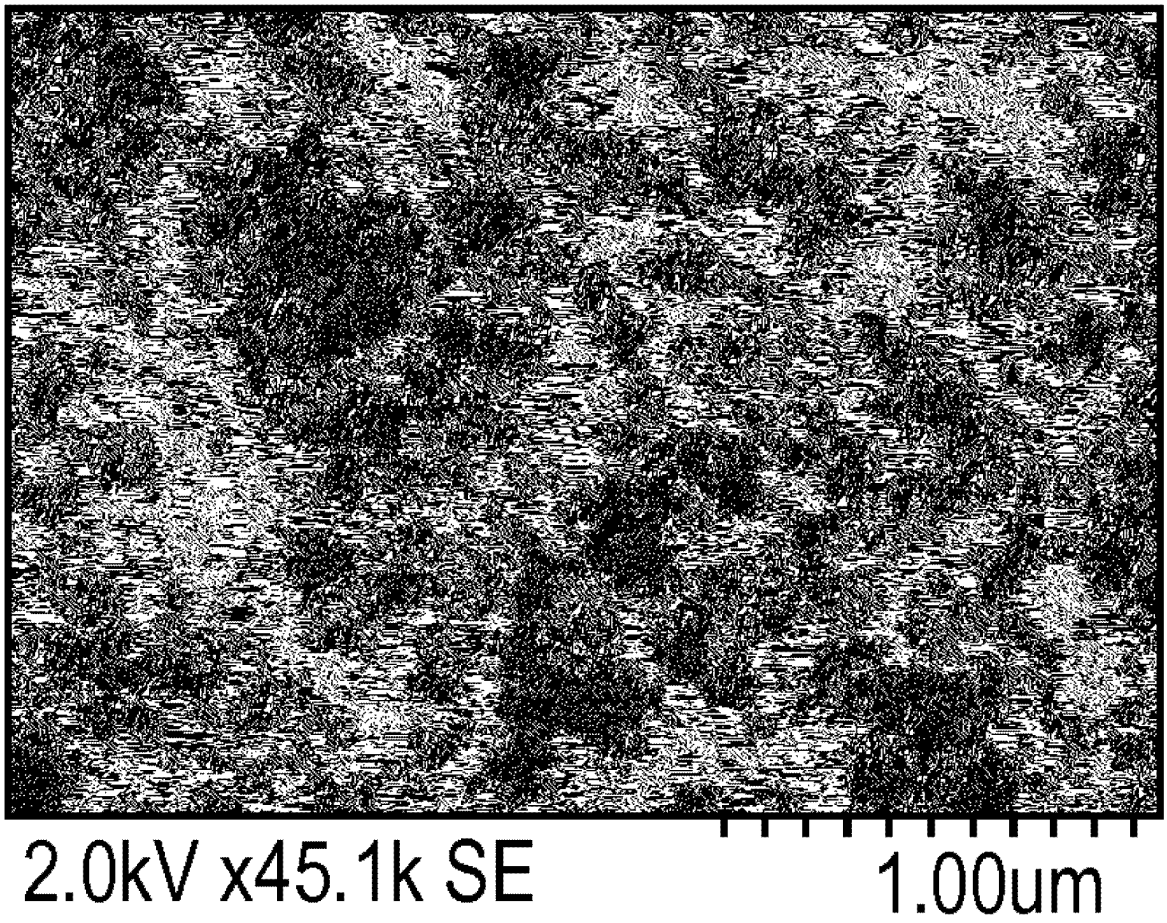

图 29A

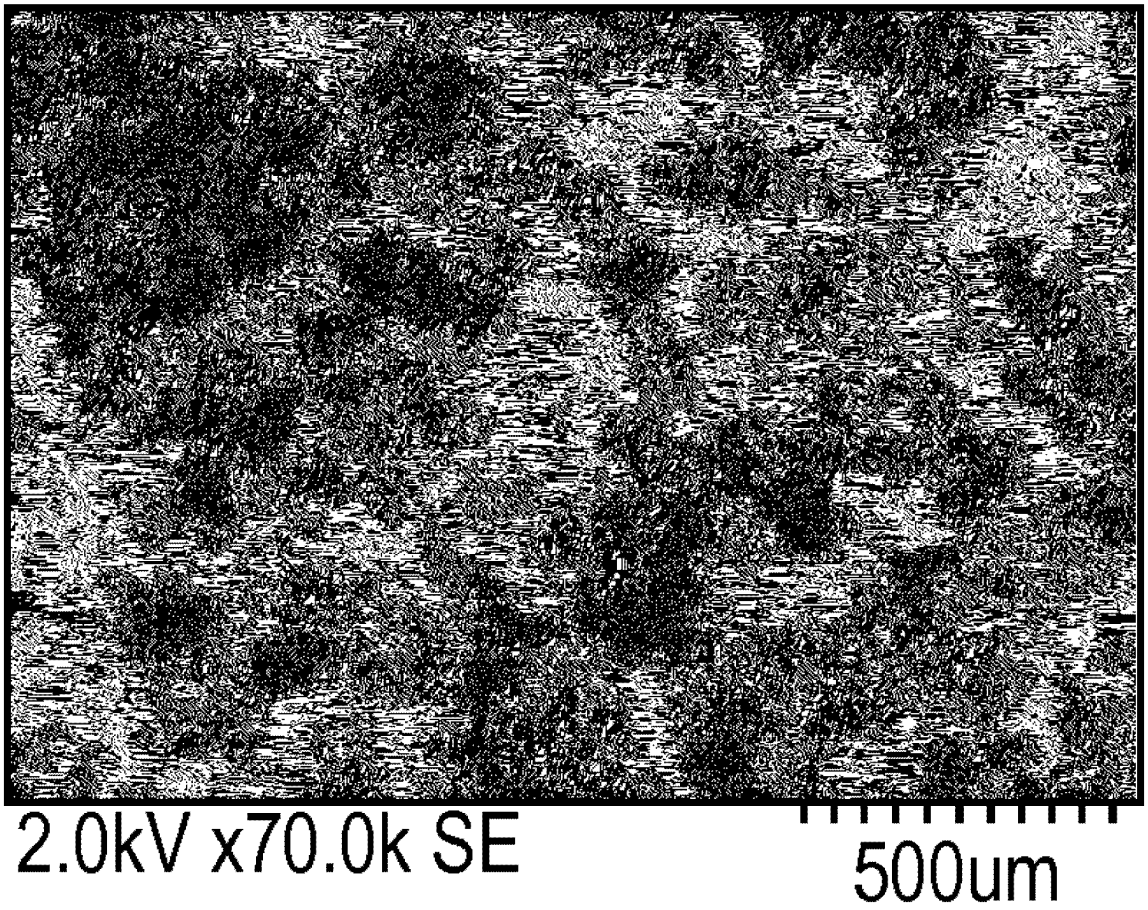

图 29B

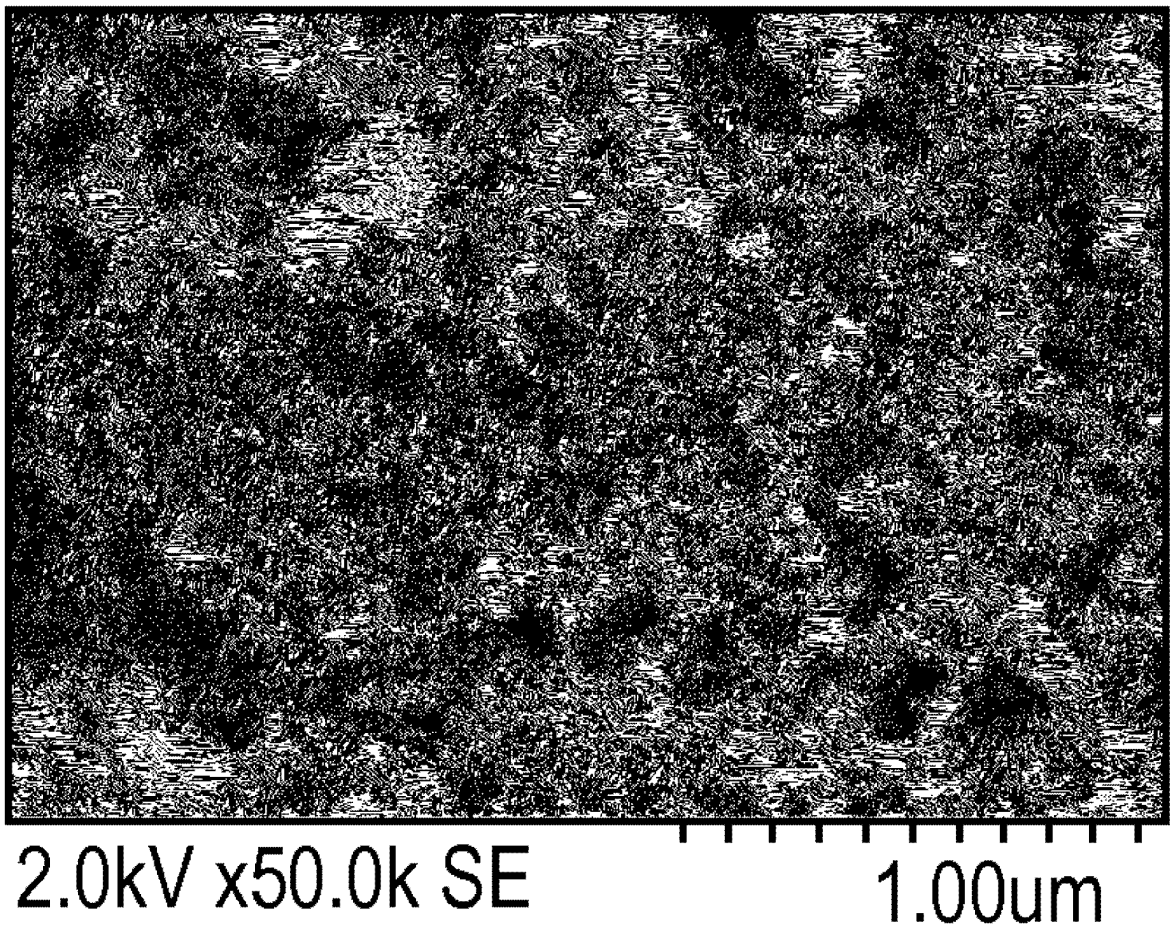

图 30A

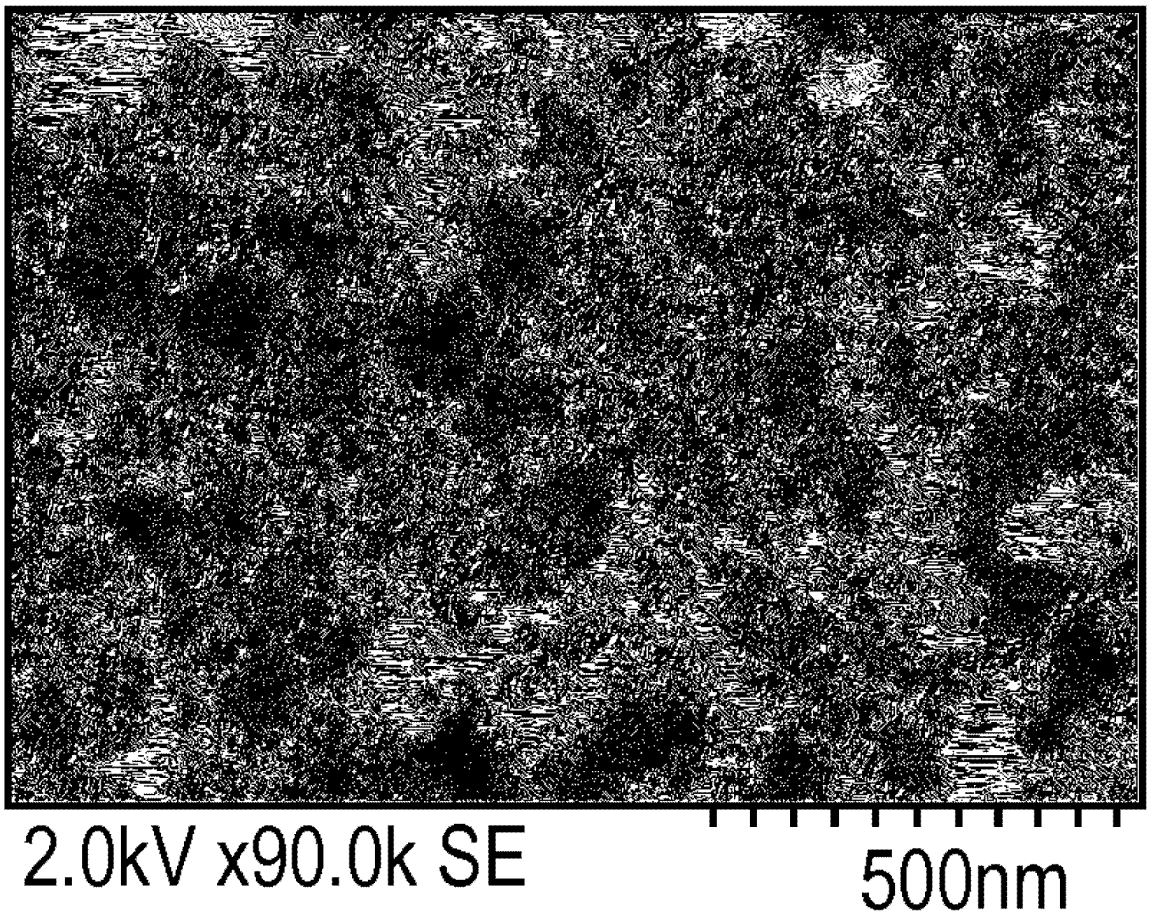

图 30B

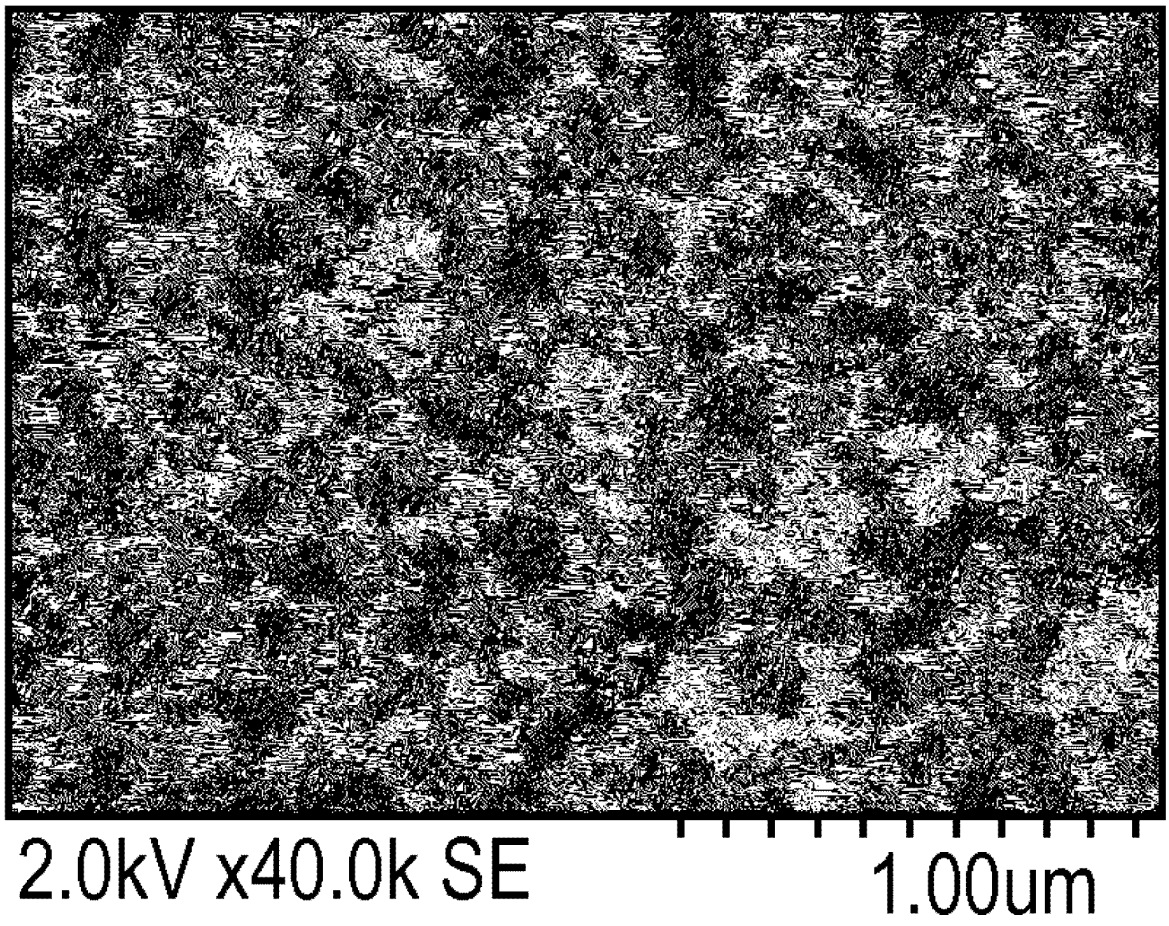

图 31A

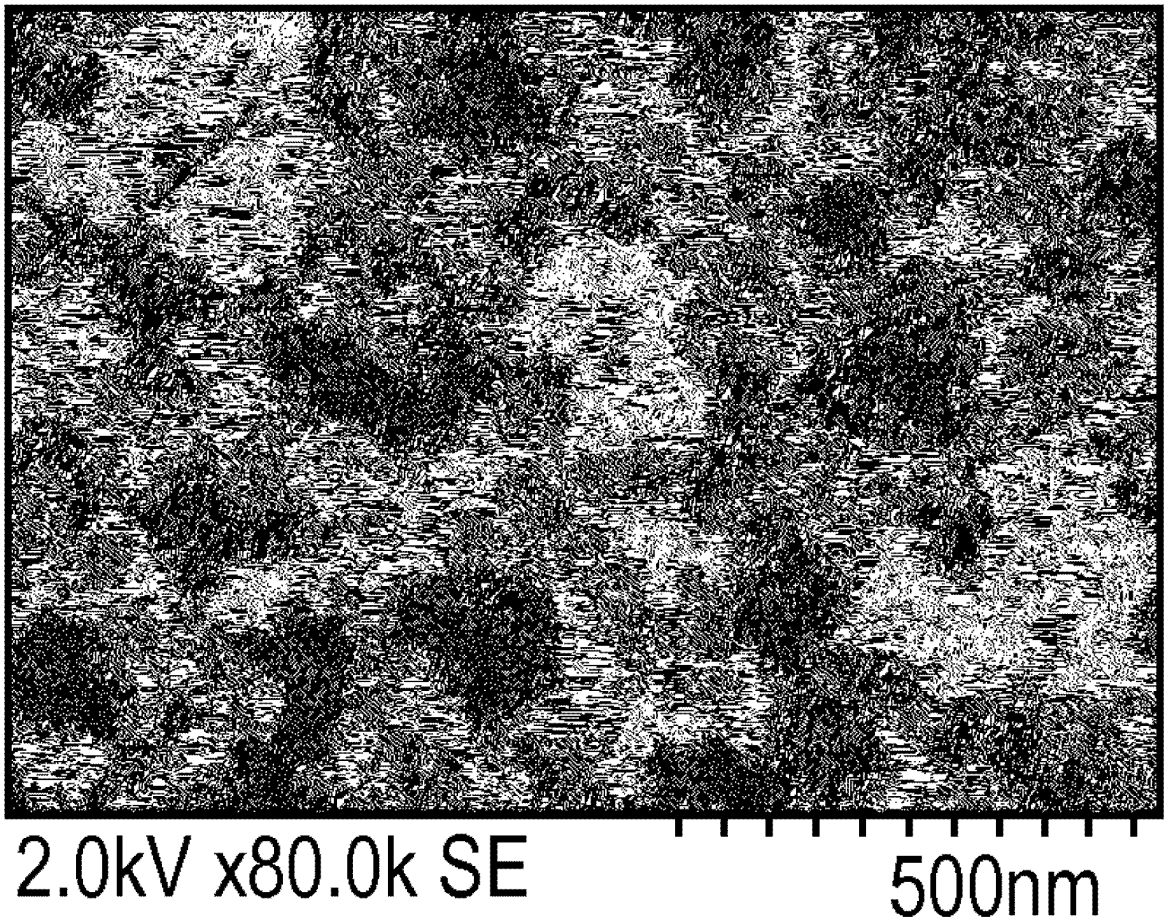

图 31B

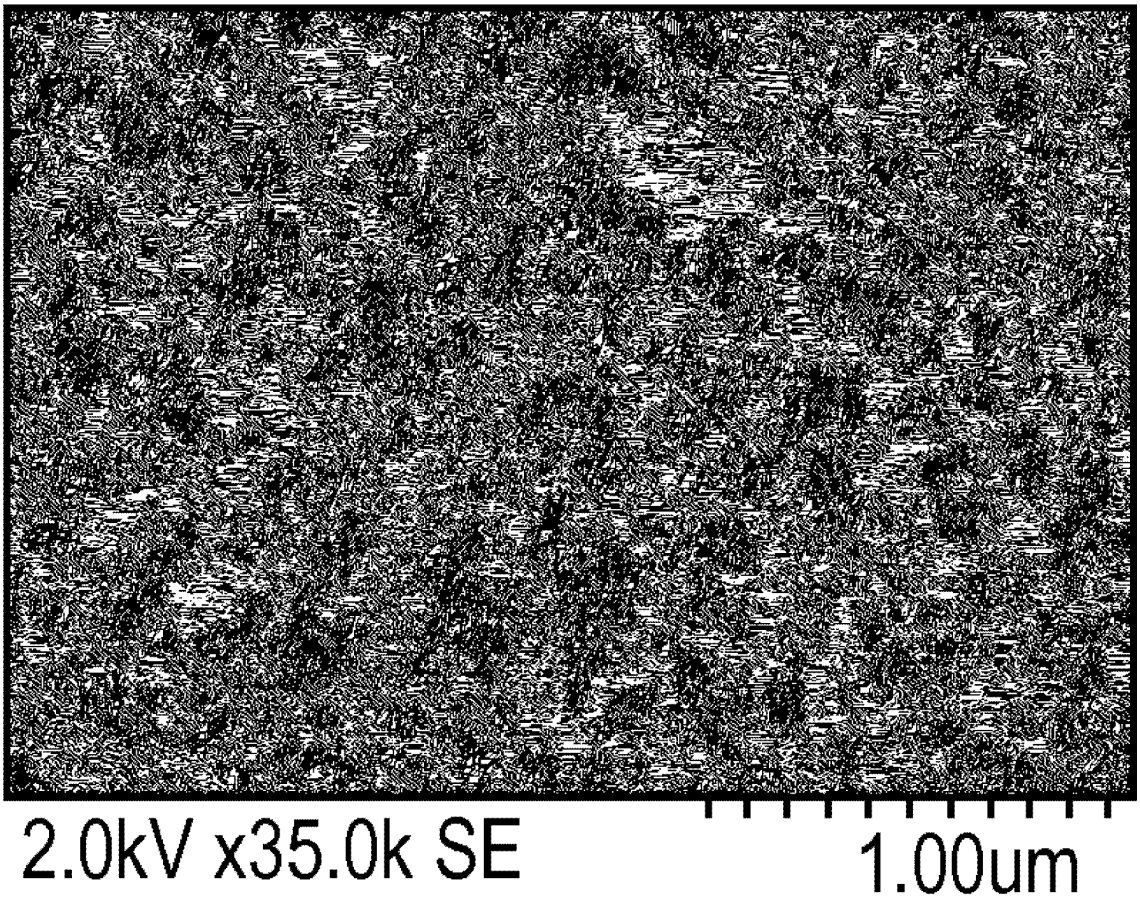

图 32A

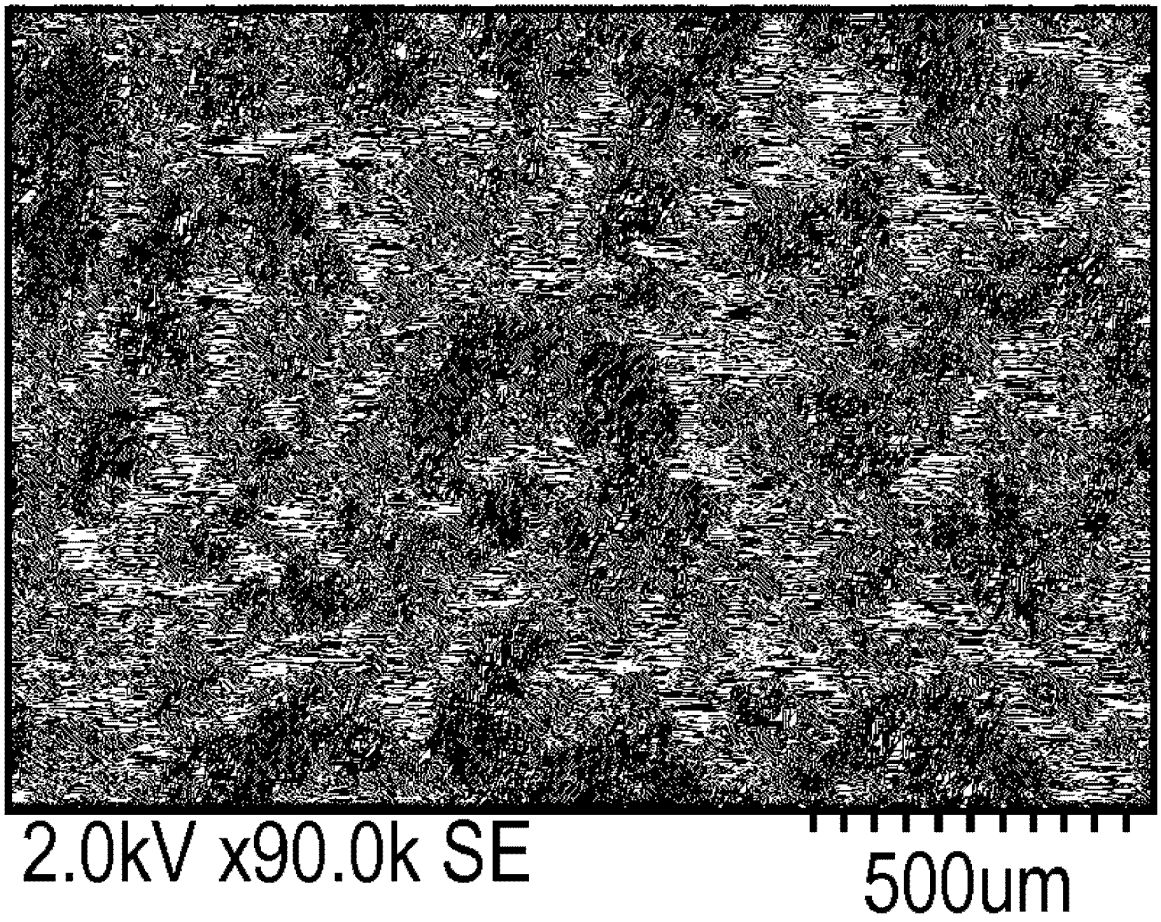

图 32B

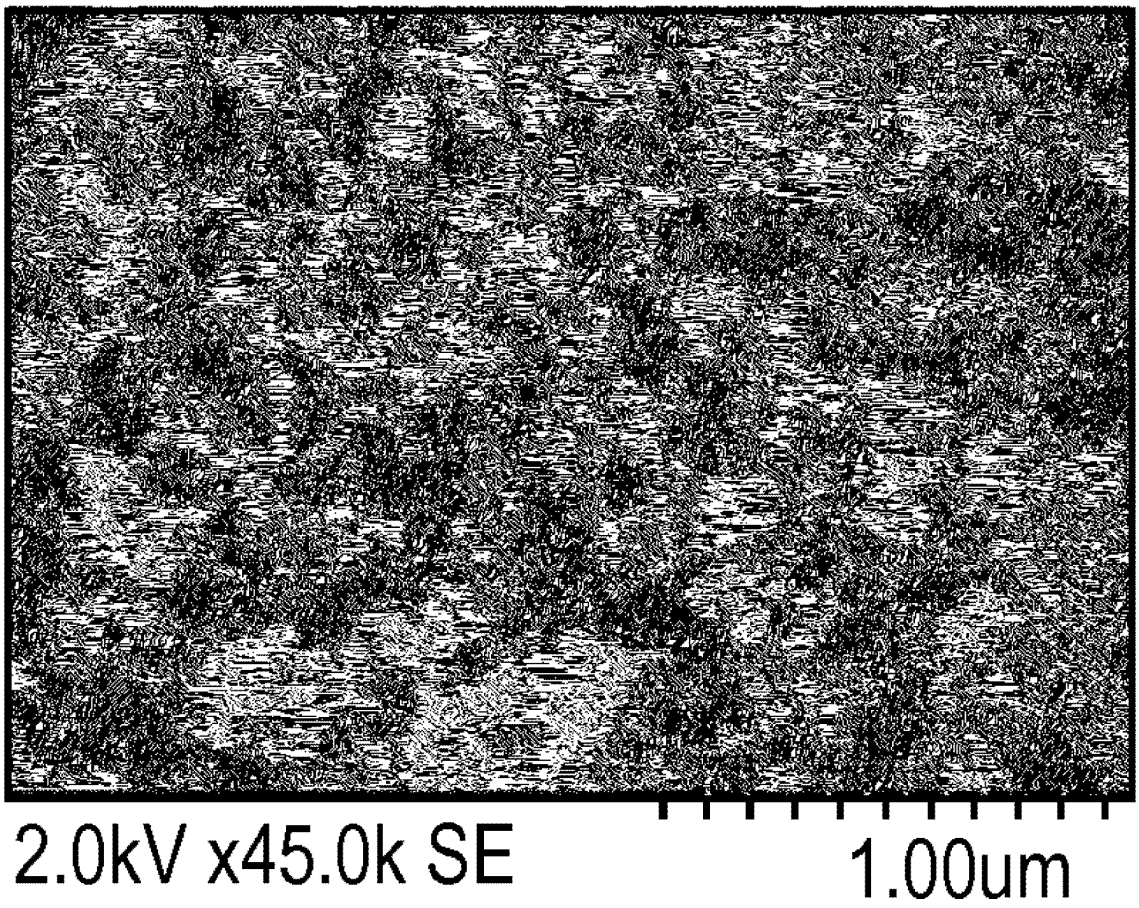

图 33A

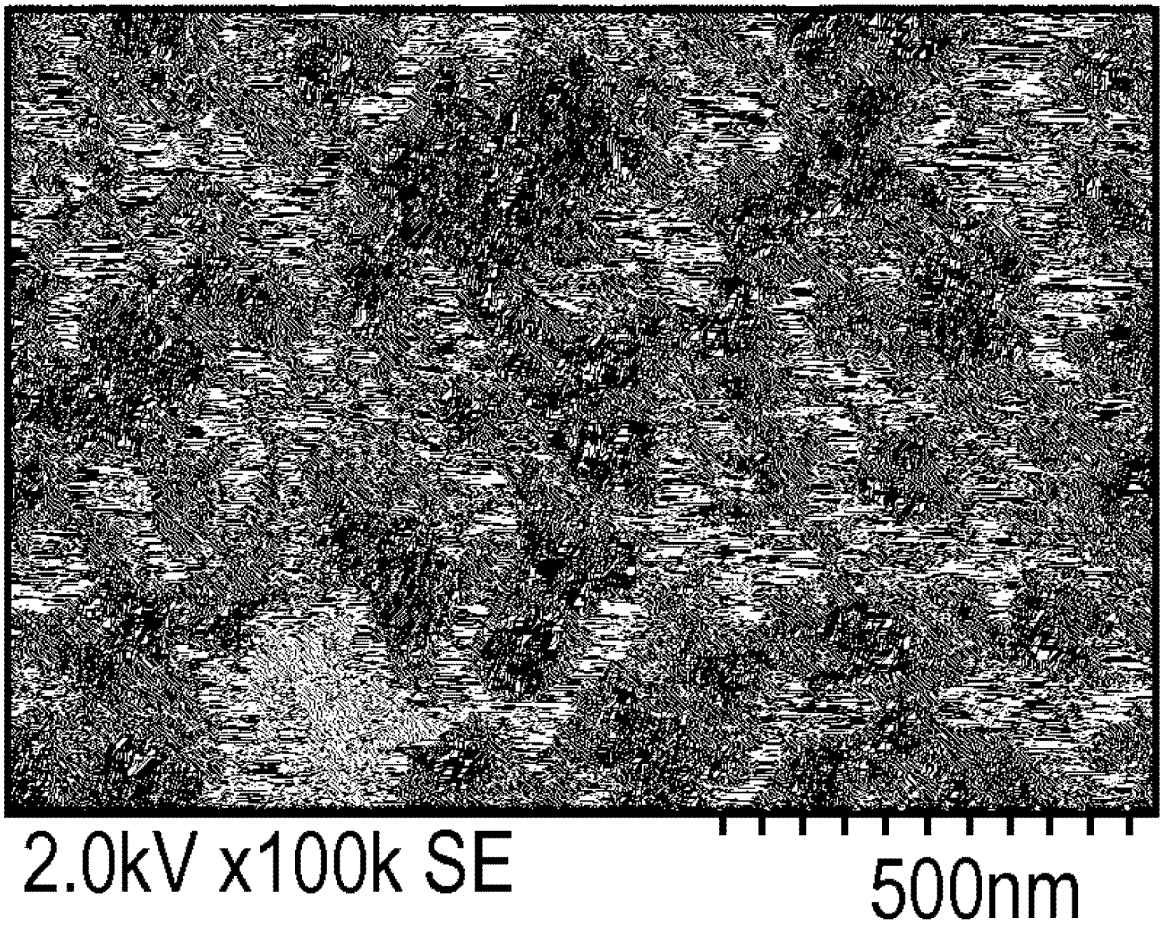

图 33B

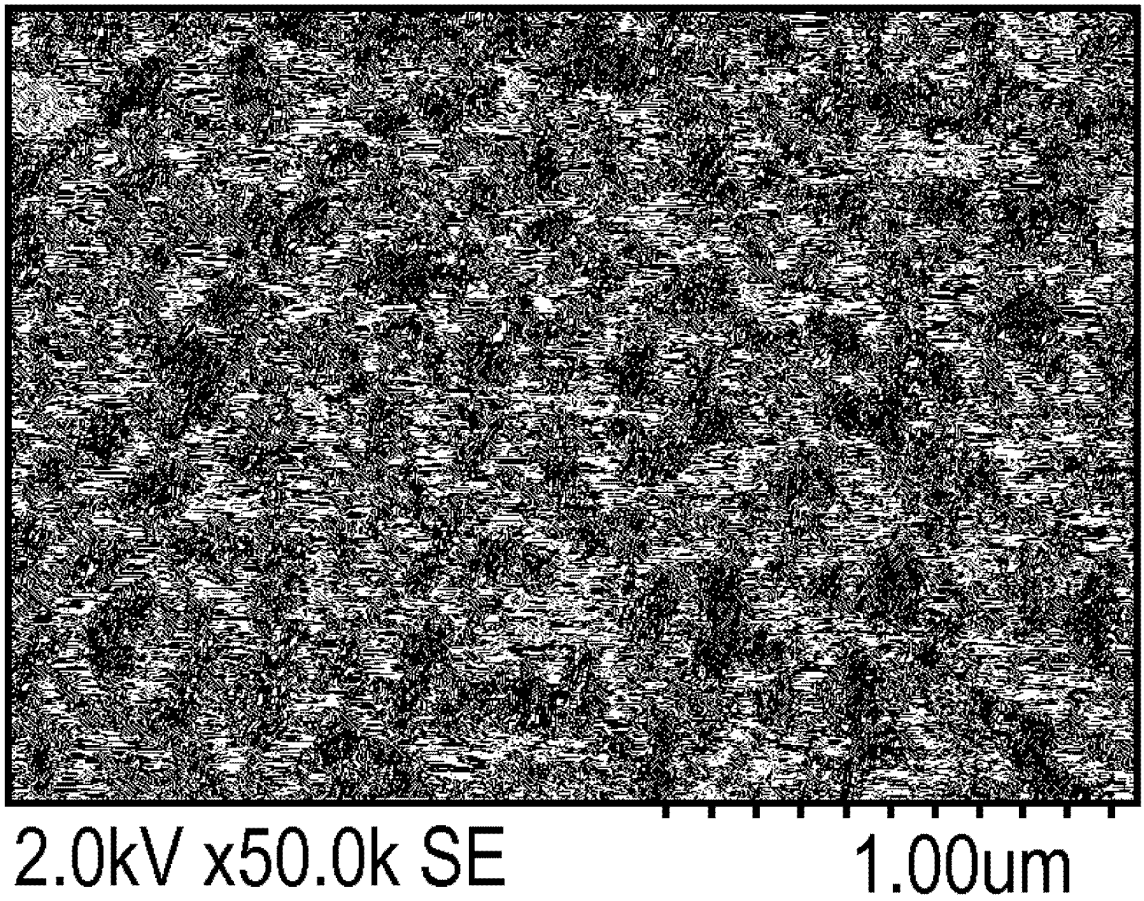

图 34A

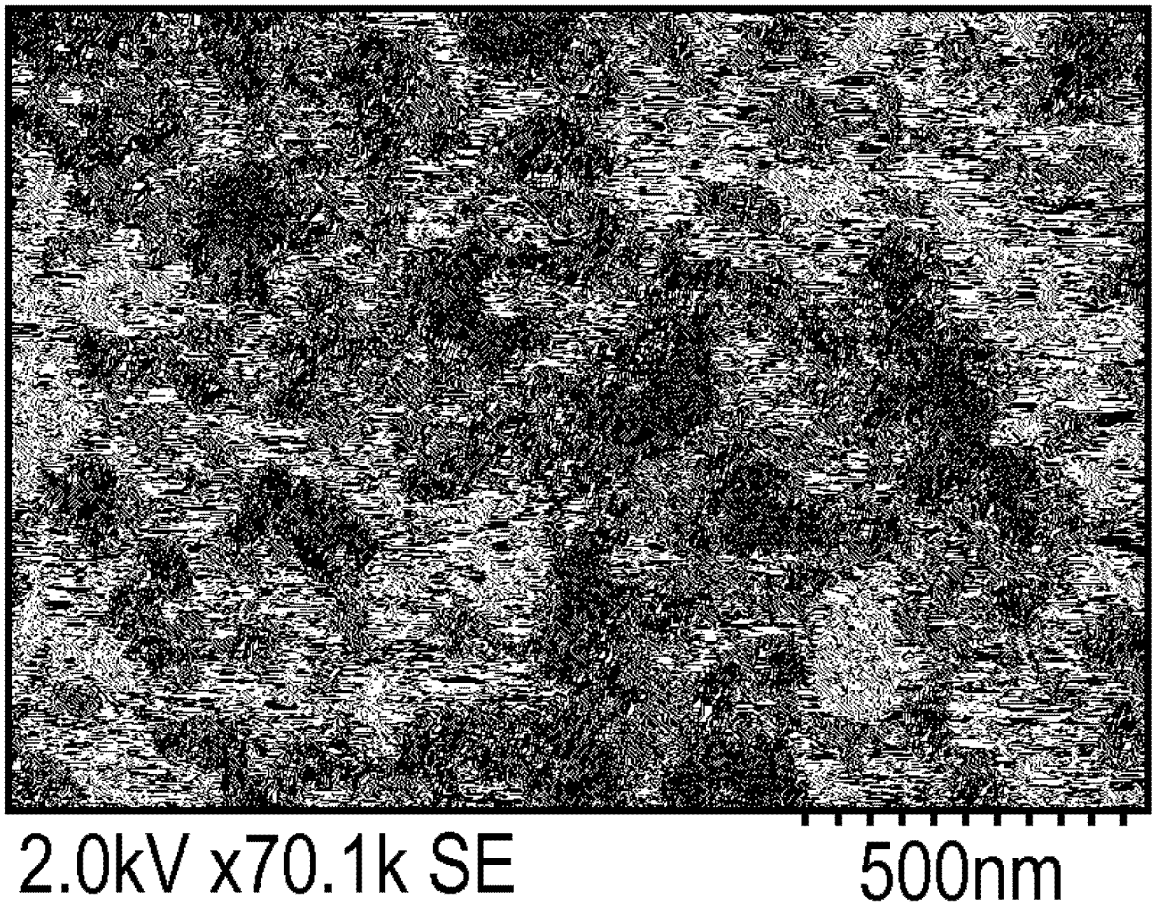

图 34B

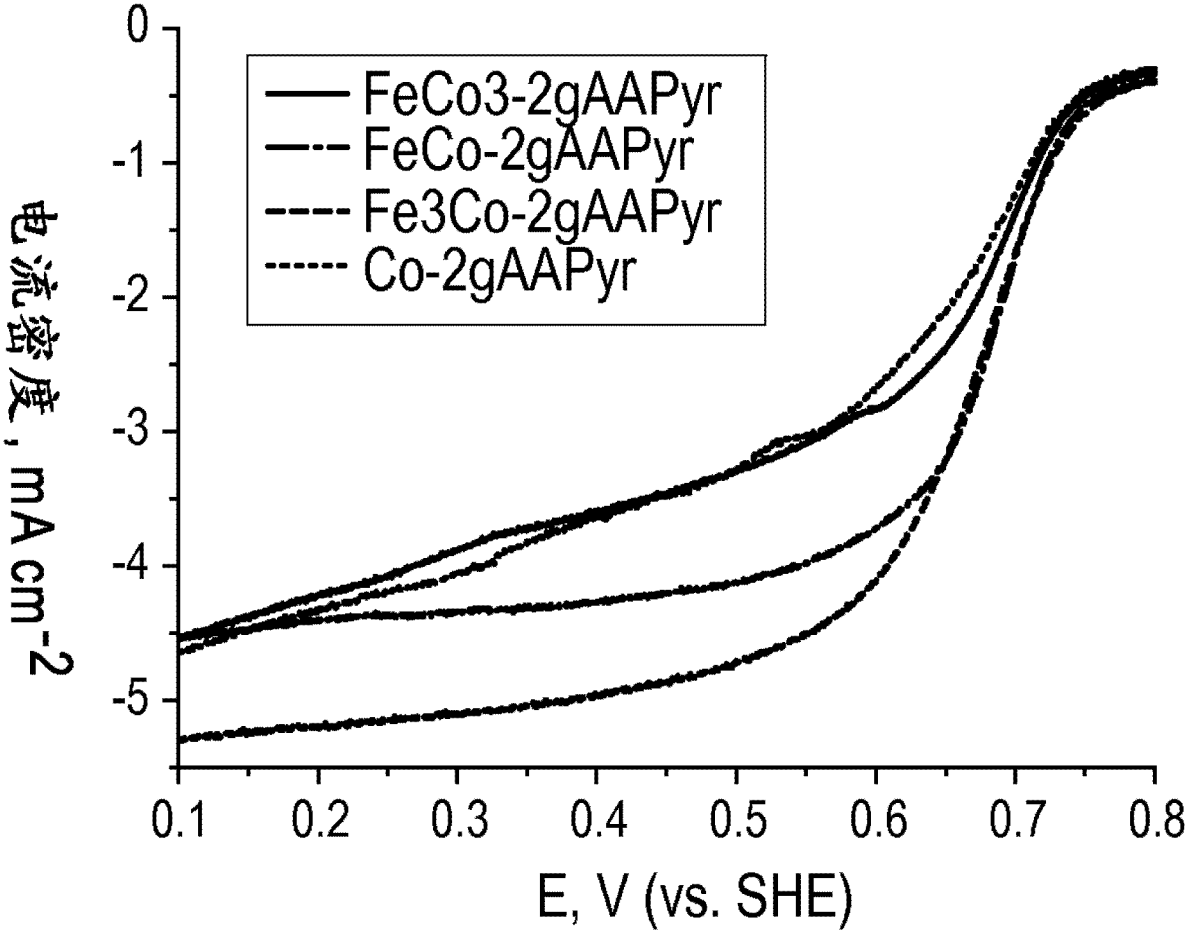
FeCo3-2gAAPyr
FeCo-2gAAPyr
Fe3Co-2gAAPyr
Co-2gAAPyr
电流密度，mA cm-2
0
-1
-2
-3
-4
-5
0.1
0.2
0.3
0.4
0.5
0.6
0.7
0.8
E, V (vs. SHE)

图 35

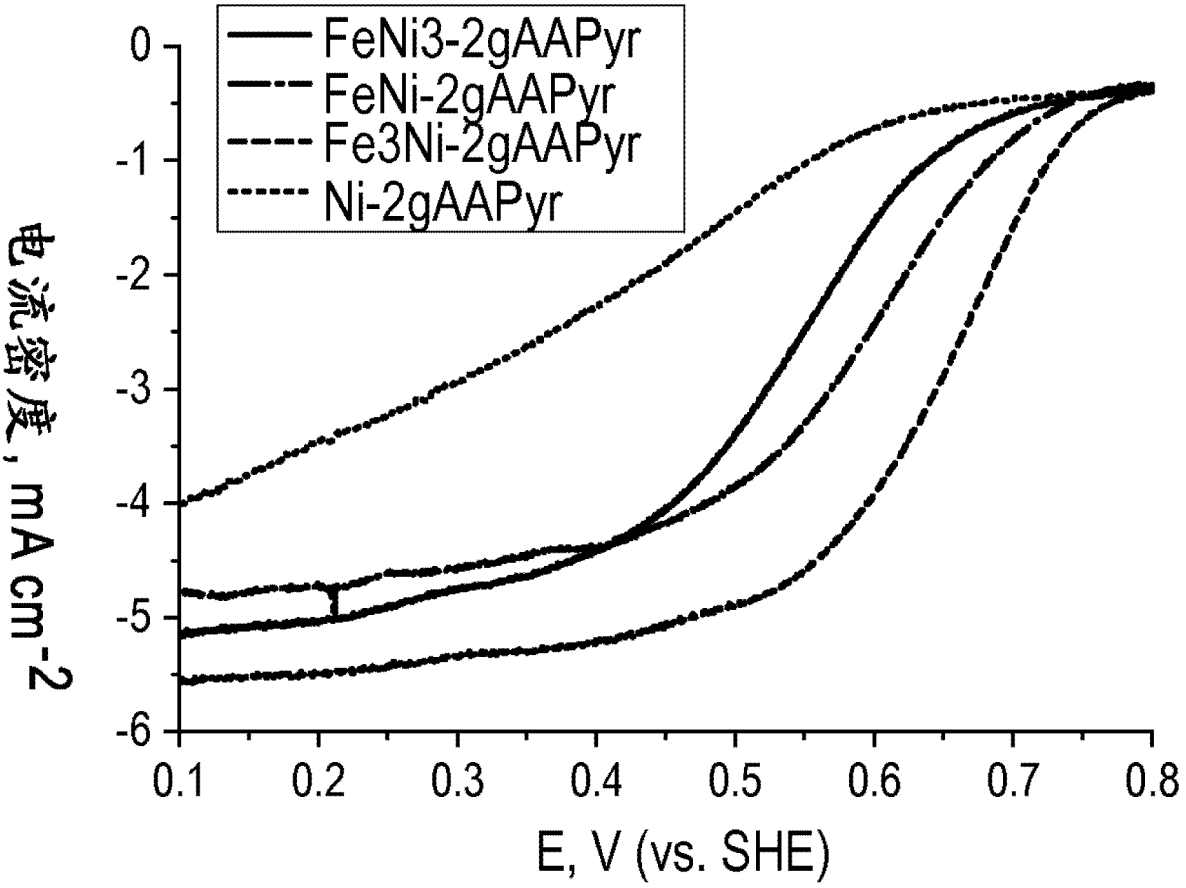
FeNi3-2gAAPyr
FeNi-2gAAPyr
Fe3Ni-2gAAPyr
Ni-2gAAPyr
电流密度，mA cm-2
0
-1
-2
-3
-4
-5
-6
0.1
0.2
0.3
0.4
0.5
0.6
0.7
0.8
E, V (vs. SHE)

图 36

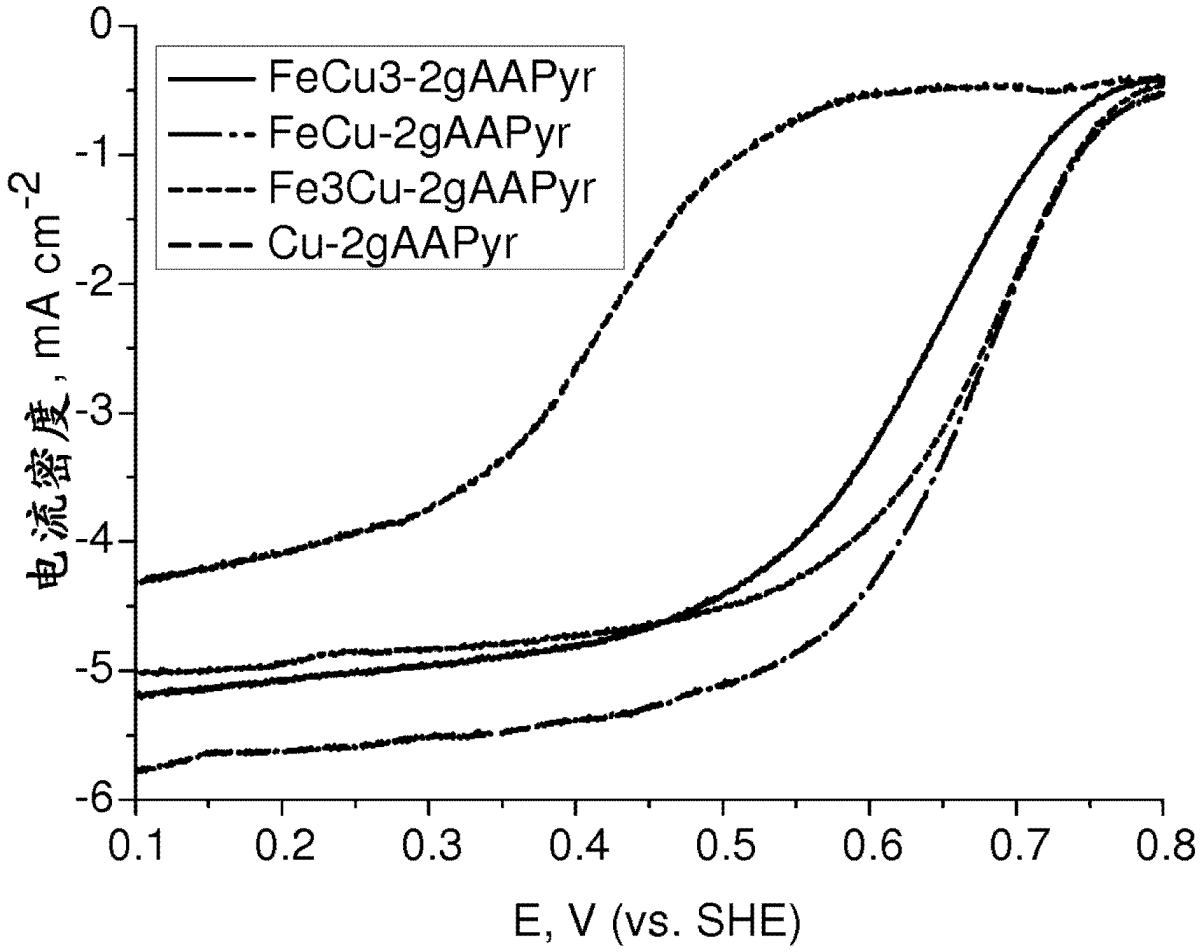
FeCu3-2gAAPyr
FeCu-2gAAPyr
Fe3Cu-2gAAPyr
Cu-2gAAPyr
电流密度, mA cm-2
0
-1
-2
-3
-4
-5
-6
0.1
0.2
0.3
0.4
0.5
0.6
0.7
0.8
E, V (vs. SHE)

图 37

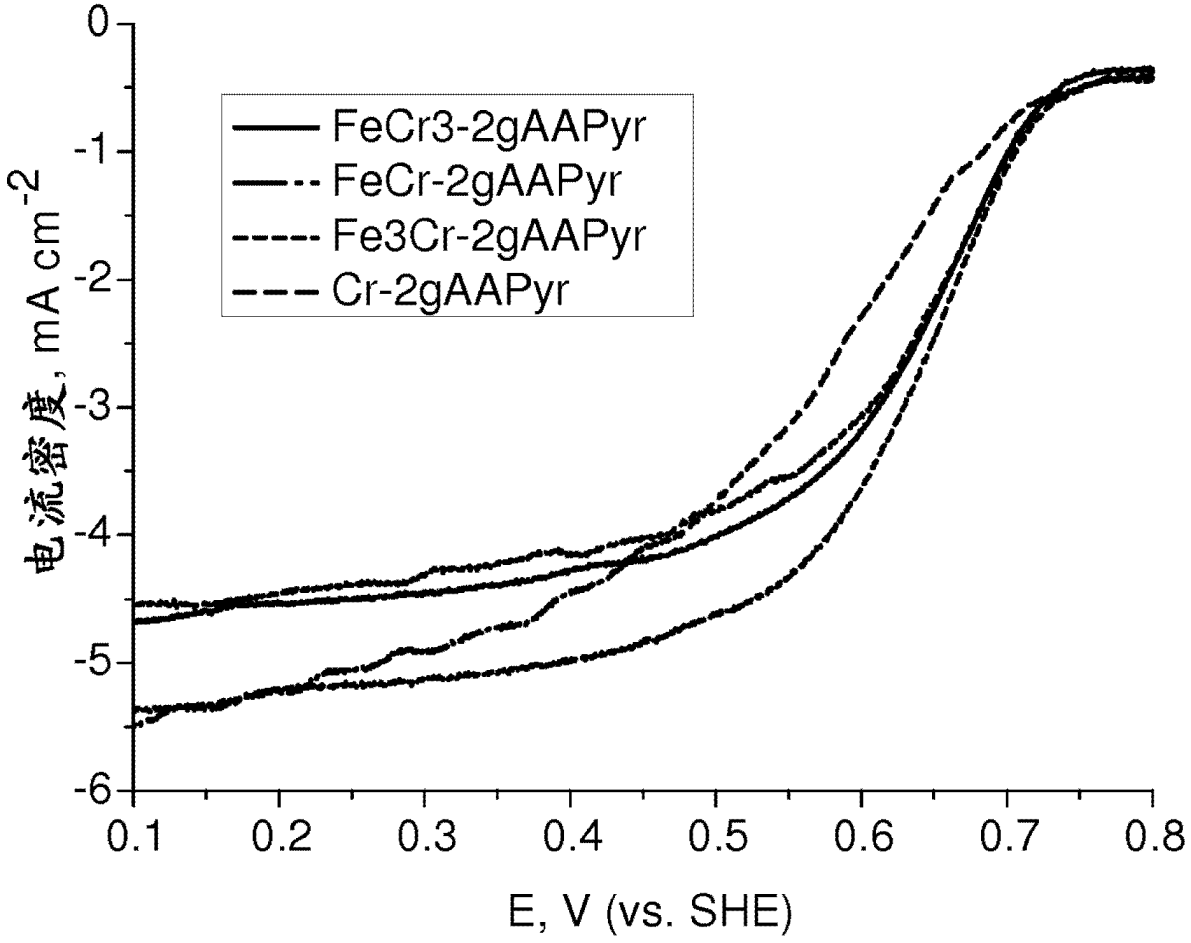
FeCr3-2gAAPyr
FeCr-2gAAPyr
Fe3Cr-2gAAPyr
Cr-2gAAPyr
电流密度, mA cm-2
0
-1
-2
-3
-4
-5
-6
0.1
0.2
0.3
0.4
0.5
0.6
0.7
0.8
E, V (vs. SHE)

图 38

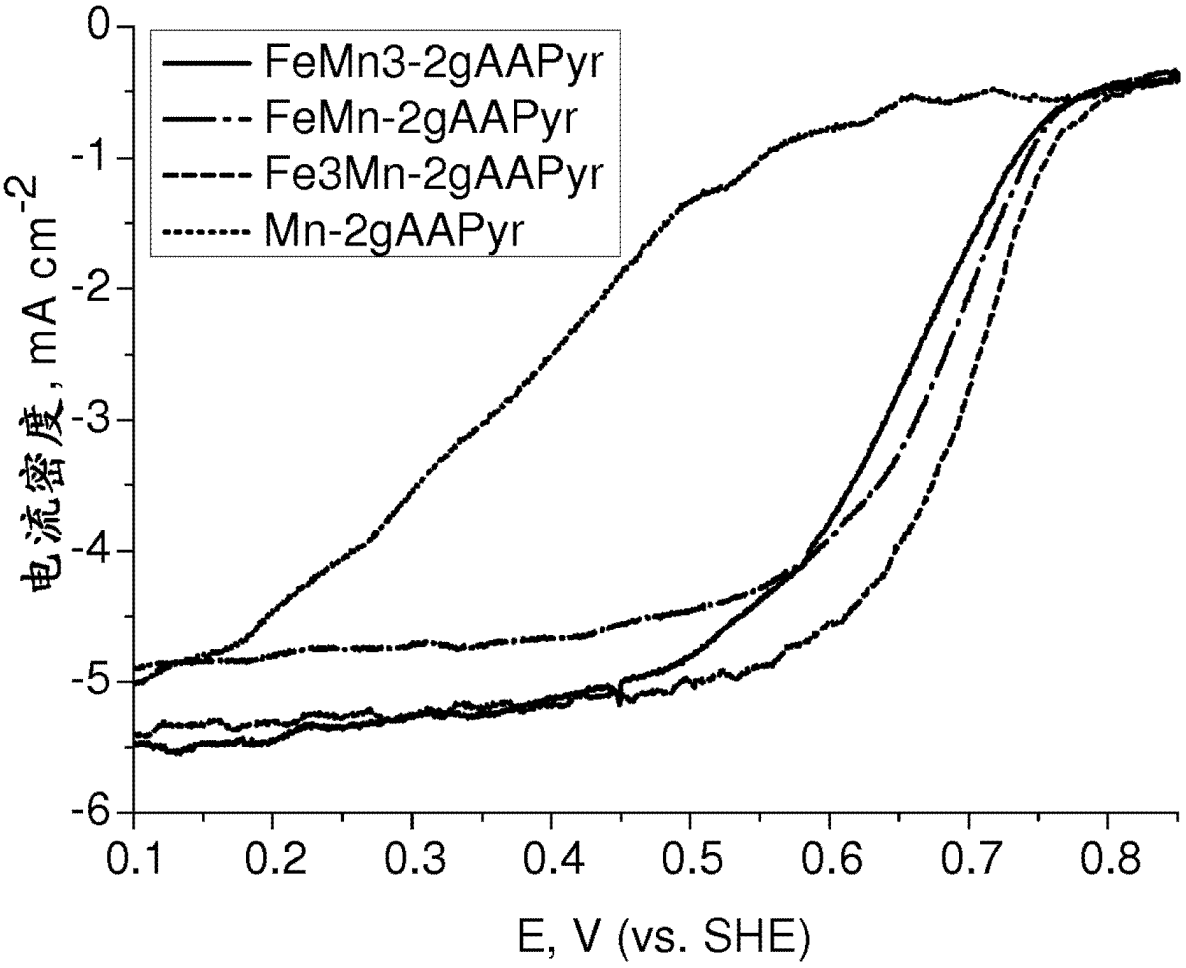
FeMn3-2gAAPyr
FeMn-2gAAPyr
Fe3Mn-2gAAPyr
Mn-2gAAPyr
电流密度, mA cm-2
0
-1
-2
-3
-4
-5
-6
0.1
0.2
0.3
0.4
0.5
0.6
0.7
0.8
E, V (vs. SHE)

图 39

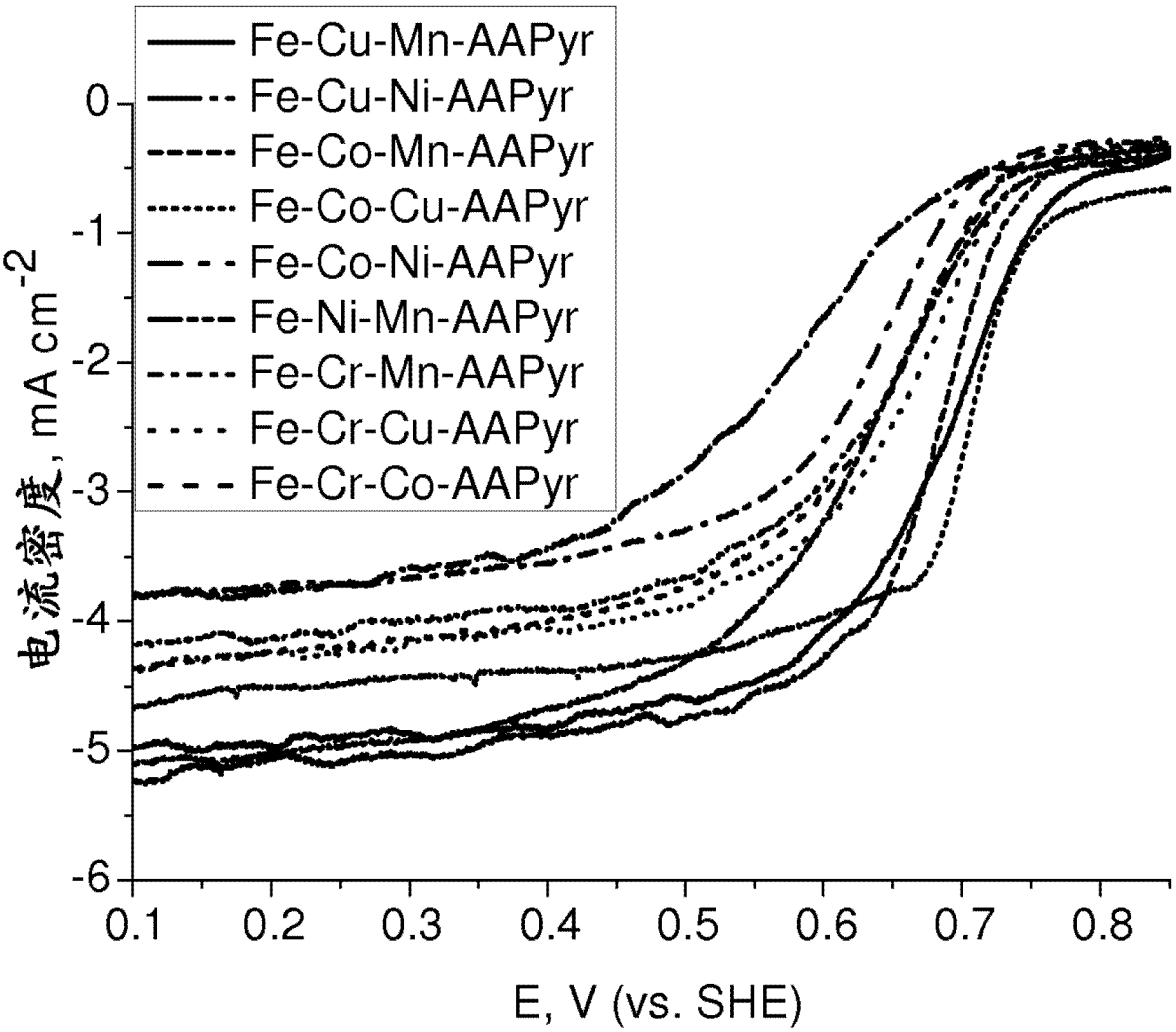
Fe-Cu-Mn-AAPyr
Fe-Cu-Ni-AAPyr
Fe-Co-Mn-AAPyr
Fe-Co-Cu-AAPyr
Fe-Co-Ni-AAPyr
Fe-Ni-Mn-AAPyr
Fe-Cr-Mn-AAPyr
Fe-Cr-Cu-AAPyr
Fe-Cr-Co-AAPyr
电流密度, mA cm-2
0
-1
-2
-3
-4
-5
-6
0.1
0.2
0.3
0.4
0.5
0.6
0.7
0.8
E, V (vs. SHE)

图 40

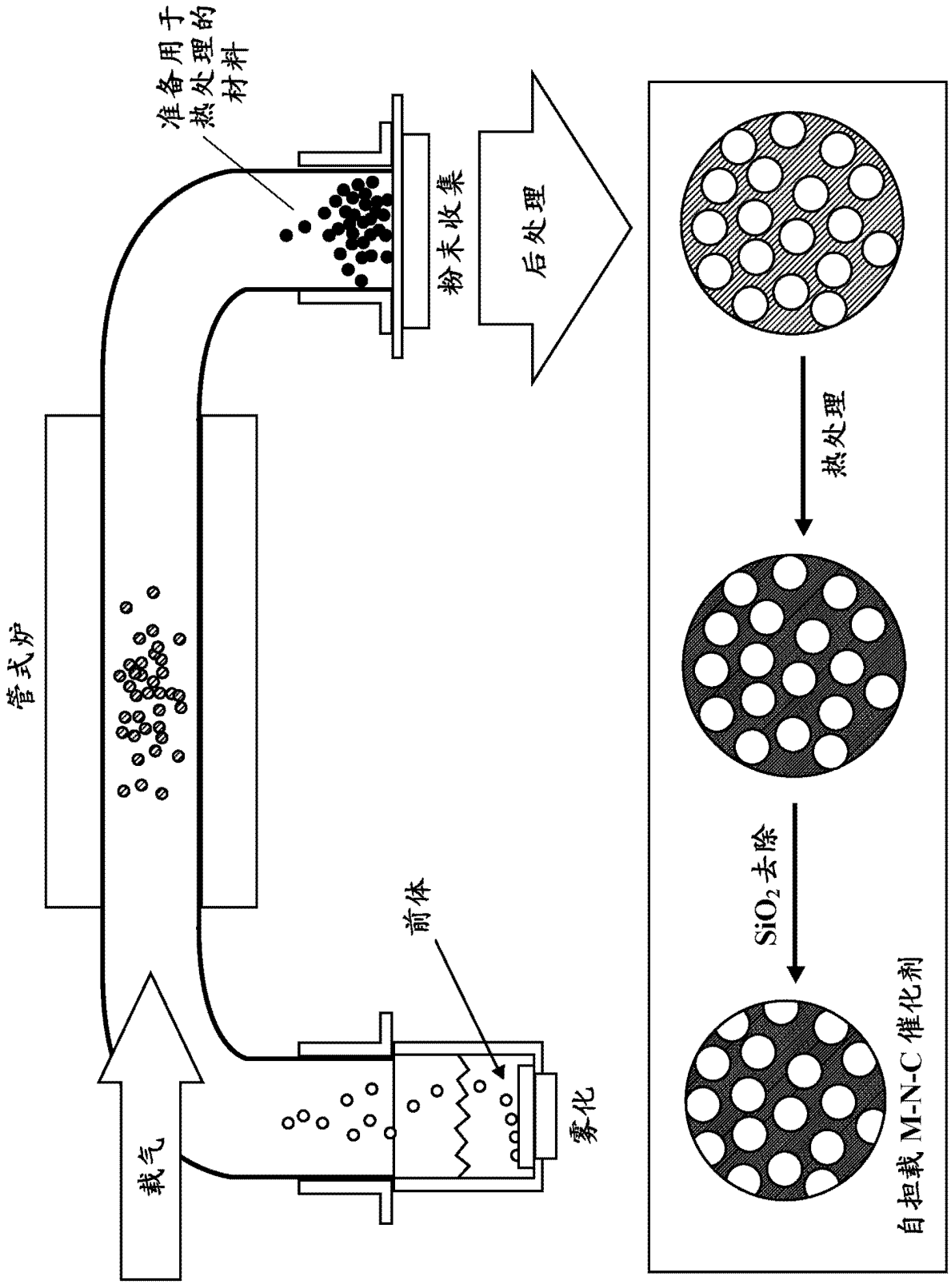

图 41

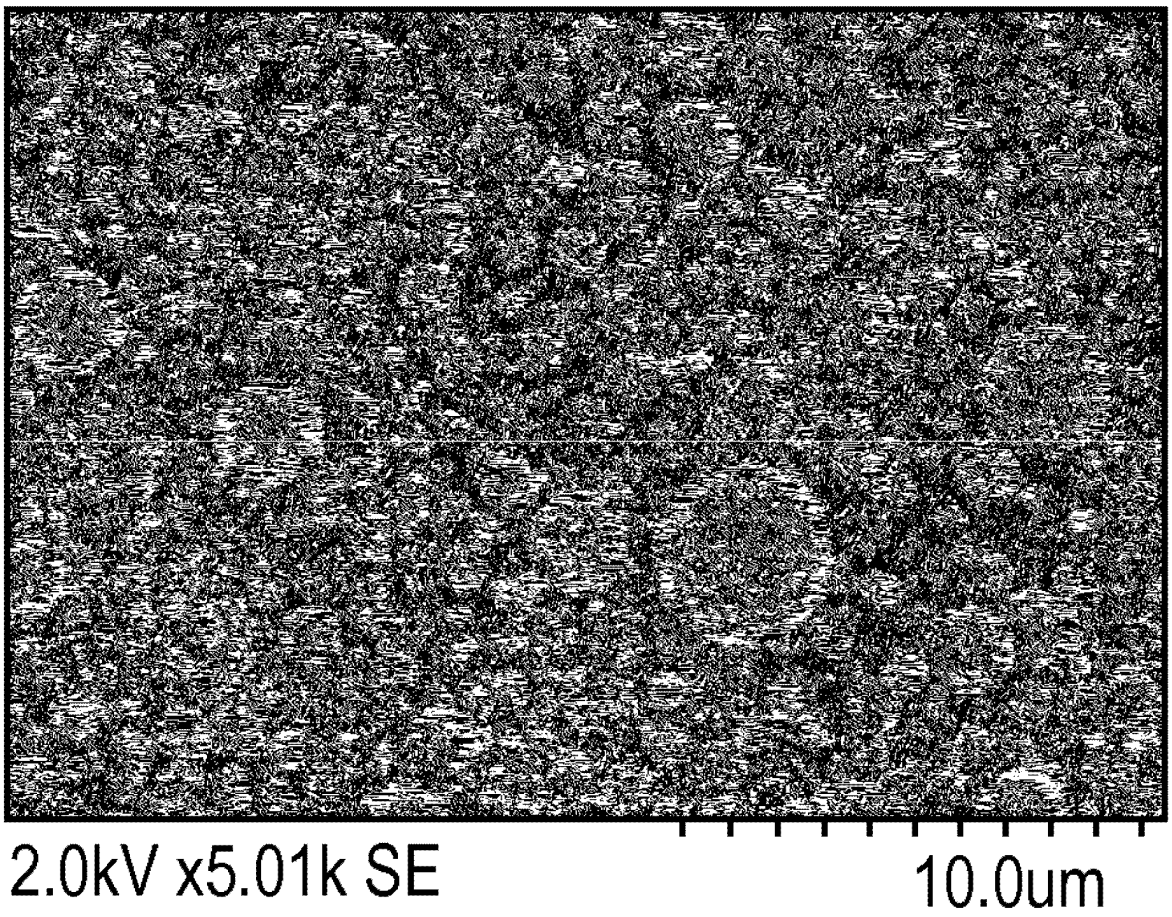

图 42A

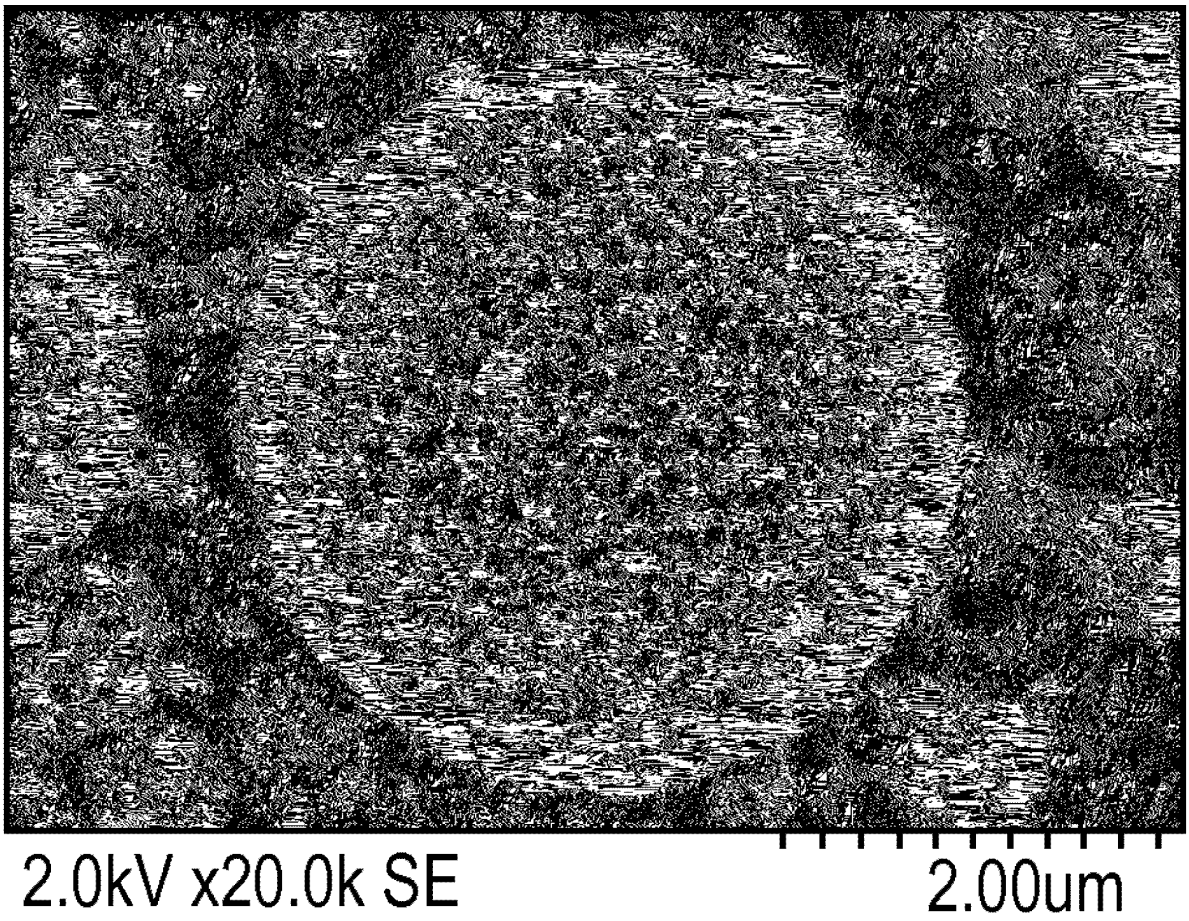

图 42B

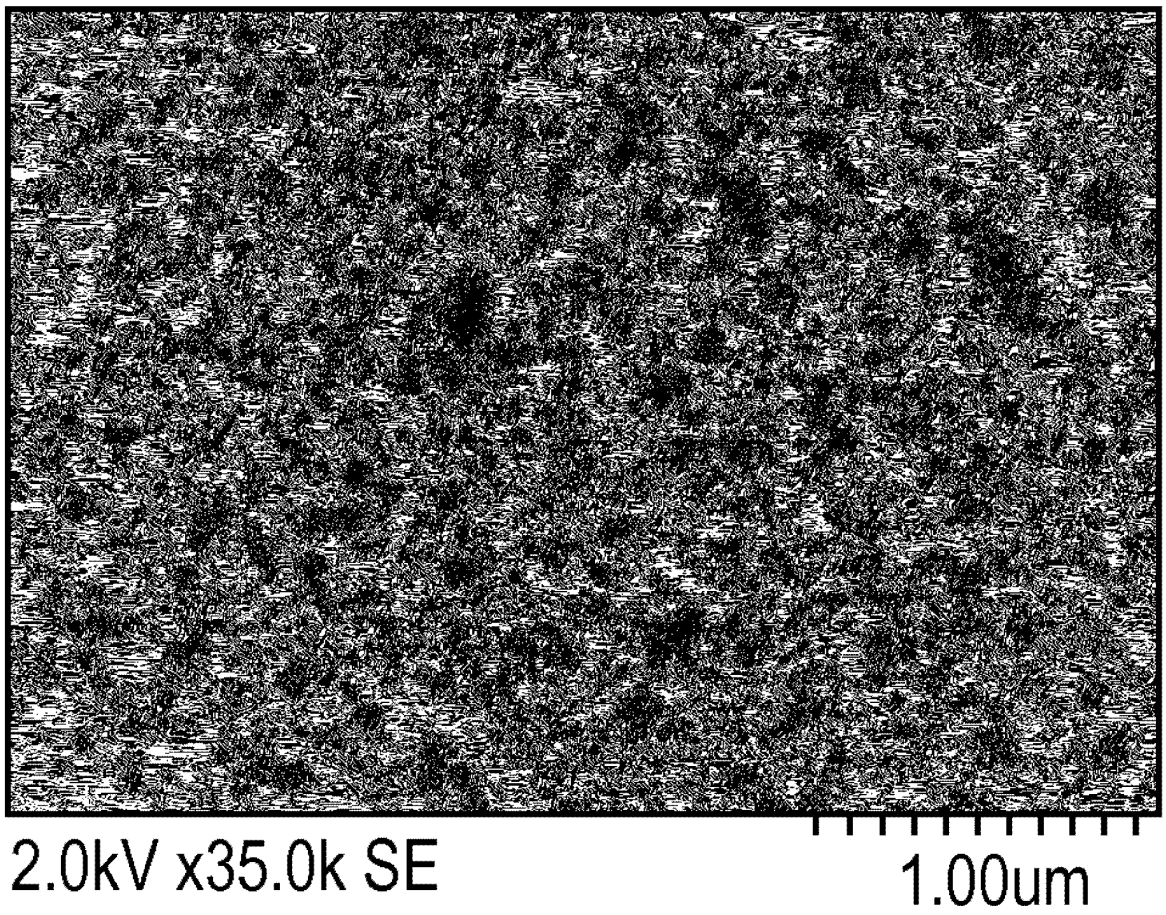

图 42C

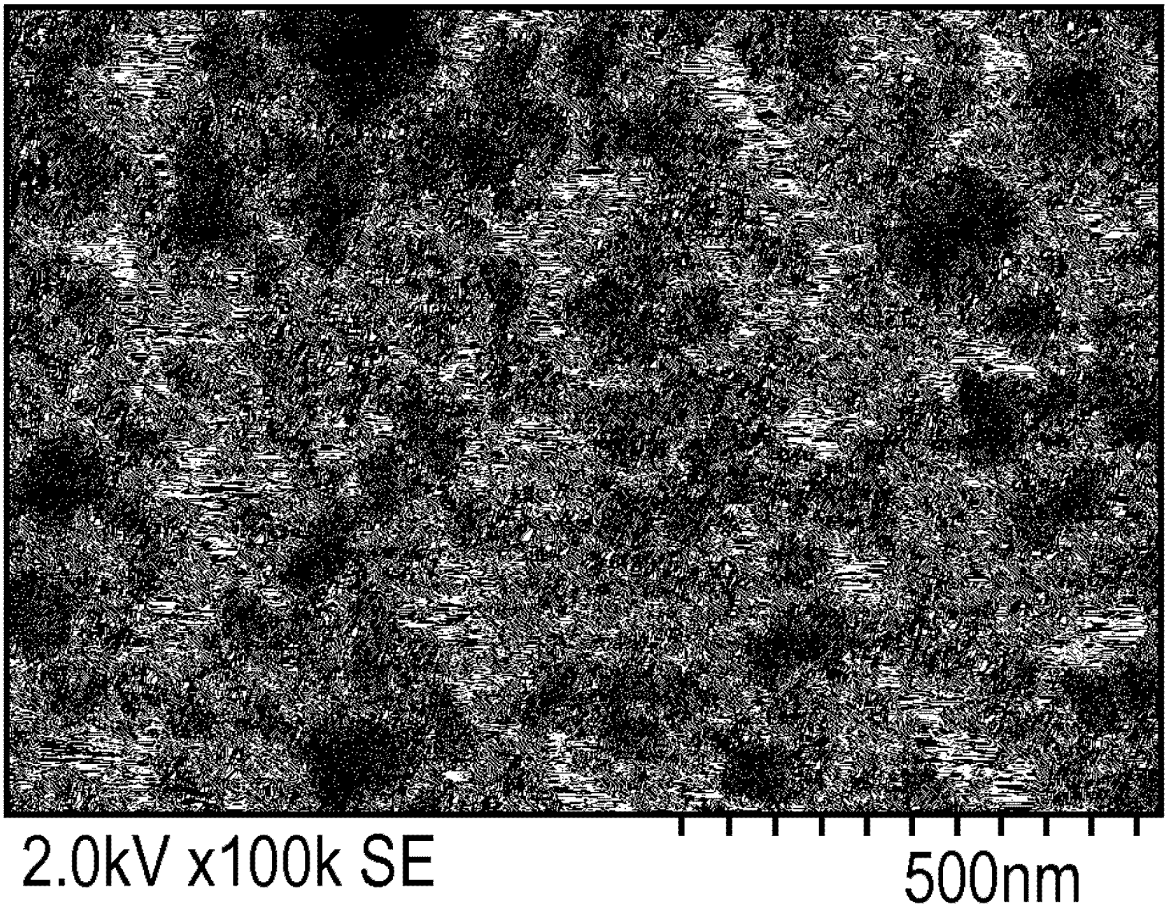

图 42D

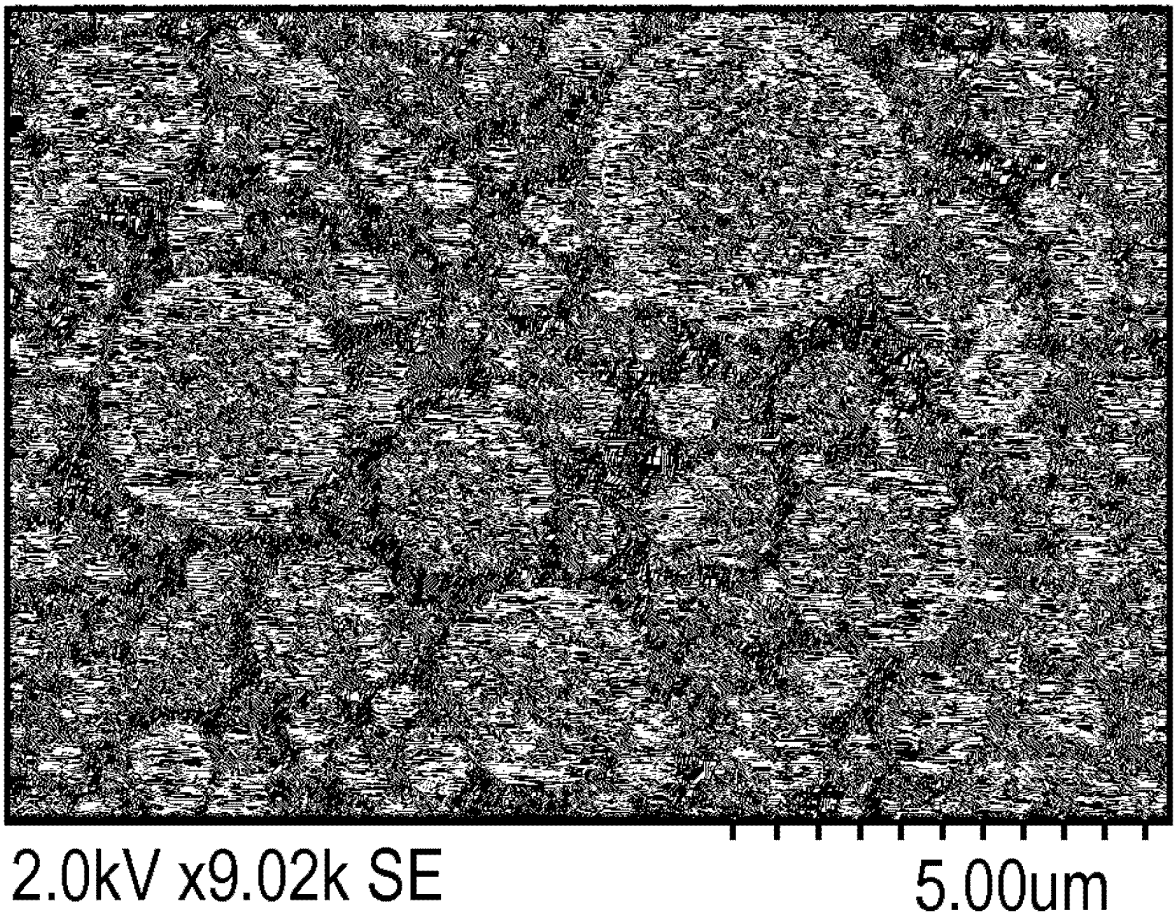

图 43A

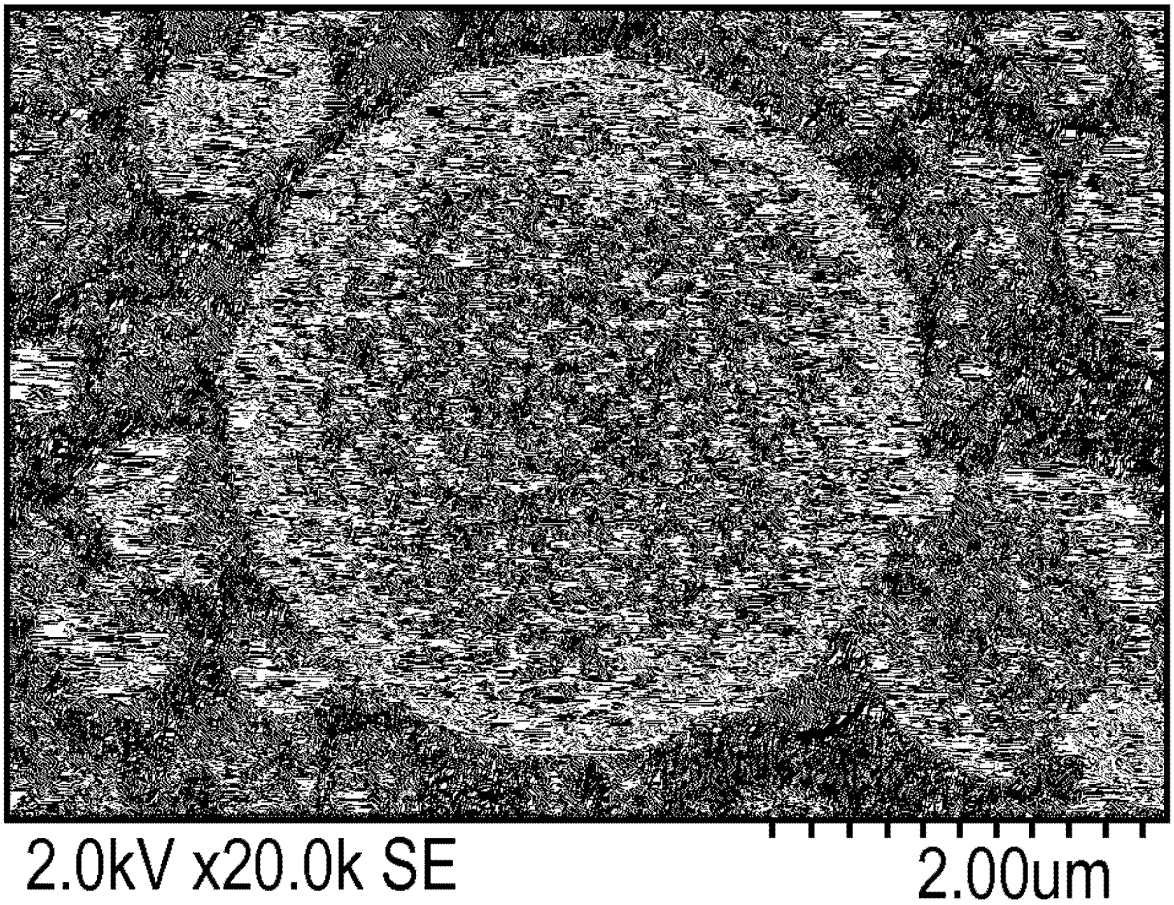

图 43B

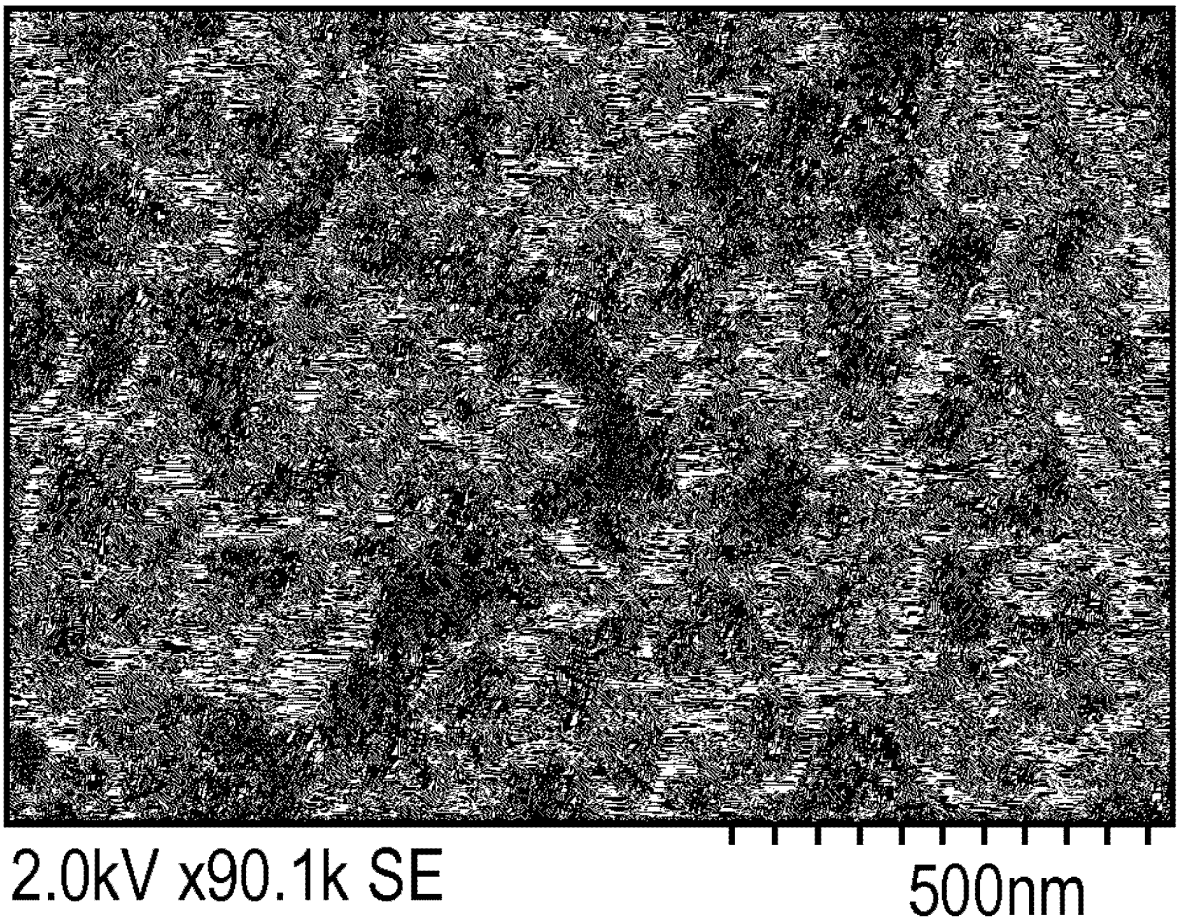

图 43C

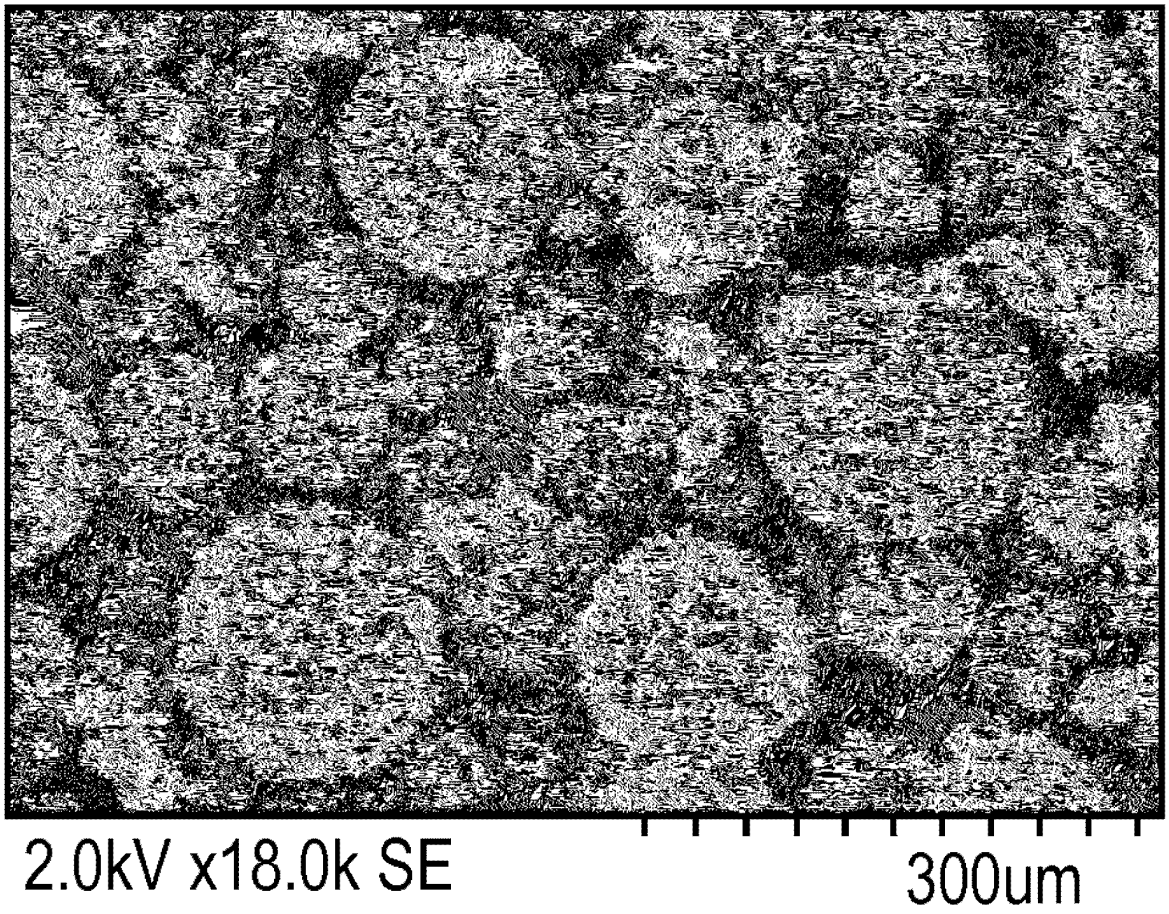

图 44A

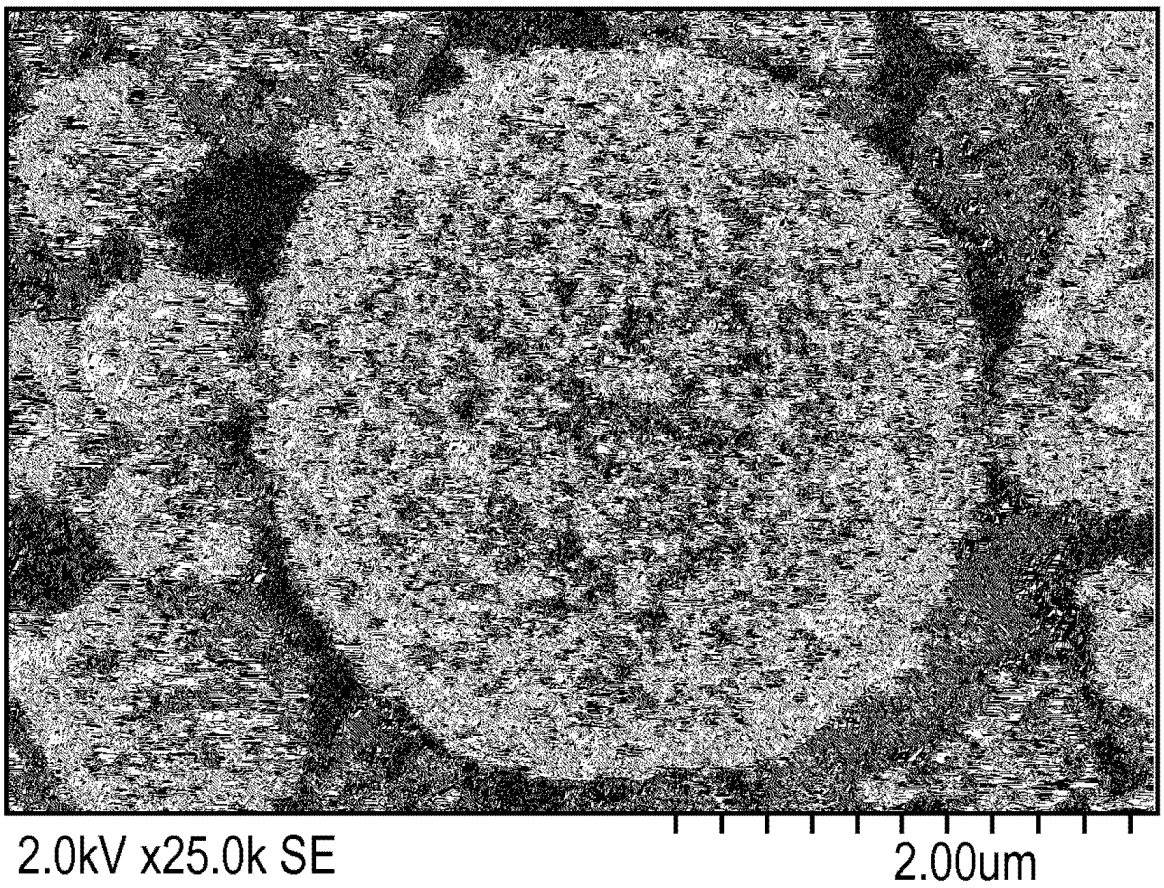

图 44B

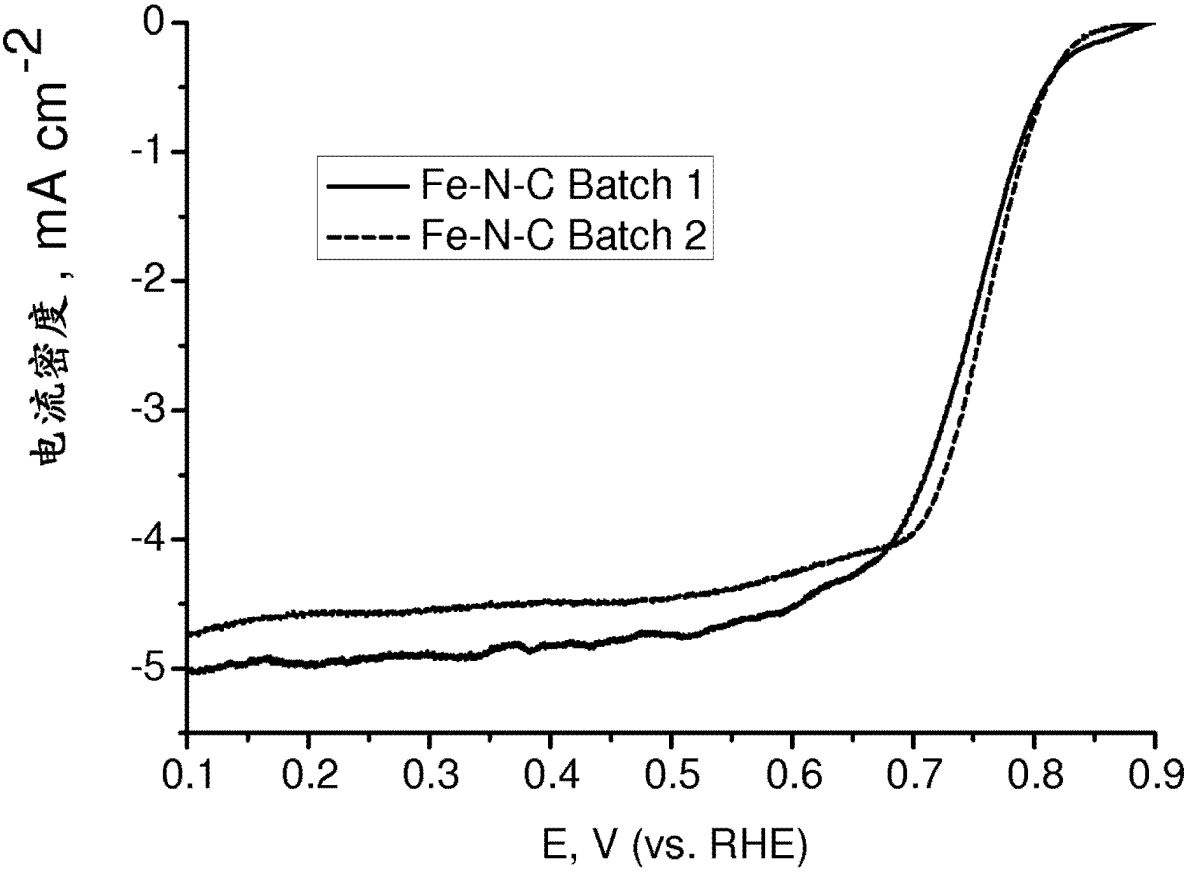
电流密度，mA cm-2
0
-1
-2
-3
-4
-5
Fe-N-C Batch 1
Fe-N-C Batch 2
0.1
0.2
0.3
0.4
0.5
0.6
0.7
0.8
0.9
E, V (vs. RHE)

图 45